



Virginia Commonwealth University
VCU Scholars Compass

Theses and Dissertations


Graduate School

2017

PREPARATION AND EVALUATION TECHNIQUES OF POROUS MATERIALS AND MIXED MATRIX MEMBRANES FOR TARGETED CO₂ SEPARATION APPLICATIONS

Tsemre Tessema

Follow this and additional works at: <https://scholarscompass.vcu.edu/etd>

 Part of the [Materials Chemistry Commons](#), [Organic Chemistry Commons](#), [Physical Chemistry Commons](#), and the [Polymer Chemistry Commons](#)

© The Author

Downloaded from

<https://scholarscompass.vcu.edu/etd/5044>

This Thesis is brought to you for free and open access by the Graduate School at VCU Scholars Compass. It has been accepted for inclusion in Theses and Dissertations by an authorized administrator of VCU Scholars Compass. For more information, please contact libcompass@vcu.edu.

© COPYRIGHT BY

Tsemre Dingel Mesfin Tessema

2017

All Rights Reserved

**PREPARATION AND EVALUATION TECHNIQUES OF POROUS MATERIALS AND
MIXED MATRIX MEMBRANES FOR TARGETED CO₂ SEPARATION
APPLICATIONS**

A dissertation submitted in partial fulfillment of the requirements for the degree of Doctor of
Philosophy at Virginia Commonwealth University

by

Tsemre Dingel Mesfin Tessema

Bachelor of Science

Kent State University, 2008

Master of Science

Villanova University, 2012

Director: Hani M. El-Kaderi,

Associate Professor, Department of Chemistry

Virginia Commonwealth University

Richmond, Virginia

July 31st, 2017

Acknowledgement

I would like to acknowledge the continued support, encouragement and guidance of Prof. Hani El-Kaderi. Without his ideas and knowledge this work would not come to fruition. I would also like to express my sincere appreciation for my committee members Prof. Julio Alvarez, Prof. Indika U. Arachchige, and Prof. Frank Gupton for their input in the pursuit of my doctorate. I also express my gratitude to our collaborators at National Energy and Technology Laboratory, U.S. Department of Energy, especially Dr. Ali Kemal Sekizkardes whose cooperation has been tremendous. I am very thankful to past and present members of the El-Kaderi Group who have been a pleasure to work with. Special thanks should be given to the Department of Chemistry at Virginia Commonwealth University; faculty and staff who all contributed to my success throughout my PhD career. I would also like to thank Altria for the fellowship granted to me in the final year of my dissertation. Finally, special thanks to my parents and siblings for their continued support throughout my endeavors.

Table of Contents

Table of Contents

List of Tables	vi
List of Schemes.....	vi
List of Figures.....	vii
List of Abbreviations	v
Abstract.....	xiii

Chapter 1-Introduction

1.1 CO ₂ emission and need for capture and sequestration	1
1.2 Processes for CO ₂ separations.....	3
1.2.1 Absorption.....	4
1.2.2 Cryogenic distillation.....	4
1.2.3 Membranes.....	5
1.2.4 Adsorption.....	9
1.2.4.1 Zeolites.....	10
1.2.4.2 Activated carbons.....	11
1.2.4.3 Metal organic frameworks	11
1.2.4.4 Porous organic polymers.....	12
1.3 Tuning the properties of POPs for CO ₂ separation	13
1.3.1 Textural properties	13
1.3.2 Chemical functionality.....	15

1.4 Dissertation Problem.....	19
References.....	24

Chapter 2- A dynamic gas mixture breakthrough instrument that complements current evaluation methods of porous materials for CO₂ separation and capture

2.1 Introduction	28
2.2 Heat of adsorption calculations using the virial equation.....	29
2.3 Selectivity calculations	29
2.4 Sorbent evaluation criteria	32
2.5 Column breakthrough evaluation of hetero-atom doped porous carbons of flue gas mixture separation	32
2.5.1 Description column breakthrough experiment setup.....	35
2.5.2 Experimental section.....	35
2.5.3 Results and Discussion	36
2.6 Conclusion	37
References.....	40

Chapter 3- Evaluation of Newly Synthesized Porous Benzimidazole Linked Polymers for CO₂ Separation

3.1 Introduction.....	42
3.2 Experimental section.....	43
3.2.1 General techniques and materials	43
3.2.2 Synthesis of Tetra(4-bromophenyl)ethylene (TBE)	44
3.2.3 Synthesis of Tetra(4-formylphenyl)ethylene (TFE)	44

3.2.4 Synthesis of 4,4',5,5'-Tetrabromo-9,9'-spirobi[fluorine] (TSF)	45
3.2.6 Synthesis of 9,9'-spirobi[fluorine]-4,4',5,5'-tetracarbaldehyde (SFTA).....	45
3.2.6 Synthesis of BILP-30.....	46
3.1.7 Synthesis of BILP-31	46
3.3 Results and Discussion	49
3.3.1 Synthesis and Characterization	49
3.3.2 Porosity measurements and textural properties	50
3.3.3 CO ₂ uptake studies.....	57
3.3.4 Gas Selectivity Studies: CO ₂ over N ₂ and CH ₄	62
3.3.5 Performance of BILP-30 and BILP-31 in CO ₂ Separation from Flue Gas Using VSA.....	66
3.3.5 Performance of BILP-30 and BILP-31 in CO ₂ Separation from Landfill Gas Using VSA.....	67
3.3.4 Conclusion.....	68
References.....	70

**Chapter 4- Highly Porous Pyrene Driven Azo-Functionalized Porous Nanofibers for CO₂
Capture and Separation Applications**

4.1 Introduction.....	73
4.2 Experimental section.....	74
4.2.1 General techniques and materials	74
4.2.2 Synthesis of 1,3,6,8-tetrabromopyrene	75
4.2.3 Synthesis of 1,3,6,8-tetra(4-aminophenyl)pyrene.....	75
4.3 Synthesis of Azo-Py.....	75

4.3 Results and Discussion	77
4.3.1 Synthesis and characterization of Azo-Py	77
4.3.2 Porosity and textural properties	81
4.3.3 Gas uptake studies.....	81
4.3.4 Selective CO ₂ capture over N ₂ and CH ₄	88
4.3.5 Sorbent evaluation criteria of Azo-Py for CO ₂ separation.....	91
4.4 Conclusion	92
4.4 References.....	94
Chapter 5- Compatible incorporation of benzimidazole linked polymers into Matrimid to yield mixed matrix membranes with superior CO₂/N₂ selectivity	
5.1 Introduction.....	98
5.2 Experimental	99
5.2.1 Materials and instrumentation.....	99
5.2.2 Synthesis of BILP-4.....	100
5.2.3 Synthesis of BILP-101.....	100
5.2.4 Membrane fabrication	100
5.2.5 Gas separation performance testing	101
5.3 Results and Discussion	101
5.3.1 Characterization of BILP-4 and BILP-4/Matrimid [®] MMMs	102
5.3.2 Gas transport properties	108
5.4 Conclusion	112
References.....	113

Chapter 6-Concluding Remarks	116
References.....	118

List of Tables

1.1: Physical parameters of selected gases.....	15
2.1: Sorbent evaluation criteria.....	32
2.2: VSA and PSA conditions for sorbent evaluation at 298 K.....	32
2.3: Textural properties and elemental analysis of PYDCs	33
2.4: CO ₂ uptake, heat of adsorption and selectivity values of PYDCs.....	34
3.1: Textural Properties of BILP-30 and -31.....	57
3.2: Gas up takes, heat of adsorption and selectivity of BILPs.....	66
3.3: VSA evaluation criteria for CO ₂ separation from flue gas.....	67
3.3: VSA evaluation criteria for CO ₂ separation from landfill gas.....	68
4.1: Textural Properties of Azo-Py	84
4.2: Gas uptakes, heat of adsorption and selectivity of Azo-Py	87
4.3: VSA evaluation criteria for CO ₂ separation from flue gas.....	91
4.4: VSA evaluation criteria for CO ₂ separation from landfill gas.....	92
5.1: Textural properties and CO ₂ uptake of BILP-4 and BILP-101.....	102
5.2: CO ₂ permeability and CO ₂ /N ₂ ideal selectivity for Matrimid as well as BILP-4/Matrimid.....	109

List of Schemes

1.1: Structures of some of the commercially relevant polymers	7
1.2: pKa values of common nitrogen functionality groups in POPs and POPs rich in nitrogen moieties	17
3.1: Synthetic route for BILP-30	47
3.2: Syntheses route for BILP-31	48
3.3: Proposed Mechanism of Imidazole Moiety Formation by the Catalytic Acid Process	49
3.2: Synthesis of DBLP-3, DBLP-4, and DBLP-5	68
4.1: Synthetic route for the preparation of Azo-Py.....	76
4.2: Proposed mechanism of Azo bond formation by the catalytic acid process	78

List of Figures

1.1: Diagrammatic representation of the life-cycle chain of fossil fuel use	2
1.2: Location of membrane in CO ₂ separation systems.....	9
1.3: Structures of some common MOFs.....	12
2.1: Schematic representation of the dynamic gas breakthrough setup.....	35
2.2: Dynamic gas breakthrough curves for PYDCs: 550-1 and 550-2.....	38
2.3: Dynamic gas breakthrough curves for PYDCs: 550-3 and 600-2.....	39
3.2: Thermogravimetric analysis of BILP-30 and BILP-31	51
3.3: Powder X-ray diffraction of BILP-30 and BILP-31.....	51
3.4: Scanning electron microscopy (SEM) images of BILPs	52
3.5: N ₂ isotherms of BILP-30 and BILP-31 at 77 K.....	53
3.6: BET plot of BILP-30 and BILP-31 from N ₂ isotherms at 77 K.....	54
3.7: Pore size distribution of BILP-30 and BILP-31 from N ₂ isotherms at 77 K.....	55
3.8: Pore size distribution of BILP-30 and BILP-31 from CO ₂ isotherms at 273 K.....	56
4.2: Thermogravimetric analysis of Azo-Py.....	79
4.3: Powder X-ray diffraction patterns of Azo-Py.....	80
4.4: Scanning electron microscopy (SEM) image of Azo-Py.....	80
4.5: N ₂ isotherm of Azo-Py at 77 K.....	82
4.6: BET plot of Azo-Py from N ₂ isotherm at 77 K.....	82
4.7: Pore size distribution of Azo-Py from N ₂ isotherms at 77 K	83
4.8: Pore size distribution of Azo-Py from CO ₂ isotherms at 273 K.....	83
4.9: CO ₂ , CH ₄ and N ₂ uptake isotherms of Azo-Py.....	85
4.10: Azo-Py isosteric heat of adsorption.....	86

4.11: IAST selectivity of Azo-Py	89
4.12: IS selectivity of Azo-Py.....	90
5.1: Structures of BILP-4, BILP-101 and Matrimid [®]	99
5.2: N ₂ isotherms of BILP-4 at 77 K and pore size distribution	103
5.3: FT-IR spectra of pristine Matrimid [®] membranes and BILP-4/Matrimid [®] MMMs.....	104
5.4: TGA of pristine Matrimid [®] membranes and BILP-4/Matrimid [®] MMMs.....	104
5.5: SEM images of pristine Matrimid [®] membrane and BILP-4/Matrimid [®] MMMs	105
5.6: Young's Modulus of Matrimid [®] membrane and BILP-4/Matrimid [®] MMMs.....	107
5.7: Tg of pristine Matrimid [®] membrane and BILP-4/Matrimid [®] MMMs	107
5.8: Interaction between benzimidazole moiety of BILPs and Mamtrimid [®]	108
5.9: Gas transport properties of Matrimid-BILP MMMs	111
5.10: performances of Matrimid-BILP MMMs in Robeson Plot 2008.....	111

Abstract

PREPARATION AND EVALUATION TECHNIQUES OF POROUS MATERIALS AND MIXED MATRIX MEMBRANES FOR TARGETED CO₂ SEPARATION APPLICATIONS

By Tsemre Dingel Mesfin Tessema,

A dissertation submitted in partial fulfillment of the requirements for the degree of Doctor of
Philosophy at Virginia Commonwealth University.

Virginia Commonwealth University, 2017

Director: Hani M. El-Kaderi, Associate Professor, Department of Chemistry

The use of porous sorbents for physisorptive capture of CO₂ from gas mixtures has been deemed attractive due to the low energy penalty associated with recycling of such materials. Porous organic polymers (POPs) have emerged as promising candidates with potential in the treatment of pre- and post- fuel combustion processes to separate CO₂ from gas mixtures. Concurrently, significant advances have been made in establishing calculation methods that evaluate the practicality of porous sorbents for targeted gas separation applications. However, these methods rely on single gas adsorption isotherms without accounting for the dynamic gas mixtures encountered in real-life applications. To this end, the design and application of a dynamic gas mixture breakthrough apparatus to assess the CO₂ separation performance of a new class of heteroatom (N and O) doped porous carbons derived from a Pyrazole precursor from flue gas mixtures is presented.

Here in, two new benzimidazole linked polymers (BILPs) have been designed and synthesized. These polymers display high surface while their imidazole functionality and microporous nature resulted in high CO₂ uptakes and isosteric heat of adsorption (Q_{st}). BILP-30 displayed very good selectivity for CO₂ in flue gas while BILP-31 was superior in CO₂ separation from landfill gas mixtures at 298 K and 1 bar. Additionally, a new POP incorporating a highly conjugated pyrene core into a polymer framework linked by azo-bonds is presented. Azo-Py displays a nanofibrous morphology induced by the π - π stacking of the electron rich pyrene core. Due to its high surface area and microporous nature, Azo-Py displays impressive CO₂ uptakes at 298 K and 1 bar. Evaluation of the *S* value for CO₂ separation of Azo-Py revealed competitive values for flue gas and landfill gas at 298 K and 1 bar.

Finally, a highly cross-linked benzimidazole linked polymer, BILP-4, was successfully incorporated into Matrimid[®] polymer to form a series of new mixed matrix membranes. The surface functionality of BILP-4 was exploited to enhance the interaction with Matrimid[®] polymer matrix to produce robust MMMs which displayed significantly improved CO₂ gas permeabilities and ideal selectivities for CO₂/N₂.

Chapter 1

Introduction

1.1 CO₂ emission and need for capture and sequestration

The warming effect of carbon dioxide on the Earth's atmosphere was first discovered as early as the 1800s. Nobel prize winner, Svante Arrhenius, spent several years investigating the effects of increasing and decreasing levels of gases particularly carbondioxide on the heat budget of the Earth. He came to the conclusion that the average global temperature would rise as a result of anthropogenic emissions.¹ In agreement with Arrhenius' prediction, the atmospheric CO₂ concentration has risen from 280 ppm to 401 ppm from preindustrial times until 2015.² Greenhouse gases like CO₂ have the ability to absorb solar heat which contributes to the global warming problem.¹ The domino effect of this phenomenon as translated in the melting of glacial ice, rising sea levels, and unpredictable weather patterns which have adverse effects on many nations whose economy is driven by the agriculture sector.^{3,4}

Anthropogenic CO₂ emission is predominantly encountered in gas mixtures of exhausts of fossil-fuel powered plants (flue gas) and in crude mixtures of methane (CH₄) based energy sources. The composition of flue gas is primarily nitrogen (N₂, > 70%) and CO₂ (10-15%). As a globally ubiquitous source of energy, flue gas accounts for 33-40% of global CO₂ emissions.⁵ This issue is of paramount environmental concern and in terms of this area of research, it highlights the need for the development of systems that can facilitate carbon capture and sequestration (CCS) in an efficient manner. The CCS involves threes steps: pure CO₂ from from the combustion of fossil fuels are isolated, the CO₂ is allowed to condense at high pressure and transferred to a storage site and finally the liquid CO₂ is deposited about 800 m below the earth surface (Figure. 1.1).⁶ This need for technologies that can have potential applications in CO₂

separation is further cemented by the fact that as of 2012, fossil fuels accounted for about 87% of the world's energy consumption.⁷ As such, the use of alternative and cleaner sources of energy is highly beneficial to our environment. CH₄-based energy sources present an attractive alternative in mitigating the emission of greenhouse gas. This is due to their significantly lower CO₂ emission per unit of energy compared to their fossil fuel counterparts. Natural gas, composed of CH₄ (80-95%) and CO₂ (5-10%) along with small amounts of other impurities, is currently a primary source of CH₄.⁸ Another source of CH₄ is municipal or industrial landfill gas, which is composed of CH₄ (40-60%) and CO₂ (40-60%).⁹ The removal of impurities (predominantly CO₂) in natural and landfill gas is a *sine qua non* measure for use of CH₄ as a source of relatively clean energy. To this end, exploring means for the selective capture of CO₂ is vital for enhancing the energy density as well as prevention of acidic CO₂ corrosion of pipelines and fuel tanks.⁹

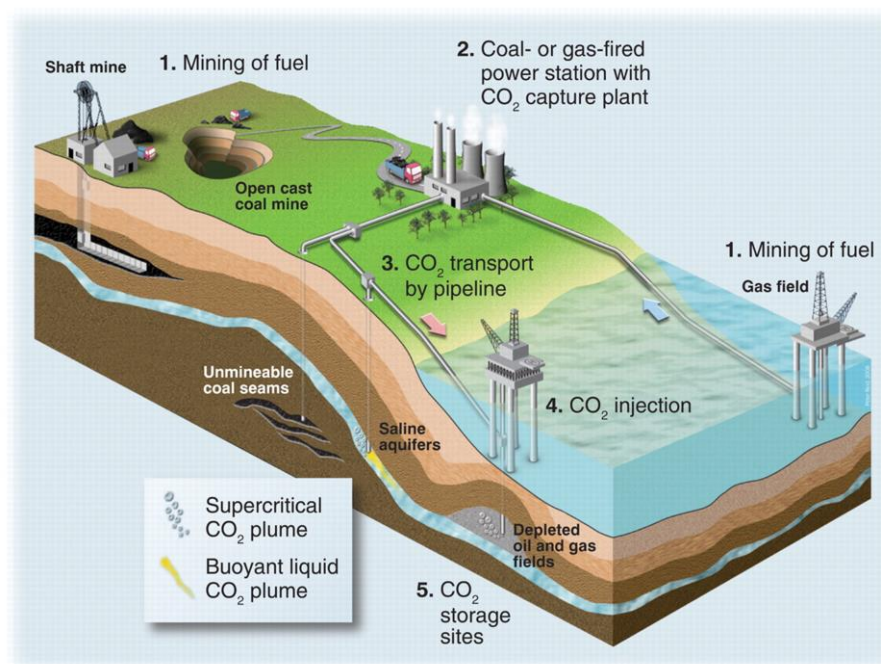


Figure 1.1 Diagrammatic representation of the life-cycle chain of fossil fuel use⁶

1.2 Processes for CO₂ separations

The CO₂ problem is one that has been recognized and seen efforts aimed at minimizing emissions both in national and global arenas. However, even with these considerations, billions of tons are released annually.¹⁰ CO₂ capture from the main sources of emissions in the form of industrial sources such as fossil-fuel power plants, cement plants, oil refineries, and steel industries is crucial in significantly reducing anthropogenic CO₂ emission. In these settings three approaches have been implemented to address this issue: pre-combustion, capture during combustion and post-combustion capture methods.¹¹ Pre-combustion treatment is mainly applied in natural gas or syngas (CO and H₂) fuel sources. Various approaches are currently available to yield the appropriate feed gas for energy generation including steam reforming and gasification of pulverized coal using O₂. A reaction between CO and H₂O yields H₂ and CO₂. The CO₂ can be removed with relative ease as it is present in large enough concentrations (15-60%).¹¹ Capture during combustion is a process that involves the use of pure oxygen for the combustion of fuels a process commonly referred to as oxy-fuel combustion. The advantages of this process are the reduced volume of exhaust generated, along with high concentration of CO₂ and minimal impurities in the exhaust which make post combustion CO₂ efficient and facile. However, the process of purifying air to obtain O₂ makes oxy-fuel combustion a challenging approach.¹¹ Post-combustion CO₂ capture from flue gas exhaust is perhaps the most abundantly used technology. It has a few drawbacks such as the need to desulfurize the flue gas, presence of impurities like SO₂ and NO_x, and the low concentration of CO₂. However, it is still favored as there are no modifications of existing combustion facilities required for this method. Four major processes have been implemented in this type of purification (Figure 1.2) and they will be discussed in the following sections

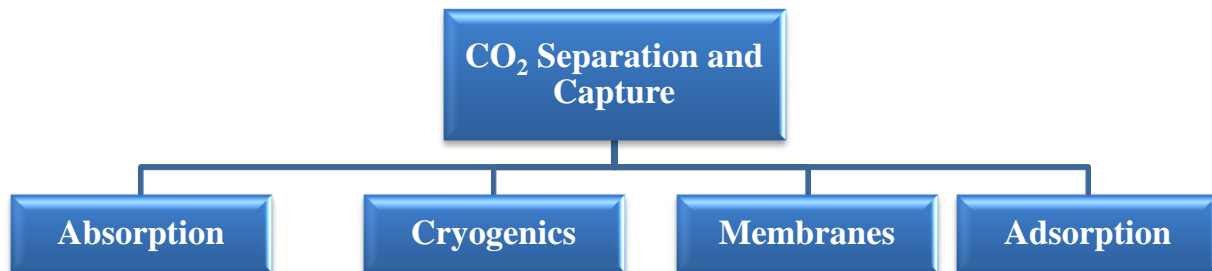


Figure 1.2. The main CO₂ separation and capture processes¹

1.2.1 Absorption

The absorption process for post-combustion CO₂ separation is perhaps the most widely used technique. Here the absorbents liquid amine solutions including monoethanolamine (MEA), diethanolamine (DEA) and methyldiethanolamine (MDEA). These solutions have been found to be highly effective in their capture of CO₂ hence their widespread application. However, they suffer from some major drawbacks including the corrosive nature of liquid amines. Additionally, a significant loss of amine is encountered from operation over time and more importantly there is a significant amount of energy required to regenerate absorbent solutions.

1.2.2 Cryogenic distillation

Cryogenic distillation is a purely physical process that utilizes condensation of gases to the liquid phase at very low temperature.¹² This process is carried out in facilities with well thought out designs and hence separations occur with high throughput.¹³ A sequence of compression, refrigeration, and separation steps are applied to separate the gas mixtures. Liquid CO₂ produced at a low pressure can easily be pumped for storage as opposed to compressing gas fractions which requires a substantial amount of energy.^{12,14} Additionally, the absence of

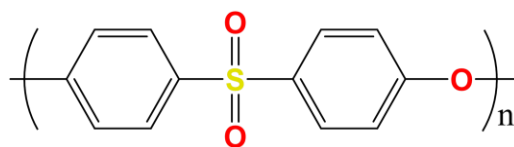
chemical agents in this purification method means there is no secondary pollution involved. However there are some challenges that are encountered with cryogenic distillations. Other components such as H₂, N₂, O₂, CH₄ etc have a lowering boiling point relative to CO₂. This leads to a drastic depreciation of the phase transition temperature of CO₂ leading a higher energy cost for refrigeration. Moreover, this can lead to CO₂ frost formation which can jeopardize the facility's safety.¹⁵

1.2.3 Membranes

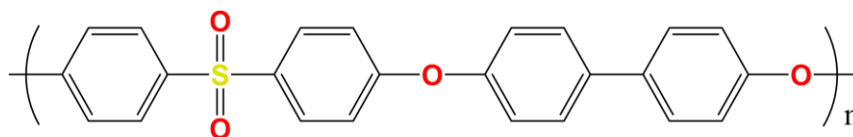
In recent decades, polymer membranes have risen in prominence as practical alternatives for industrial gas separation processes. As such numerous classes of membranes have come into play with the need to enhance the efficiency of such processes. Presented in Scheme 1.1 are the structures of some of the commercially relevant polymer membranes. One of such classes of membranes are polysulfones which are composed of repeating units of diphenylene sulfones.¹⁶ Polysulfones possess some desirable characteristics such as high glass transition temperatures (T_g), good mechanical strength, dimensional stability and heat deflection temperature.¹⁶ These are induced by the phenylene rings which result in a rigid backbone, limited molecular rotation and π - π interaction between adjacent molecules. Poly(phenylene oxides) are another class of polymers that have been deployed as membranes. Poly(2,6-dimethyl-1,4-phenylene oxides) (PPO) is the first of such polymers to be commercialized. PPO serves as a high-performance engineering thermoplastic possessing desirable mechanical characteristics and thermo-oxidative stability due to limited rotation and electronic resonance rotation induced by its aromatic ether bond.¹⁷ Aromatic polyamides more commonly known as aramids are another family of polymers that found commercial use as membranes. These are produced by the polymerization reactions between aromatic diacid chlorides and aromatic diamines. Two of the most common aramids

include poly(p-phenylene terephthalamide) (i.e., Kevlar[®]) and poly(m-phenylene isophthalamide) (i.e., Nomex[®]).¹⁸ Polyester carbonates which are copolymers possessing ester and carbonate linkages make up another family of membrane polymers. Polyester carbonates like tetrabromo bisphenol A polycarbonate (TB-BisA-PC) are synthesized by the reaction of tetrabromobisphenol A with a dicarboxylic acid.¹⁹

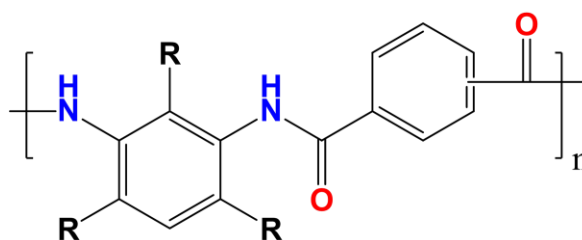
Polyimide based polymer membranes are widely employed in several gas separation applications due to their high gas permeability and selectivity as well as their attractive physical properties. Matrimid is one of such commercial polyimides prepared from the polycondensation reaction between 3,3'-4,4'-benzophenone tetracarboxylic dianhydride (BTDA) and diaminophenylindane (DAPI). The DAPI monomer (5(6)-amino-1-(4-aminophenyl)-1,3,3-trimethylindane) contains an isomeric phenyl indane leading to a mixture of 6-amino and 5-amino isomers. Its isomeric nature along with the bent phenyl indane ring bearing four out of plane bulky groups by way of a three methyl and one phenyl group stiffen the polymer backbone and minimize efficient chain packing.²⁰ These structural details are manifested in Matrimid[®]'s solubility in common organic solvents, impressive mechanical strength and high T_g upon casting.^{20,21} All of which are important as solution processability and durability under harsh working conditions are crucial properties of polymer membranes in gas separation applications.



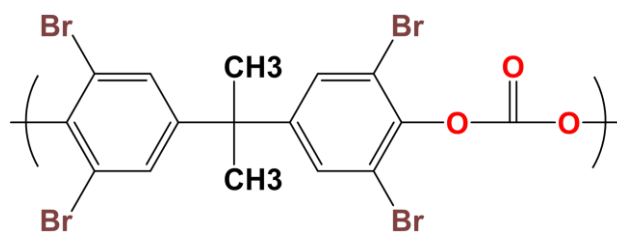
Polysulfone, Victrex[®] PES, Ultrason[®] E¹⁶



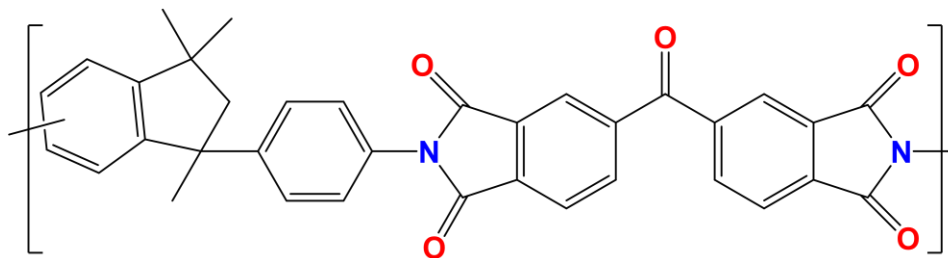
Udel[®], Ultrason[®] S¹⁶



General structure of aramids¹⁸



Polyestercarbonate, tetrabromo bisphenol A polycarbonate (TB-BisA-PC)¹⁹



Chemical structure of Matrimid[®] polyimide

Scheme 1.1. Structures of some of the commercially relevant polymer²⁰

Membranes have been industrially used in post-combustion flue gas CO₂ separation as they are suitable for installation on stationary power plants. In such plants, the membranes are housed downstream of the combustion units (Figure 1.2) to allow selective CO₂ separation over N₂ before storage. For single-stage membrane configuration a high CO₂/N₂ selectivity of about 100 has been set as the benchmark to rival processes like amine solution absorptions due to the low concentration levels of CO₂ as those found in flue gas.²² However, this can be addressed by installing multi-stage membrane configurations. For example Polaris™ membranes with a CO₂/N₂ selectivity of 50 have been configured into a dual-stage system by introducing a slight feed compression, partial permeate vacuum and a sweep operation which yielded a system that can compete with current technologies.²³

For pre-combustion carbon capture, the use of membranes for CO₂ separation faces some serious challenges. In this setting, high pressure CO₂ is separated from syn gas (CO and H₂ mixtures) before the combustion process (Figure 1.2). In terms of gas composition, pre-combustion carbon capture is favorable for CO₂ separation: 40% CO₂, 56% H₂ and parts of CO, CH₄, Ar and H₂S. However, the extremely high temperatures reaching 700 °C needed for reforming reactions make the plausibility of effectively sieving CO₂ difficult given most polymers are not stable at such temperatures. However, advancements in the preparation of H₂ selective membranes that are stable at relatively high temperatures have been reported. Polybenzimidazole membranes which have displayed promising performance in a plethora of applications have been tested at operation temperatures as high 200 °C.

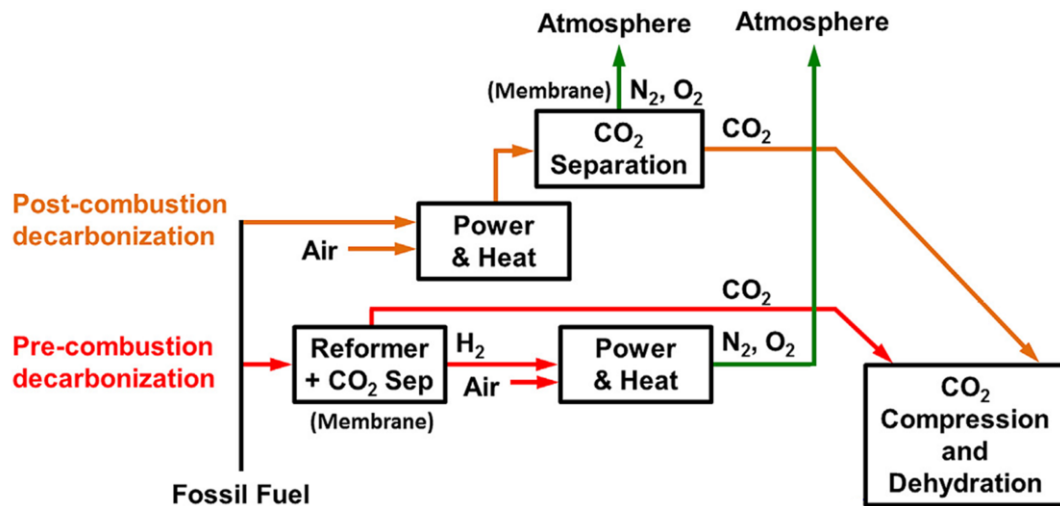


Figure 1.2 Location of membrane in CO₂ separation systems²³

1.2.4 Adsorption

Adsorption processes in CO₂ capture involve the use of solid sorbents in packed beds or in fluidic adsorbents. This method is advantageous to the currently used absorption processes in that the regeneration of materials does not have a huge energy penalty. In fact, one of the properties to consider in designing such systems is the preparation of materials that have an optimum compromise between the binding energy of CO₂ to the adsorbent and low heat of regeneration. Adsorption processes can be classified into two forms: chemisorption and physisorption. Chemisorption involves a chemical reaction between the adsorbate and adsorbent components.²⁴ This process generally results in a high heat of adsorption and requires a significant amount of energy for adsorbent regeneration. Meanwhile, physisorption is a process where adsorbate particles bind to adsorbents by weak forces such as H-bonding and Van der Waal's forces. As such, the physisorption process involves a weaker mode of interaction between adsorbate and adsorbent and offers a process for the easy recovery of sorbents.

Porous solid sorbents made of inorganic, inorganic-organic hybrids, and purely organic materials offer a class of adsorbent materials with properties suitable for CO₂ capture and separation. The porosity of such materials can be classified into three groups depending on the average diameter of their pores: microporous (< 2 nm), mesoporous (2-50 nm) and macroporous (> 50 nm).²⁵ Another characteristic of such materials is the degree of order within the structure of the materials. Porous solid sorbents exist in crystalline, semi-crystalline and amorphous forms. To date a vast number of porous materials differing in chemical nature, textural properties and physical and chemical stability which are all influential in their performance in selective CO₂ capture have been reported. These types of materials include zeolites, activated carbons, metal organic frameworks (MOFs) and porous organic polymers (POPs).

1.2.4.1. Zeolites

Zeolites are porous aluminosilicate solid sorbents that have been used in various industrial applications including CO₂ capture. Zeolites have been reported to display a very high uptake for CO₂ at dry flue gas stream conditions. For example, zeolite Ca-A was reported to have a CO₂ uptake of 3.72 mmol g⁻¹ with a CO₂/N₂ selectivity of 250 at such conditions.²⁶ These values are impressive and amongst the highest reported to date. However, zeolites generally are extremely hydrophilic which leads to H₂O saturation of CO₂ binding sites. In real life, flue gas stream conditions where there is water vapor present; this will prove detrimental to CO₂ capture. Additionally, zeolites have a high binding affinity to CO₂, 58 kJ mol⁻¹ for zeolite Ca-A, as well as H₂O.²⁶ The need to dry the flu gas stream and high temperatures to regenerate the materials and hence high operational costs complicate the wide spread use of zeolites for CO₂ capture.²⁷

1.2.4.2. Activated carbons

Activated carbons are another class of porous sorbents that have been implemented in CO₂ separation applications. Activated carbons are obtained from the physical or chemical activation of carbon rich precursors. In physical activation, the precursor is carbonized at high temperatures, 600-900 °C, under a N₂ or Ar atmosphere followed by a gasification step using air, CO₂, CO etc.²⁸ Meanwhile, in chemical activation, the carbon precursor is mixed with an activation agent before carbonization under an inert atmosphere. Common activation agents that have been used include ZnCl₂,²⁹ H₃PO₄,³⁰ NaOH³⁰ and KOH.³¹ Activated carbons present numerous desirable features for CO₂ capture processes including physico-chemical stability, tunable textural properties, high surface areas, ease of regeneration and cost effective preparation from abundantly available precursors.³² Moreover, studies have shown that employing certain chemical activation agents has led to higher levels of hetero-atom doping (N, O, P, S) in activated carbons which improve CO₂ uptakes and CO₂/N₂ selectivities by inducing CO₂-philic sites on the carbons' pore walls.³¹

1.2.4.3. Metal Organic Frameworks (MOFs)

Metal organic frameworks, MOFs, are porous networks of metal ions or clusters coordinated to organic ligands (Figure 1.3). Research in this class of materials has seen a tremendous growth due to the ability to effectively tune the structure and porosity of MOFs to explore their viability in CO₂ capture. For instance, the pore size of porous sorbents plays a crucial role in its ability to selective capture a specific gas from a mixture. This is due to the difference in the kinetic diameter of various gases (CO₂ = 3.3 Å, CH₄ = 3.8 Å and N₂ = 3.64 Å). As such, the targeted design of MOFs can be implemented to induce selective CO₂ over N₂ or CH₄.³³ The activation of open metal sites that are occupied by guest molecules MOFs has also

been reported to enhance CO₂ capture.³³ Perhaps, the most explored approach for enhancing CO₂ capture and selectivity in MOFs is the incorporation of polar functional groups in the pore structures. The vast array of synthetic chemistry methods available has expanded the limits of improving selective CO₂ capture by using direct assembly and post-synthesis modification methods.³⁴ For instance, exploiting the amino and pyrimidine groups of an adenine based monomer; bio-MOF-11 has been reported to exhibit high CO₂ uptake and selectivities as well high heat of adsorption (45 kJ mol⁻¹).³⁴ Following a post-synthesis modification approach, Farrah *et. al.* have demonstrated a significant enhancement in CO₂/N₂ and CO₂/CH₄ selectivities by incorporating a *p*-(CF₃)NC₅H₄ ligand into a 4',4'',4'''-benzene-1,2,4,5-tetrayltetrabenzonic acid and Zn(II) based MOF.³⁵

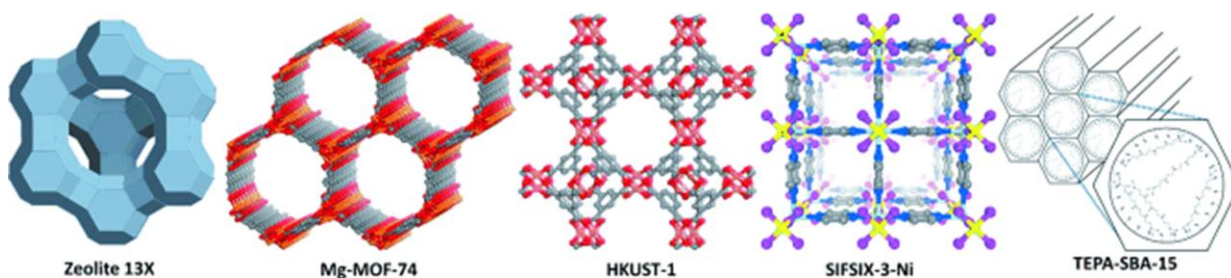


Figure 1.3. Structures of some common MOFs⁴⁷

1.2.4.4. Porous organic polymers (POPs)

Porous organic polymers are another class of porous materials that have garnered a broad range of research efforts for applications such as gas storage and separation, catalysis, chemical sensing and optoelectronics. POPs consist of light weight elements that are linked by covalent bonds and their synthesis often considers the strategic selection of building blocks to target desired properties for the targeted application. This has been aided by the ability to exploit broad

synthetic methods available to prepare polymers using reactions such as: Suzuki coupling,³⁶ Friedel-Crafts alkylation,³⁷ Sonogashira reaction,³⁸ Yamamoto reaction,³⁹ imine formation⁴⁰ etc. Generally, POPs display a high level of microporosity and ultra-microporosity (pore sizes < 7 Å) due to the use of rigid and star shape building blocks and also interpenetration of pores within the polymer frameworks. This factor is advantageous for CO₂ capture and separation applications. Various classes of POPs have been reported to date including but not limited to: porous polymer networks (PPNs),³⁹ polymer organic networks (PONs),³⁶ porous organic frameworks (POFs),⁴¹ crystalline organic frameworks (COFs),⁴² conjugated microporous polymers (CMPs),³⁸ hyper-cross-linked polymers (HCPs),³⁷ and polymers of intrinsic microporosity (PIMs).⁴³ As sorbents for CO₂ separation, POPs prove to be promising candidates due to their low density, high thermal and chemical stability, high porosity and tunable pore size and functionality. Most POPs are amorphous in nature with the exception of COFs which are polymerized using reversible reactions and display partial crystallinity.⁴²

1.3. Tuning the properties of POPs for CO₂ separation

1.3.1. Textural properties

As in any porous material, one of the most prominent features of POPs is their surface area due to its direct correlation with their CO₂ capacity. The surface area along with pore size distribution is generally deduced from N₂ (at 77 K) or Ar (77 or 87 K) adsorption isotherms at cryogenic temperatures. The isotherms are collected in pressure ranges of 10⁻⁶ - 1 bar. The extremely low starting pressure, 10⁻⁶ bar, and cryogenic temperatures provide a clear depiction of the pore volume, pore size and surface area. Here, minimal amounts of adsorbate gas are sequentially dosed on to the polymer surface at very low kinetic energy (induced by the cryogenic temperatures). Consequently, specific volumes of adsorbed gases as a function of

relative pressure (P/P_0) are obtained. From this raw isotherm data the surface area can be determined using Langmuir model or Brunauer-Emmett-Teller (BET) model.⁴⁴ The Langmuir model follows four assumptions which make it inferior to the BET model. These assumptions include: a single monolayer formation at maximum loading; uniform adsorbent surface; lack of interaction between adsorbed molecules; a single adsorption mechanism. Therefore, the BET model, an extension of Langmuir model, assuming the formation of multi-layers is prevalently employed for surface area in POPs and porous materials alike. Pore sizes are also deduced from N_2 or Ar isotherms at cryogenic temperatures. As gas adsorption is a multilayer process, the trends in the isotherms generated are a reflection of the type of pores present in the adsorbent. Furthermore, models such as Non-Local Density Functional Theory (NLDFT) and Barrett-Joyner-Halend can be used to fit experimental isotherms to generate pore size distribution curves.

Given the impact of surface area on CO_2 uptake, studies have reported the design and synthesis of POPs with impressive porosity levels. This is critical as a high surface area POP can be a candidate for high pressure CO_2 storage. Thus researchers have targeted high surface area POPs. PPNs, a class of POPs synthesized by Yamamoto coupling of tetrahedral(4-bromophenyl)X (where X = adamantane, silicon, germanium) have achieved extremely high surface areas up to $6461 \text{ m}^2 \text{ g}^{-1}$ (BET). This resulted in exceptional CO_2 storage capacity of 48.2 mmol g^{-1} at 50 bar and 295 K observed for PPN-4. However, such extremely high surface areas do not necessarily lead to a sorbent with viable application in CO_2 separation. For instance, PAF-1 from which PPNs were derived, display a surface area of $5600 \text{ m}^2 \text{ g}^{-1}$. At 40 bar and 298 K it has very high CO_2 uptake of 29.5 mmol g^{-1} . However, it only adsorbs 2.05 mmol g^{-1} of CO_2 at 1 bar and 273 K.³⁹ This is due to the lack of chemical functionality on the pore walls of PAF-1 that

induce strong interaction sites for CO₂ adsorption. The pore size distribution of sorbents is also a feature that plays a critical role in CO₂ capture. The tailoring of pore sizes in POPs to be narrowly distributed in the ultramicro-pore range is one approach to improve CO₂ (kinetic diameter =3.3 Å) selectivity. This approach can separate CO₂ from other gases by a mechanism known as a molecular sieving effect where the kinetic diameters of undesired gases are larger than the pore size of the sorbent. This was recently demonstrated in the ultra-microporous BILP-10 synthesized by a metal free acid catalyzed condensation reaction to achieve high IAST selectivity of 70 at 298 K.⁴⁵

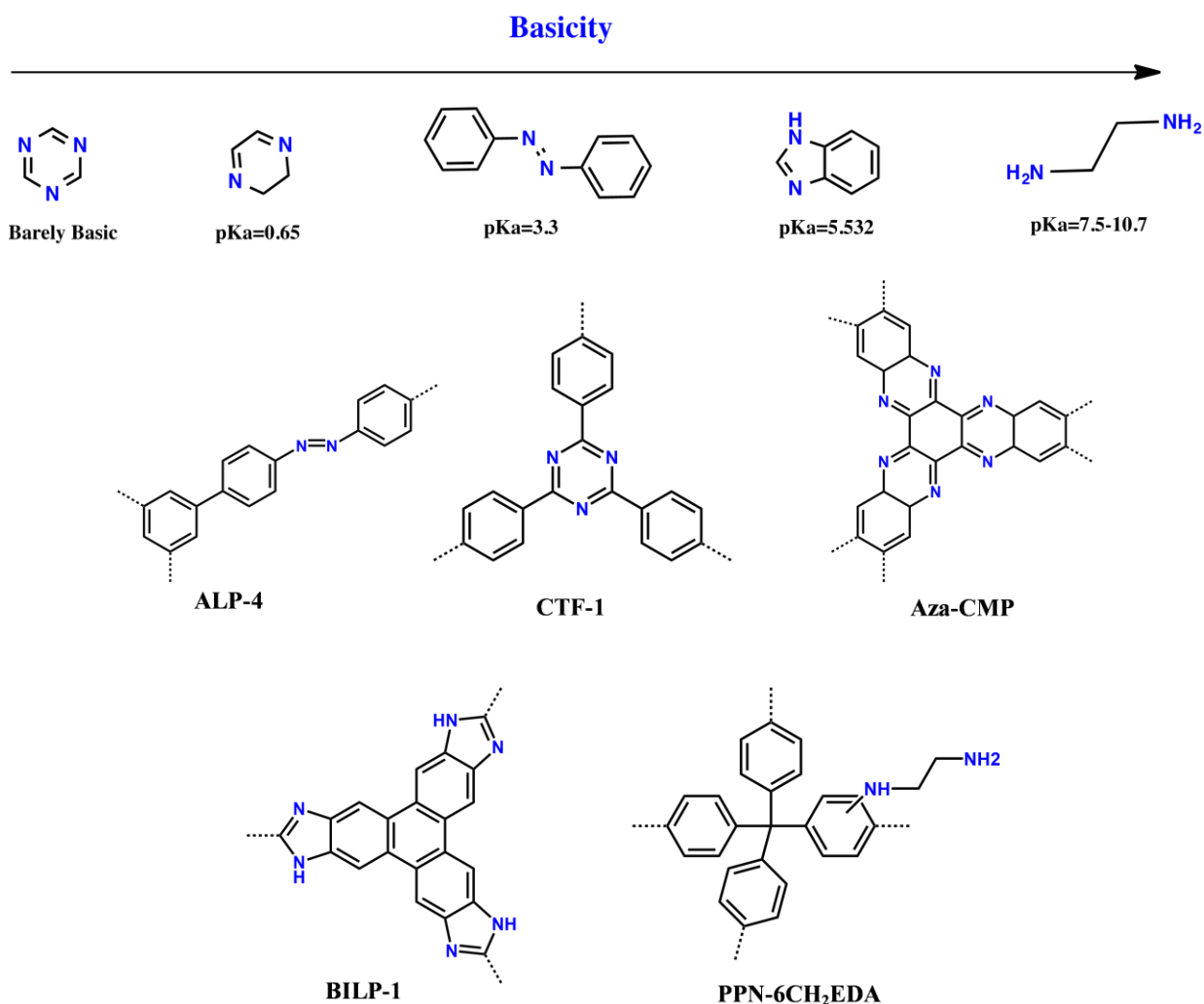
1.3.2. Chemical functionality

The polarizable nature of CO₂ molecules due to their high quadrupole moment (Table 1.1) relative to other gases offers an avenue that can be exploited by scientists to improve CO₂ interaction with POP pore walls. In turn, this can increase the CO₂ uptake capacity and selectivity of POPs. Many research efforts have thus explored incorporating heteroatom moieties such as nitrogens, oxygens, sulphur and phosphorus in POPs to attain higher CO₂ capacity and selectivity. Particularly, both experimental and theoretical studies have demonstrated that nitrogen lone pair electrons in POPs with nitrogen moieties in their skeleton act as Lewis basic sites⁴⁶ (Scheme 1.2). This results in a dipole-quadrupole interaction between polymer surface and CO₂ molecules.

Table 1.1 Physical parameters of selected gases⁴⁷

Gas	Kinetic Diameter (Å)	Polarizability ($\times 10^{-25}$ cm ³)	Quadrupole Moment ($\times 10^{-26}$ esu cm ²)
He	2.55	2.00	0.00
Ar	3.54	16.40	0.00
N ₂	3.64	17.40	1.50
CH ₄	3.82	25.90	0.00
CO ₂	3.30	29.10	4.30

A plethora of reports have been published on POPs with nitrogen functionality. The preparation of covalent triazine frameworks (CTFs) synthesized by trimerization reactions of cyano group bearing monomers with ZnCl_2 acting both as a solvent and Lewis acidic catalyst at high temperatures have been reported.⁴⁸ The nitrogen rich triazine groups in CTFs lead to high CO_2 uptakes reaching 4.28 mmol g^{-1} at 273 K and 1 bar.⁴⁸ Carbazole based POPs prepared by the carbazole-based oxidative coupling polymerization reactions also yield a class of POPs identified as CPOP. CPOP-1 has attractive textural properties with a surface area of $2220 \text{ m}^2 \text{ g}^{-1}$ and pore size centered at 0.62 nm.⁴⁹ These properties render CPOP-1 as a viable POP for CO_2/CH_4 separations with a selectivity of 33 which is one of the highest for POPs reported to date. Recently, benzimidazole linked polymers (BILPs) bearing nitrogen rich imidazole groups have been developed by the El-Kaderi group. BILPs are synthesized by the acid catalyzed polymerization reaction between aryl aldehydes and diamines.⁵⁰ BILPs display high porosity reaching surface areas of up to $1458 \text{ m}^2 \text{ g}^{-1}$.⁵¹ BILP-101 a POP rich in ultramicropores also shows great CO_2/N_2 selectivity of 70 at 298 K.⁴⁵ POPs possessing azo-bonds (nitrogen to nitrogen double bonds) have also been explored for their CO_2 capture and separation feasibility. Azo-linked polymers (ALPs) synthesized by the CuBr catalyzed homo-coupling of aryl primary amines have also been reported. ALP-1 displayed high surface areas of $1235 \text{ m}^2 \text{ g}^{-1}$ and CO_2 uptake of $5.37 \text{ m}^2 \text{ g}^{-1}$.



Scheme 1.2 pKa values of common nitrogen functionality groups in POPs and POPs rich in nitrogen moieties.^{38,39,48,54,55}

An alternative approach for enhancing the performance of POPs for CO₂ separation and storage is the incorporation of CO₂-philic amine moieties via post-synthetic modifications. The nano-porous organic frameworks, NPOF-4, prepared by the cyclotrimerization of acetyl functional groups has been post-synthetically modified by nitration followed by reduction to yield NPOF-4-NO₂ and NPOF-4-NH₂ POPs respectively. This modification showed improved CO₂ uptake from 61.6 to 82.8 mg g⁻¹ at 298K as well as increased CO₂/N₂ selectivity from 49 to

81.⁵² A modified study employed a controlled nitration step in the post-synthetic modification of NPOF-1 to yield NPOF-1-NO₂ which was further reduced to aniline-like amine functionalized NPOF-1-NH₂. This has resulted in POPs with highly improved working capacity for CO₂ in flue gas separation under vacuum swing adsorption setting.⁵³

1.4 Dissertation Problem

Over the years, an extensive amount of effort has been implemented in designing and synthesizing POPs for the goal of CO₂ capture and separation pressure, temperature and vacuum swing adsorption mechanisms. For the purpose of gas capture, a high binding affinity between the sorbent framework and the desired gas is suitable. As such, POPs synthesis is generally tailored towards targeting materials possessing high surface areas and enhanced gas-binding affinity. However, the inherent open structures present in materials of high surface area desired for high-pressure gas storage applications generally induce poor selectivity and heat of adsorption (Q_{st}) under ambient conditions (1 bar and 298K). Therefore, synthesis of porous adsorbents for such applications requires using an approach that yields materials possessing unique hybrid properties. POPs synthesized for the application of gas capture and separation particularly CO₂ have been found to be effective when their surface is modified with polar groups. This results from an increase in their CO₂ binding energy which enhances their CO₂ uptake as well as selectivity over N₂ and CH₄. The principle behind the stronger interaction of CO₂ with the polymer framework is due to dipole-quadrupole interactions and/or hydrogen bonding between the polar functional groups and CO₂. Such polar groups have been incorporated into POPs by using nitrogen and oxygen bearing monomers as well as via post synthetic modifications. The introduction of nitrogen motifs in POPs has been accomplished by benzimidazole and nitrogen-nitrogen double bond (azo bond) incorporation into the polymer frameworks. An insight into how a careful consideration of the building blocks used for polymer synthesis in order to tune structural properties has been provided. This complemented with such nitrogen rich functionalities can be used to tap into new POPs that explore the advancement of these materials to address the carbon capture and sequestration problem. Additionally, besides

the fabrication of porous materials that can prove feasible for CO₂ separation applications it is equally important that their evaluation for such applications is as accurate and thorough as possible. There have been impressive and widely accepted computational and analysis methods for deducing the viable performance of porous sorbents for CO₂ separation applications. However, these are based on single gas isotherms rather than dynamic gas mixtures that mimic real life flue gas streams.

This dissertation presents the current calculation methods used to evaluate the porous sorbents for CO₂ separation of flue gas and landfill gas mixtures including: Henry's law, ideal adsorbed solutions theory, and five sorbent evaluation criteria. These methods are complemented by a newly assembled dynamic gas mixture breakthrough setup. The breakthrough setup was used to evaluate a series of pyrazole derived heteroatom doped porous carbons (PYDCs) for flue gas separation applications.

References

- (1) Aaron, D.; Tsouris, C. Separation of CO₂ from Flue Gas: A Review. *Sep. Sci. Technol.* **2005**, *40* (1–3), 321–348.
- (2) Trends in Atmospheric Carbon Dioxide <https://www.esrl.noaa.gov/gmd/ccgg/trends/> (accessed Jul 5, 2017).
- (3) Tuwati, A.; Fan, M.; Russell, A. G. .; Wang, J.; Dacosta, H. F. M. New CO₂ Sorbent Synthesized with Nanoporous TiO(OH)₂ and K₂CO₃. *Energy and Fuels* **2013**, *27* (12), 7628–7636.
- (4) He, L.; Fan, M.; Dutcher, B.; Cui, S.; Shen, X.; Kong, Y.; Russell, Armistead G.; McCurdy, P. Dynamic Separation of Ultradilute CO₂ with a Nanoporous Amine-Based Sorbent. *Chem. Eng. J. (Amsterdam, Netherlands)* **2012**, *189–190*, 1385–8947.
- (5) Yang, H.; Xu, Z.; Fan, M.; Gupta, R.; Slimane, R. B.; Bland, A. E.; Wright, I. Progress in Carbon Dioxide Separation and Capture: A Review. *J. Environ. Sci.* **2008**, *20* (1), 14–27.
- (6) Haszeldine, R. S. Carbon Capture and Storage: How Green Can Black Be? *Science (80-.)*. **2009**, *325*, 1647–1652.
- (7) J, T.; Monastersky, R. The Global Energy Challenge: Awash with Carbon. *Nature* **2012**, *491*, 654–655.
- (8) Naber, J. D.; Siebers, D. L. Effects of Natural Gas Composition on Ignition Delay under Diesel Conditions. *Combust. Flame* **1994**, *99*, 192–200.
- (9) Bae, Y. S.; Mulfort, K. L.; Frost, H.; Ryan, P.; Punnathanam, S.; Broadbelt, L. J.; Hupp, J. T.; Snurr, R. Q. Separation of CO₂ from CH₄ Using Mixed-Ligand Metal-Organic Frameworks. *Langmuir* **2008**, *24* (16), 8592–8598.

- (10) Metz, B. .; Davidson, O. .; de Coninck, H. C. .; Loos, M. .; Meyer, L. A. *Special Report on Carbon Dioxide Capture and Storage. Prepared by Working Group III of the Intergovernmental Panel on Climate Change*; Cambridge, U.K., and New York, 2005.
- (11) Sanz-Pérez, E. S.; Murdock, C. R.; Didas, S. A.; Jones, C. W. Direct Capture of CO₂ from Ambient Air. *Chem. Rev.* **2016**, *116* (19), 11840–11876.
- (12) Pierce, W. F. .; Riemer, P. .; William, G. O. International Perspectives and the Results of Carbon Dioxide Capture Disposal and Utilisation Studies. *Energy Convers. Manag* **1995**, *36*, 813–818.
- (13) Deng, S. .; Jin, H. .; Cai, R. Novel Cogeneration Power System with LNG Cryogenic Exergy Utilization. *Energy* **2004**, *29*, 497–512.
- (14) Wang, B. Q. Process Mechanism and System Synthesis for CO₂ Capture in IGCC System, 2004.
- (15) Song, C. F. .; Kitamura, Y. .; Li, S. H. Evaluation of Stirling Cooler System for Cryogenic CO₂ Capture. *Appl. Energy* **2012**, *98*, 491–501.
- (16) McGrail, P. T. *Polymer International*. 1996, p 41(2):103-121.
- (17) Aycock, D. . Poly(phenylene Ether). *In Encyclopedia of polymer science and technology*; NY: Interscience Publishers, 1974.
- (18) Ekiner, O. M. .; Vassilatos, G. . Polyaramide Hollow Fibers for H₂/CH₄ Separation. II. Spinning and Properties. *J. Memb. Sci.* **2001**, *186* (1), 71–84.
- (19) Anand, J. N.; Bales, S. E.; Feay, D. C.; Jeanes, T. O. Tetrabromo Bisphenol Based Polyestercarbonate Membranes and Method of Using. Patent 4,840,646, 1989.
- (20) Farr, I. V.; Kratzner, D.; Glass, T. E.; Dunson, D.; Ji, Q.; McGrath, J. E. Synthesis and Characterization of Polyimide Homopolymers Based on 5(6)-Amino-1-(4-Aminophenyl)-

- 1,3,3-Trimethylindane. *J. Polym. Sci. Part A Polym. Chem.* **2000**, 38 (15), 2840–2854.
- (21) Farr, I. V.; Glass, T. E.; Ji, Q.; McGrath, J. E. Synthesis and Characterization of Diaminophenylindane Based Polyimides via Ester-Acid Solution Imidization. *High Perform. Polym.* **1997**, 9 (3), 345–352.
- (22) Basic Research Needs for Carbon Capture: Beyond 2020, US Department of Energy Basic Energy Sciences Workshop for Carbon Capture; 2010.
- (23) Merkel, T. C.; Lin, H.; Wei, X.; Baker, R. Power Plant Post-Combustion Carbon Dioxide Capture: An Opportunity for Membranes. *J. Memb. Sci.* **2010**, 359, 126–139.
- (24) Gunnarsson, Maria Theliander, H.; Hasani, M.; Hasani, M. Chemisorption of Air CO₂ on Cellulose: An Overlooked Feature of the cellulose/NaOH(aq) Dissolution System. *Cellulose* **2017**, 24 (6), 2427–2436.
- (25) Thommes, M.; Kaneko, K.; Neimark, A. V.; Olivier, J. P.; Rodriguez-Reinoso, F.; Rouquerol, J.; Sing, K. S. W. Physisorption of Gases, with Special Reference to the Evaluation of Surface Area and Pore Size Distribution (IUPAC Technical Report). *Pure Appl. Chem.* **2015**, 87, 1051–1069.
- (26) Bae, T.-H. .; Hudson, M. R. .; Mason, J. A. .; Queen, W. L. .; Dutton, J. J. .; Sumida, K. .; Micklash, K. J. .; Kaye, S. S. .; Brown, C. M. .; Long, J. R. Evaluation of Cation-Exchanged Zeolite Adsorbents for Post-Combustion Carbon Dioxide Capture. *Energy Environ. Sci.* **2013**, 6, 128–138.
- (27) Lin, L.-C.; Berger, A. H. .; Martin, R. L. .; Kim, J.; Joseph, A. Swisher Jariwala, K.; Rycroft, C. H.; Bhowan, A. S.; Deem, M. W.; Haranczyk, Maciej Smit, B. In Silico Screening of Carbon-Capture Materials. *Nat. Mater.* **2012**, 11, 633–641.
- (28) Demiral, H.; Demiral, İ.; Karabacakoğlu, B.; Tümsük, F. Production of Activated Carbon

- from Olive Bagasse by Physical Activation. *Chem. Eng. Res. Des.* **2011**, *89* (2), 206–213.
- (29) Özhan, A.; Ömer, Ş.; Küçük, M. M.; Saka, C. Preparation and Characterization of Activated Carbon from Pine Cone by Microwave-Induced ZnCl₂ Activation and Its Effects on the Adsorption of Methylene Blue. *Cellulose* **2014**, *21* (4), 2457–2467.
- (30) Li, Y.; Zhang, X.; Yang, R.; Li, G.; Hu, C. The Role of H₃PO₄ in the Preparation of Activated Carbon from NaOH-Treated Rice Husk Residue. *RSC Adv.* **2015**, *5*, 32626–32636.
- (31) Ashourirad, B.; Sekizkardes, A. K. ; Altarawneh, S.; El-Kaderi, H. M. Exceptional Gas Adsorption Properties by Nitrogen-Doped Porous Carbons Derived from Benzimidazole-Linked Polymers. *Chem. Mater.* **2015**, *27* (4), 1349–1358.
- (32) White, R. J. .; Budarin, V. .; Luque, R. .; Clark, J. H. .; Macquarrie, D. Tuneable Porous Carbonaceous Materials from Renewable Resources. *Chem. Soc. Rev.* **2009**, *38*, 3401–3418.
- (33) Bae, Y.-S.; Spokoyny, A. M.; Farha, O. K.; Snurr, R. Q.; Hupp, J. T.; Mirkin, C. A. Carborane-Based Metal-Organic Frameworks as Highly Selective Sorbents for CO₂ over Methane. *Chem. Commun.* **2010**, *46*, 3478.
- (34) Bae, Y.-S.; Snurr, R. Q. Development and Evaluation of Porous Materials for Carbon Dioxide Separation and Capture. *Angew. Chemie - Int. Ed.* **2011**, *50* (49), 11586–11596.
- (35) Farha, O. K.; Mulfort, K. L.; Hupp, J. T. An Example of Node-Based Postassembly Elaboration of a Hydrogen-Sorbing, Metal–Organic Framework Material. *Inorg. Chemistry* **2008**, *47*.
- (36) Jeon, H. J.; Choi, J. H.; Lee, Y.; Choi, K. M.; Park, J. H.; Kang, J. K. Highly Selective CO₂-Capturing Polymeric Organic Network Structures. *Adv. Energy Mater.* **2012**, *2* (2),

- 225–228.
- (37) Woodward, R. T. .; Stevens, L. A. .; Dawson, R.; Vijayaraghavan, M.; Hasell, T.; Silverwood, I. P. .; Ewing, A. V. .; Ratvijitvech, T.; Exley, J. D. .; Chong, S. Y. .; et al. Swellable, Water- and Acid-Tolerant Polymer Sponges for Chemoselective Carbon Dioxide Capture. *J. Am. Chem. Soc.* **2014**, *136* (25), 9028–9035.
- (38) Jiang, Jia-Xing.; Su, Fabing; Wood, Colin D.; Campbell, Neil L.; Niu, Hongjun; Dickinson, Calum; Ganin, Alexey Y.; Rosseinsky, Matthew J.; Khimyak, Yaroslav Z.; Cooper, Andrew I.; Trewin, A. Conjugated Microporous Poly(aryleneethynylene) Networks. *Angew. Chemie, Int. Ed.* **2007**, *46* (45), 8574–8578.
- (39) Yuan, D.; Lu, W.; Zhao, D.; Zhou, H.-C. Highly Stable Porous Polymer Networks with Exceptionally High Gas-Uptake Capacities. *Adv. Mater. (Weinheim, Ger.)* **2011**, *23* (32), 3723–3725.
- (40) Islamoglu, T.; Behera, S.; Kahveci, Z.; Tessema, T. D.; Jena, P.; El-Kaderi, H. M. Enhanced Carbon Dioxide Capture from Landfill Gas Using Bifunctionalized Benzimidazole-Linked Polymers. *ACS Appl. Mater. Interfaces* **2016**, *8* (23), 14648–14655.
- (41) Katsoulidis, Alexandros P.; Kanatzidis, M. G. Phloroglucinol Based Microporous Polymeric Organic Frameworks with -OH Functional Groups and High CO₂ Capture Capacity. *Chem. Mater.* **2011**, *23* (7), 1818–1824.
- (42) Rabbani, M. G. .; Sekizkardes, A. .; Kahveci, Z. .; Reich, T. E. .; Ding, R. .; El-Kaderi, H. M. A 2D Mesoporous Imine-Linked Covalent Organic Framework for High Pressure Gas Storage Application. *Chem. Eur. J.* **2012**, *19* (10), 3324–3328.
- (43) Sekizkardes, A. K.; Kusuma, V. A.; Dahe, G.; Roth, E. A.; Hill, L. J.; Marti, A.; Macala,

- M.; Venna, S. R.; Hopkinson, D. Separation of Carbon Dioxide from Flue Gas by Mixed Matrix Membranes Using Dual Phase Microporous Polymeric Constituents. *Chem. Commun.* **2016**, 52 (79), 11768–11771.
- (44) Brunauer, S.; Emmett, P. H. .; Teller, E. Adsorption of Gases in Multimolecular Layers. *J. Am. Chem. Soc.* **1938**, 60 (2), 309–319.
- (45) Sekizkardes, A. K.; Culp, J. T.; Islamoglu, T.; Marti, A.; Hopkinson, D.; Myers, C.; El-Kaderi, H. M.; Nulwala, H. B. An Ultra-Microporous Organic Polymer for High Performance Carbon Dioxide Capture and Separation. *Chem. Commun. (Camb)*. **2015**, 51 (69), 13393–13396.
- (46) Altarawneh, S.; Behera, S.; Jena, P.; El-Kaderi, H. M. New Insights into Carbon Dioxide Interactions with Benzimidazole-Linked Polymers. *Chem. Commun. (Camb)*. **2014**, 50 (27), 3571–3574.
- (47) Sumida, K.; Rogow, D. L.; Mason, J. A.; McDonald, T. M.; Bloch, E. D.; Herm, Z. R.; Bae, T. H.; Long, J. R. Carbon Dioxide Capture in Metal-Organic Frameworks. *Chem Rev.* **2012**, 112 (2), 724–781.
- (48) Hug, S.; Mesch, M. B. .; Oh, H.; Popp, N.; Hirscher, M.; Senker, J.; Lotsch, B. V. A Fluorene Based Covalent Triazine Framework with High CO₂ and H₂ Capture and Storage Capacities. *J. Mater. Chem. A Mater. Energy Sustain.* **2014**, 2 (16), 2050–7496.
- (49) Chen, Q.; Luo, M.; Hammershoej, Peter; Zhou, D.; Han, Y.; Laursen, B. W.; Yan, C.-G.; Han, B.-H. Microporous Polycarbazole with High Specific Surface Area for Gas Storage and Separation. *J. Am. Chem. Soc.* **2012**, 134 (14), 6084–6087.
- (50) Altarawneh, S.; Islamoglu, T.; Sekizkardes, A. K.; El-kaderi, H. M. Effect of Acid-Catalyzed Formation Rates of Benzimidazole-Linked Polymers on Porosity and Selective

- CO₂ Capture from Gas Mixtures. *Environ. Sci. Technol.* **2015**, *49* (7), 4715–4723.
- (51) Islamoglu, T.; Behera, S.; Kahveci, Z.; Tessema, T.-D.; Puru, J.; El-kaderi, H. M. Enhanced Carbon Dioxide Capture from Landfill Gas Using Bifunctionalized Benzimidazole-Linked Polymers. *ACS Appl. Mater. Interfaces* **2016**, *8*, 14648–14655.
- (52) Islamoglu, T.; Rabbani, Mohammad Gulam El-Kaderi, H. M. Impact of Post-Synthesis Modification of Nanoporous Organic Frameworks on Small Gas Uptake and Selective CO₂ Capture. *J. Mater. Chem. A* **2013**, *1*, 10259–10266.
- (53) Islamoglu, T. .; Kim, T. .; Kahveci, Z. .; El-Kadri, O. M. .; El-Kaderi, M. H. Systematic Postsynthetic Modification of Nanoporous Organic Frameworks for Enhanced CO₂ Capture from Flue Gas and Landfill Gas. *J. Phys. Chem. C* **2016**, *120* (5), 2592–2599.
- (54) Arab, P.; Rabbani, M. G.; Sekizkardes, A. K.; Islamoglu, T.; El-kaderi, H. M. Copper(I)-Catalyzed Synthesis of Nanoporous Azo-Linked Polymers: Impact of Textural Properties on Gas Storage and Selective Carbon Dioxide Capture. *Chem. Mater.* **2014**, *26*, 1385–1392.
- (55) Rabbani, M. G.; El-Kaderi, H. M. Synthesis and Characterization of Porous Benzimidazole-Linked Polymers and Their Performance in Small Gas Storage and Selective Uptake. *Chem. Mater.* **2012**, *24* (8), 1511–1517.

Chapter 2

A dynamic gas mixture breakthrough instrument that complements current evaluation methods of porous materials for CO₂ separation and capture

2.1 Introduction

With the rapid growth in the development of materials that utilize the process of adsorption for selective CO₂ capture, it is that much critical to develop methods that provide a thorough evaluation of the viability of these materials in their performance for targeted applications. Typically, the single-gas isotherms of CO₂, CH₄, and N₂ have been collected to assess the gas uptake capacity of the sorbent material at ambient conditions. A high CO₂ uptake in particular has been deemed to be a characteristic of a sorbent with potential for CO₂ capture and sequestration. However, this parameter is far from conclusive in determining the performance of a sorbent in realistic conditions involving pressure-swing adsorption or vacuum swing adsorption processes. As such further analysis on single gas isotherms have been implemented to elucidate the potential of sorbents selective CO₂ capture applications. Despite the detailed methods that have been implemented, they do not mimic the multicomponent and dynamic gas mixture environment as those encountered in post-combustion flue gas exhaust.

In this chapter, we cover some of the single gas isotherm analysis methods used to evaluate sorbents for CO₂ separation including: binding affinity of gases using heat of adsorption calculations, selectivity using Henry's law, selectivity at specific partial pressure,¹ ideal adsorbed solutions theory (IAST) selectivity as well as the five sorbent evaluation criteria outlined by Bae and Snurr.² Additionally, we detail the assembly and employment of a dynamic gas mixture column breakthrough instrument to evaluate the performance of a new series of hetero-atom doped porous carbons for the separation of CO₂ from flue gas mixtures.

2.2 Heat of adsorption calculations using the virial equation

The virial equation is one method used to determine the binding affinity and isosteric heats of adsorption of gas molecules to sorbent pore walls.³⁻⁵ The following virial equation is used to fit the single gas adsorption isotherms at 273 and 298 K.

$$\ln p = \ln n + \frac{1}{T} \sum_{i=0}^M a_i n^i + \sum_{i=0}^N b_i n^i$$

Here, n is the amount adsorbed (mmol/g) at pressure p (Torr), T is temperature (K) and a_i and b_i are temperature independent empirical parameters, and M and N determine the number of terms required to adequately describe the isotherm. The resulting virial coefficients a_0 through a_M can be used to calculate the isosteric heats of adsorption as a function of uptake:

$$Q_{st} = -R \sum_{i=0}^M a_i n^i$$

Here, R is the gas constant (8.314 J K⁻¹ mol⁻¹). At zero-coverage, the isosteric heat of adsorption is given by:

$$Q_{st} = -R \sum_{i=0}^M a_0$$

2.3 Selectivity calculations

In a two component gas mixture, the selective adsorption of one gas over the other ($S_{1,2}$) is defined as the ratio of molar uptakes on sorbent surface to the ratio of the molar fractions of the bulk phase at equilibrium. This parameter is a ubiquitous gauge used in evaluating the performance of sorbents for selective gas capture. The most common way it has been calculated in literature is by taking the ratio of the Henry's law constant of the strongly adsorbed gas to that

of the weakly adsorbed gas.^{2,6} This method, commonly referred to as initial slope, is limited to reflecting the selectivity only at very low pressure and loading on the adsorbent. An alternative for calculating selectivity has been executed with the following equation:¹

$$S = \frac{[q_1]}{[q_2]} / \frac{[p_1]}{[p_2]}$$

Here, S is the selectivity value, q_1 is the quantity adsorbed of component 1, and p_1 is the partial pressure of component 1.

Perhaps, the most thorough method for calculating selectivity is the IAST method. Here, selectivity can be calculated from single gas isotherms with respect to uptake at specific partial pressures of gas mixtures present in the industrial application of interest.^{4,7} For all IAST calculations performed in this dissertation, the following steps were followed. To begin, the CO₂ isotherms were fitted to Dual Site Langmuir (DSL) model while CH₄ and N₂ isotherms were fitted to Single Site Langmuir (SSL) model given by the equations below:⁴

Duals Site Langmuir model = $q_A + q_B$; Single Site Langmuir = q_A

$$q = q_A + q_B = q_{sat,A} \frac{b_A * \exp\left(\frac{E_A}{R*T}\right) * p}{1 + b_A * \exp\left(\frac{E_A}{R*T}\right) * p} + q_{sat,B} \frac{b_B * \exp\left(\frac{E_B}{R*T}\right) * p}{1 + b_B * \exp\left(\frac{E_B}{R*T}\right) * p}$$

Here, q is the total amount of gas adsorbed (mmol/g), p is the total system pressure (bar), q_{sat} is the saturation capacity (mmol/g), b is the Langmuir constant (bar⁻¹). For CO₂ isotherms dual-site Langmuir-Freundlich ($q = q_A + q_B$) was employed to get a reasonable fitting. The parameters obtained from fittings were used for ideal adsorption solution theory (IAST) selectivity calculations. IAST is composed of a set of equations.

$$\pi_i^0(p_i^0) = \frac{RT}{A} \int_{p=0}^{p_i^0} n_i^0(p) d \ln p \quad i = 1,2,3,\dots,N$$

$$\pi_i^0 = \pi_j^0$$

$$py_i = p_i^0 x_i$$

$$\sum_{i=0}^N x_i = 1 \quad \sum_{i=0}^N y_i = 1$$

where π^0 is spreading pressure, p^0 is the equilibrium pressure of the single component gas corresponding to π^0 , A is the available surface area, n is experimentally measured gas uptake as a function of pressure p , R is ideal gas constant, T is temperature, x_i is the mole fraction of component i in the adsorbed phase and y_i is the mole fraction of component i in the bulk phase.

The integrals were computed numerically by using *Mathematica*® in order to get the adsorbed phase compositions (x_i). Adsorption selectivity of component 1 over component 2 was then calculated according to following equation:

$$S_{1,2} = \frac{p_2^0}{p_1^0} = \frac{x_1/y_1}{x_2/y_2}$$

The total amount adsorbed, n_t can be calculated by assuming ideal mixing at constant π^0 and T , as follows:

$$\frac{1}{n_t} = \sum_{i=1}^N \left[\frac{x_i}{n_i^0(p_i^0)} \right]$$

where n_t is the total number of adsorbed moles of gas per unit mass of adsorbent and n_i^0 is the number of moles of component i in the adsorbed phase per unit mass of adsorbent at spreading pressure π^0 and temperature T in the absence of the competing gas component.

The adsorption amount for the component i (n_i^{ads}) in the binary mixture adsorption is calculated employing the following equation:

$$n_i^{ads} = n_t x_i \quad (\text{Equation 8})$$

2.4 Sorbent evaluation criteria

The five sorbent evaluation criteria recently outlined by Bae and Snurr have been comprehensive in assessing a sorbent's performance for both pressure swing adsorption (PSA) and vacuum swing adsorption (VSA) processes. These criteria are summarized in Table 2.1 below

Table 2.1. Sorbent evaluation criteria^a

Criteria	Units and Denotation
1. CO ₂ uptake under adsorption conditions (mol kg ⁻¹)	N_1^{ads}
2. Working CO ₂ capacity (mol kg ⁻¹)	$\Delta N = N_1^{ads} - N_1^{des}$
3. Regenerability %	(%), $R = (\Delta N_1 / N_1^{ads}) 100$
4. Selectivity under adsorption conditions	$\alpha_{12}^{ads} = (N_1^{ads} / N_2^{ads})(y_2 / y_1)$
5. Sorbent selection parameter	$S = (\alpha_{12}^{ads})^2 / (\alpha_{12}^{des}) (\Delta N_1 / \Delta N_2)$

N is the adsorbed amount and *y* is the mole fraction in the gas phase. The subscripts 1 and 2 indicate CO₂ and either CH₄ or N₂, respectively. The superscripts “ads” and “des” refer to adsorption and desorption conditions, respectively.

Following the above sorbent evaluation criteria, the performance of sorbents can be evaluated in four scenarios involving the separation of CO₂ from either N₂ or CH₄ at pressures (VSA and PSA) and gas mixture compositions of application interests. The four scenarios are presented in Table 2.2.

Table 2.2. VSA and PSA conditions for sorbent evaluation at 298 K

Application	Mixture composition	Adsorption and desorption pressures (p ^{ads} and p ^{des})
1. Natural gas purification using PSA	CO ₂ /CH ₄ : 10/90	p ^{ads} = 5 bar, p ^{des} = 1 bar
2. Landfill gas separation using PSA	CO ₂ /CH ₄ : 50/50	p ^{ads} = 5 bar, p ^{des} = 1 bar
3. Landfill gas separation using VSA	CO ₂ /CH ₄ : 50/50	1 bar, p ^{des} = 0.1 bar
4. Flue gas separation using VSA	CO ₂ /N ₂ : 10/90	1 bar, p ^{des} = 0.1 bar

2.5 Column breakthrough evaluation of hetero-atom doped porous carbons of flue gas mixture separation

There are well established methods for evaluating the performance of porous sorbents in gas separation applications. Selectivity calculations from initial slope ratios, IAST and the sorbent evaluation criteria discussed above have proven to be standards in reports pertaining to such applications. However, all of these methods rely on single-component isotherms to deduce

the performance of sorbents in mixed gas adsorption. As such, these methods even though widely accepted need to be at least complemented with a technique that mimics the real industrial conditions where dynamic gas mixtures are encountered. To this end, we present here in the in-house assembly of a dynamic gas mixture breakthrough apparatus for studies of CO₂ separation in flue gas composition mixtures.

The sorbents studied are pyrazole/KOH derived hetero-atom (N and O) doped porous carbons. The pyrazole-derived carbons (PYDCs) have high nitrogen doping levels (14.9-15.5 wt. %) induced by high nitrogen to carbon ratio in pyrazole (43 wt. %) as well as high oxygen content (16.4-18.4 wt. %). PYDCs have superior porosity ($S_{\text{BET}} = 1266\text{--}2013 \text{ m}^2 \text{ g}^{-1}$) and CO₂ isosteric heat of adsorption ($Q_{\text{st}} = 33.2\text{--}37.1 \text{ kJ mol}^{-1}$). The textural properties of PYDCs are summarized in Table 2.3.

Table 2.3. Textural properties and elemental analysis of PYDCs

Sample	$S_{\text{BET}}^{\text{a}}$ ($\text{m}^2 \text{ g}^{-1}$)	$V_{\text{TOT}}^{\text{b}}$ ($\text{cm}^3 \text{ g}^{-1}$)	$V_{\text{Mic}}^{\text{c}}$ ($\text{cm}^3 \text{ g}^{-1}$)	$V_{\text{meso}}^{\text{c}}$ ($\text{cm}^3 \text{ g}^{-1}$)	V_0^{d} ($\text{cm}^3 \text{ g}^{-1}$)	C (wt. %)	O (wt. %)	N (wt. %)
PYDC-550-1	1266	0.69	0.47(68)	0.22	0.058	66.6	18.4	14.9
PYDC-550-2	2013	1.173	0.75(63)	0.42	0.065	68	16.9	15.1
PYDC-550-3	1400	0.78	0.53 (68)	0.25	0.046	68.1	16.4	15.5
PYDC-600-2	1398	0.88	0.61 (69)	0.27	0.069	68.2	16.5	15.3

^aBrunauer–Emmett–Teller (BET) surface area. ^bTotal pore volume at $P/P_0 = 0.95$. ^cDetermined by PSD assuming slit-shaped pores and the QSDFT model from nitrogen adsorption data at 77 K (the values in parentheses are the percentage of micropore volume relative to total pore volume). ^dPore volume of ultramicropores (<0.7 nm) obtained from CO₂ adsorption data at 273 K.

These properties render PYDCs with the ability to adsorb high amounts of CO₂ up to 2.15 mmol g⁻¹ and 6.06 mmol g⁻¹ at 0.15 and 1 bar, respectively, at 298 K. While at 273 K, PYDCs

display CO₂ uptake up to 3.7 mmol g⁻¹ and 8.59 mmol g⁻¹ at 0.15 and 1 bar, respectively. Due to a desirable combination of micropores and mesopores, PYDCs show significantly high adsorption selectivity for CO₂/N₂ (128) and CO₂/CH₄ (13.4) as determined by the Ideal Adsorbed Solution Theory (IAST) calculation using pure gas isotherms at 298 K. The gas uptake and selectivity values of PYDCs are summarized in Table 2.4. Due to the ease of scalability using a single precursor and solvent free preparation method along with their superior CO₂ uptake and selectivity, we deemed them suitable for flue gas mixture breakthrough studies.

Table 2.4. CO₂ uptake, heat of adsorption and selectivity values of PYDCs

	CO ₂ capacity (mmol g ⁻¹)					CH ₄ capacity (mmol g ⁻¹)			Selectivity(298)			
	0.15 bar		1.0 bar			1.0 bar			CO ₂ /N ₂		CO ₂ /CH ₄	
	273K	298K	273K	298K	Q _{st} ^a	273K	298K	Q _{st} ^a	IS ^b	IAST ^c	IS ^b	IAST ^d
	PYDC-550-1	2.99	1.79	6.3	4.62	35.28	1.92	1.32	20.54	85	49.6	19
PYDC-550-2	3.714	2.15	8.59	6.06	34.14	2.26	1.78	18.6	52	40.4	13	9.8
PYDC-550-3	2.69	1.5	6.24	4.05	33.249	1.89	1.07	24.33	99	114.9	12	13
PYDC-600-2	3.46	2.05	7.219	4.96	37.102	2.26	1.46	23.17	150	128	17	13

^aObtained from CO₂ isotherm data at 273 and 298 K using the Virial equation, kJ mol⁻¹. ^bObtained from the initial slope of adsorption isotherms at 298 K in the linear low pressure region. ^cCalculated using the IAST method at 298 K for the mixture of 0.1/0.9 for CO₂/N₂ at 1 bar. ^dcalculated using the IAST method at 298 K for the mixture of 0.5/0.5 for CO₂/CH₄ at 1 bar.

2.5.1 Description column breakthrough experiment setup

The dynamic gas mixture adsorption properties of the razole derived carbons were assessed using a custom built breakthrough gas separation setup (Figure 2.1). The setup is equipped with three adsorbate gas sources: helium which is used to activate the packed sample

column, CO₂ and N₂. The flows of the feed gases were regulated using respective mass flow controllers which allow mimicking composition of industrial gases for targeted applications. Once a uniform gas mixture is obtained in the mixing chamber, the feed gas can be introduced into the sample column via a three-way valve. The sample column is made of stainless steel with dimensions of 200 mm in length and 4 mm i.d. A Swagelok back pressure regulator fitted at the opposite end of the sample column is used to regulate experiments at desired pressures. The effluent/breakthrough gas is analyzed using an RGA200 mass analyzer.

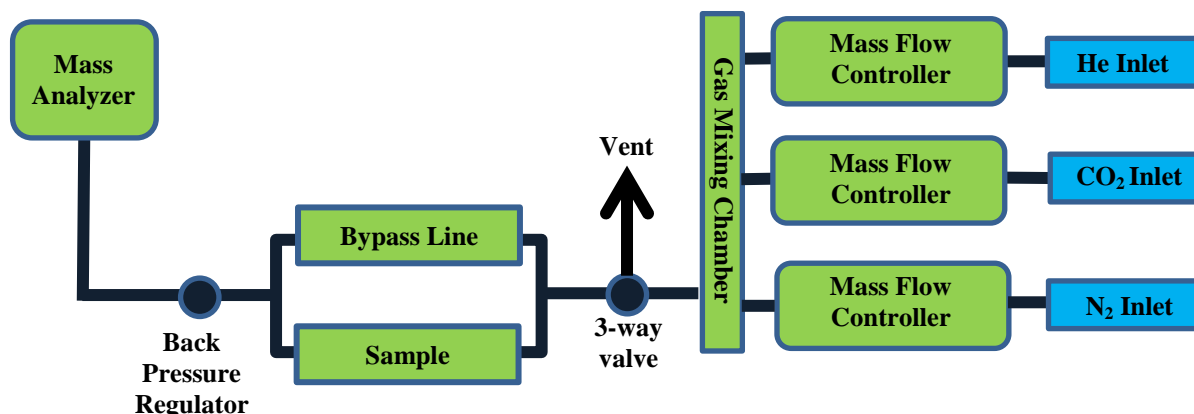


Figure 2.1: Schematic representation of the dynamic gas breakthrough setup

2.5.2 Experimental section

In a typical experiment, the sample column was loaded with 150-200 mg of -carbon. The sample was activated at 150 °C and a 5ml/min He flow. Breakthrough experiments were conducted at 298 K and 1 bar. For flue gas settings, a CO₂/N₂: 0.5/4.5 ml min⁻¹ (10:90) mixture is fed through the column and the breakthrough time for each gas is assessed by recording P vs T curves. The complete breakthrough time is denoted as the time it takes for downstream gas to reach the total signal of the feed gas. The selectivity (S) of CO₂ over N₂ is determined by applying the following equation:⁸

$$S_{\text{CO}_2/\text{N}_2} = \frac{(\text{Uptake CO}_2/\text{Uptake CO}_2 \text{ and N}_2) / (\text{Uptake CO}_2/\text{Uptake CO}_2 \text{ and N}_2)}{\text{Composition CO}_2 / \text{Composition N}_2}$$

2.5.3 Results and discussion

The CO₂ separation ability of the PYDCs determined from IAST calculations was complemented using column breakthrough studies. The breakthrough of binary gas mixtures of CO₂/N₂: 10/90 flown through a PYDC packed column at 298K and atmospheric pressure in dry conditions were used to determine the breakthrough times of the gas components. The breakthrough time for N₂ (within seconds) were very short compared to CO₂ (Figure 2.2 and 2.3) in all four PYDCs indicative of high selectivity toward CO₂ in a practical setting. The CO₂ signals of PYDCs were observed after 67, 65.1, 77.7 and 81 min g⁻¹ for 550 1, 550 2, 550 3 and 600 2. Subsequently, the CO₂/N₂ breakthrough selectivities were calculated and were found to be 175, 167, 181 and 193 for PYDC-550-1, -550-2, -550-3 and -600-2 respectively. Even though these values are different from those derived from IAST calculations, they display a similar trend. Such variations in selectivity values between equilibrium and dynamic experiments are not to be unexpected due to the different processes by which the results from the two methods are obtained. Besides their dynamic nature, breakthrough experiments are also influenced by factors such as adsorbent packing density, column size, column shape, effluent gas flow rate as well as extra-column effects.^{9,10} The breakthrough selectivity values have a much smaller range (26) compared to the IAST values (123) which suggests that the factors that determine breakthrough selectivity are different from the IAST method. Since the breakthrough experiments are a dynamic process, the nature of pores of the materials contributes significantly to gas separation ability.¹¹ Relatively, PYDC-550-2 has the highest percentage of mesopores (35%) and the lowest percentage of micropores (64%) and hence has the poorest capability of selectively sieving N₂ under dynamic conditions which has a higher kinetic diameter than CO₂. Whereas, PYDC-600-2

bearing the lowest percentage of mesopores (31%) and highest micropores (69%) displayed the best CO₂/N₂ performance.

2.6 Conclusion

We have successfully assembled a system that can be used to study the separation of dynamic gas mixtures. The breakthrough selectivity of hetero-atom doped porous carbons bearing a range of textural properties was tested. It was illustrated that under dynamic conditions, the textural properties, particularly the nature of pores in the sorbent, plays a far more significant role than the chemical functionalities. This was evident in the high breakthrough selectivity value recorded for PYDC-600-2 which had the highest percentage of micropores.

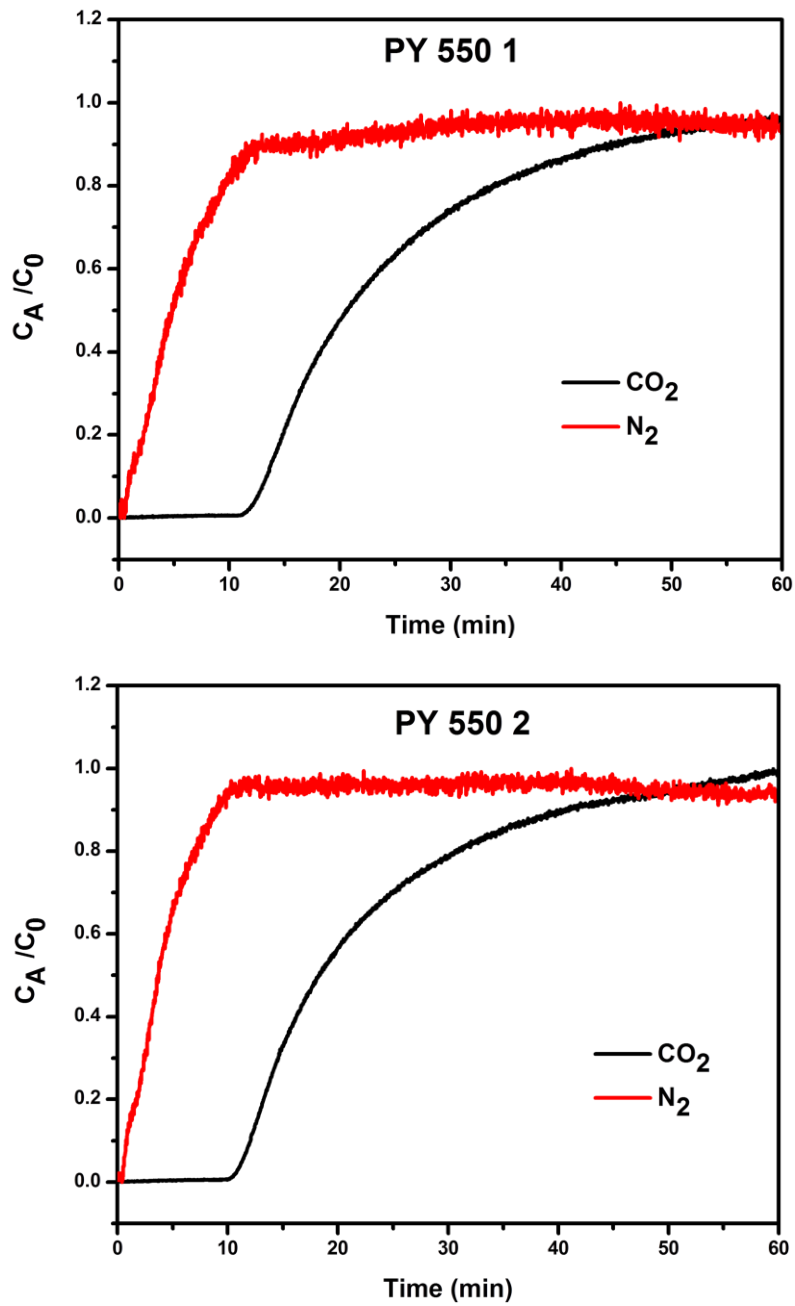


Figure 2.2. Dynamic gas breakthrough curves for PYDCs: -550-1 (top), -550-2 (bottom)

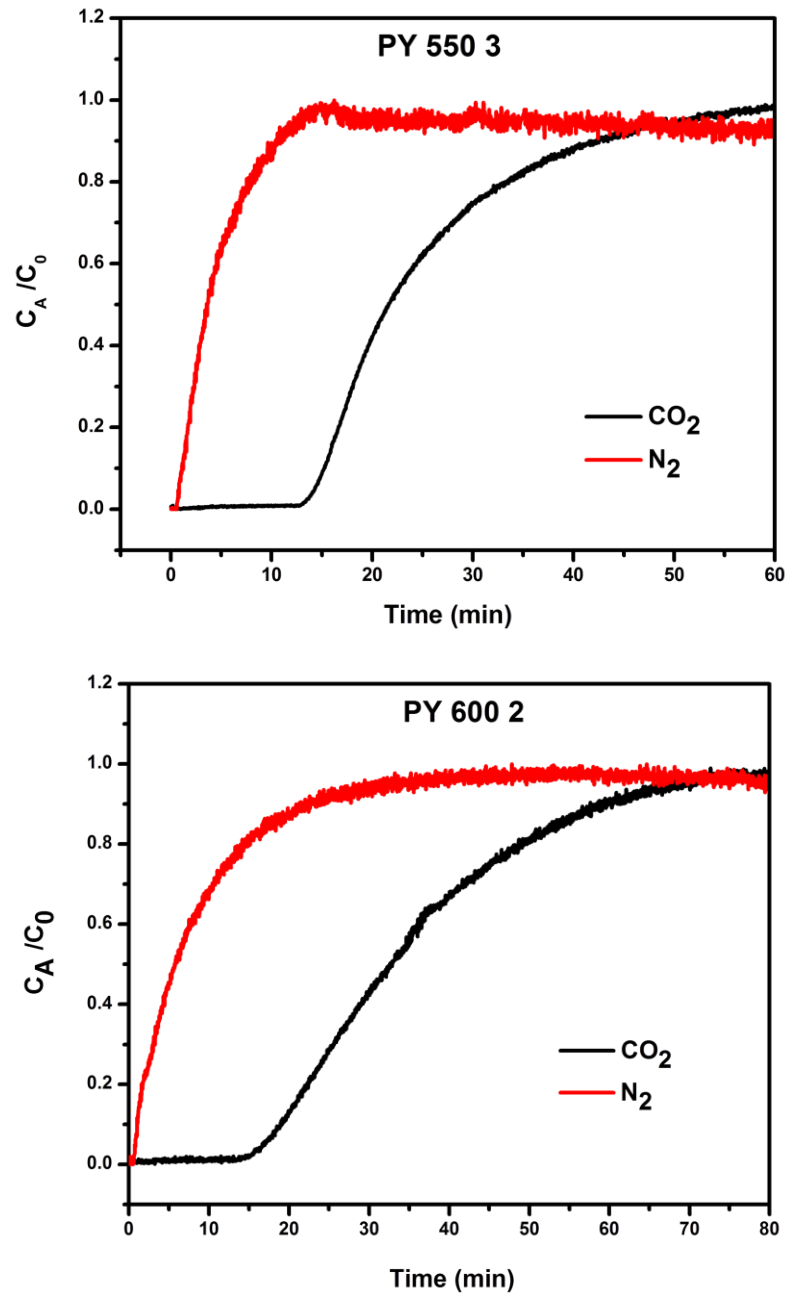


Figure 2.3. Dynamic gas breakthrough curves for PYDCs: -550-3 (top) and -600-2 (bottom)

References

- (1) Sumida, K.; Rogow, D. L.; Mason, J. A.; McDonald, T. M.; Bloch, E. D.; Herm, Z. R.; Bae, T. H.; Long, J. R. Carbon Dioxide Capture in Metal-Organic Frameworks. *Chem Rev.* **2012**, *112* (2), 724–781.
- (2) Bae, Y.-S.; Snurr, R. Q. Development and Evaluation of Porous Materials for Carbon Dioxide Separation and Capture. *Angew. Chemie - Int. Ed.* **2011**, *50* (49), 11586–11596.
- (3) Zhao, X. B. .; Villar-Rodil, S. .; Fletcher, A. J. .; Thomas, K. M. Kinetic Isotope Effect for H- 2 and D-2 Quantum Molecular Sieving in Adsorption/desorption on Porous Carbon Materials. *J. Phys. Chem. B* **2006**, *110* (20), 9947–9955.
- (4) Sekizkardes, A. K.; Kahveci, Z.; El-kaderi, H. M. Application of rene-Derived Benzimidazolelinked Polymers to CO2 Separation under Pressure and Vacuum Swing Adsorption Settings. *J. Mater. Chem. A* **2014**, *2*, 12492–12500.
- (5) Islamoglu, T.; Behera, S.; Kahveci, Z.; Tessema, T.-D.; Puru, J.; El-kaderi, H. M. Enhanced Carbon Dioxide Capture from Land Fi Ll Gas Using Bifunctionalized Benzimidazole-Linked Polymers. *ACS Appl. Mater. Interfaces* **2016**, *8*, 14648–14655.
- (6) Yang, R. T. *Adsorbents: Fundamentals and Applications*; Wiley, 2003.
- (7) Myers, A. L.; Prausnitz, J. M. Thermodynamics of Mixed-Gas Adsorption. *AIChE J.* **1965**, *11* (1), 121–127.
- (8) Shekhah, O.; Belmabkhout, Y.; Chen, Z.; Guillerm, V.; Cairns, A.; Adil, K.; Eddaoudi, M. Made-to-Order Metal-Organic Frameworks for Trace Carbon Dioxide Removal and Air Capture. *Nat. Commun.* **2014**, *5* (May), 4228.
- (9) Mason, J. A.; McDonald, T. M.; Bae, T. H.; Bachman, J. E.; Sumida, K.; Dutton, J. J.; Kaye, S. S.; Long, J. R. Application of a High-Throughput Analyzer in Evaluating Solid Adsorbents for Post-Combustion Carbon Capture via Multicomponent Adsorption of

- CO₂. *J. Am. Chem. Soc.* **2015**, *137* (14), 4787–4803.
- (10) Hofman, P. S.; Rufford, T. E.; Chan, K. I.; May, E. F. A Dynamic Column Breakthrough Apparatus for Adsorption Capacity Measurements with Quantitative Uncertainties. *Adsorption* **2012**, *18* (3–4), 251–263.
- (11) Zhao, Y.; Yao, K. X.; Teng, B.; Zhang, T.; Han, Y. A Perfluorinated Covalent Triazine-Based Framework for Highly Selective and Water-Tolerant CO₂ Capture. *Energy Environ. Sci.* **2013**, *6* (12), 3684–3692.

Chapter 3

Evaluation of Newly Synthesized Porous Benzimidazole Linked Polymers for CO₂ Separation

3.1. Introduction

Porous organic polymers (POPs) as discussed earlier have emerged as promising candidates for their potential in treatment of post combustion flue gas to reduce CO₂ emission into the atmosphere as well as treatment of landfill gas to enhance energy density and eliminate the corrosive CO₂ gas for longevity of fuel vessels and pipelines. It has also been well established that the incorporation of nitrogen containing functionalities in such porous frameworks enhances their CO₂ uptake and separation ability.^{1,2} This is achieved via Lewis acid-base interactions as well hydrogen bonding sites introduced by these nitrogen rich moieties.^{3,4} Imidazole functionalized polymers have garnered attention by way of benzimidazole linkages due to their basicity (pKa = 5.532). Specifically, the CO₂ interaction sites on the imidazole moiety are the lone pairs on the double bonded nitrogen and through a hydrogen bonding of the secondary amine.

Moreover, the use of star shaped and rigid building blocks for a topology targeted approach has been shown to influence the textural properties of polymers which can be complemented with functional groups conducive for CO₂ capture.⁵ Thus, the right combination of textural properties along with chemical functionality can lead to the realization of a porous framework that could be implemented for use in targeted gas separation applications.⁶ With the above considerations, we present the synthesis and characterization of two new BILPs for their potential application in selective CO₂ capture from flue gas and landfill gas mixtures.

3.2. Experimental Section

3.2.1 General Techniques and Materials

All solvents, starting materials and reagents were purchased from Acros Organics and used without any further purification unless otherwise noted. Tetrahydrofuran (THF) was dried using a distillation setup under nitrogen flow. Air sensitive materials and reactions were handled or carried out in an inert atmosphere (nitrogen gas) using glove box or Schlenk line techniques. Elemental analyses were done at American University of Sharjah, UAE. Liquid ^1H NMR were conducted using a Varian Mercury-400 MHz NMR spectrometer. FT-IR spectra were obtained using a Nicolet-Nexus 670 spectrometer equipped with an attenuated total reflectance accessory. Thermal stability of the synthesized polymers was assessed using a Perkin thermo-gravimetric analyzer with a temperature ramp rate of $5\text{ }^\circ\text{C}/\text{min}$ under N_2 flow. Scanning electron microscope (SEM) images were used to determine the morphology of the polymers using a Hitachi SU-70 FE-SEM. The samples were prepared by dispersion onto a double sided carbon tape attached to a sample holder followed by a platinum coating for 70 seconds at 1×10^{-6} bar. Powder X-ray diffraction data were collected using a Panalytical X'pert pro multipurpose diffractometer by a $\text{Cu K}\alpha$ radiation with a 2θ range of 2-30. Porosity and gas uptake studies were conducted using a Quantachrome Autosorb iQ volumetric analyzer using gases of ultra- high purity (UHP) grade. Typically, a sample ($\sim 40\text{-}50$ mg) was loaded into a pre-weighed 9 mm large bulb Quantachrome cell which was then hooked up to the degassing station of the gas analyzer. The sample was then degassed at $120\text{ }^\circ\text{C}$ and 1.0×10^{-5} bar for 12h. The degassed sample and cell were refilled with helium, weighed and hooked up to the analysis station of the gas analyzer. Adsorption temperatures were attained using a temperature controlled water/ethylene glycol mixture bath for 273 and 298 K and a refrigerated bath of liquid nitrogen for 77 K.

3.2.2 Synthesis of Tetra(4-bromophenyl)ethylene (TBE)

Tetra(4-bromophenyl)ethylene was synthesized following a previously published method.⁷ Briefly, bromine (6.0 mL, 117 mmol) in an open vial and tetraphenylethylene (5.0 g, 15.04 mmol) spread on a watch glass were placed at the bottom and top rack in a desiccator. The reaction was carried out for 5 days with an outlet tube installed on the desiccator to vent HBr that is formed during the reaction. A dark green solid product was collected and recrystallized from dichloromethane/methanol (2:1) to isolate white crystals that were dried using vacuum. ¹H NMR (400 MHz, CDCl₃, 25 °C): δ = 7.06 (d, 8H), 7.51 (d, 8H).

3.2.2 Synthesis of Tetra(4-formylphenyl)ethylene (TFE)⁸

Tetra(4-formylphenyl)ethylene was synthesized by dissolving Tetra(4-bromophenyl)ethylene (1.5 g, 3.5 mmol) in anhydrous THF (200 mL) under the flow of N₂ gas. While stirring *n*-BuLi (2.5 M solution in *n*-hexane, 14 mL, 35 mmol) was added dropwise at -78 °C. Stirring was continued for 1 hour and the temperature allowed to warm up to -60 °C forming a bright yellow solution. At this point anhydrous N,N-dimethylformamide (DMF) (5.4 mL, 70 mmol) was added after cooling the reaction mixture to -78 °C. The reaction mixture was allowed to warm up to room temperature overnight while stirring. The resultant white mixture was treated with 3 M HCl (50 mL) and the organic layer removed by rotary evaporation. The remaining aqueous layer was extracted by CHCl₃ and the extract washed with water, dried over MgSO₄ and filtered. The crude light yellow product was isolated by rotary evaporation and further purified by flash column chromatography using silica gel and CH₂Cl₂ as an eluent to afford cream colored solid product in 54% yield (0.81 g, 1.89 mmol). ¹H NMR (400 MHz, CDCl₃, 25 °C): δ = 7.49 (d, 8H), 7.71 (d, 8H), 9.85 (s, 4H) Anal. Calcd. for C₃₀H₂₀O₄: C, 81.07%; H, 4.54%; O 14.04% Found C, 76.67%; H, 6.37%; O (N/A)

3.2.3 Synthesis of 4,4',5,5'-Tetrabromo-9,9'-spirobi[fluorine] (TSF)

The compound 4,4',5,5'-Tetrabromo-9,9'-spirobi[fluorine] (TSF) was synthesized by adopting a previously published method.⁷ Briefly, bromine (4.1 mL, 80 mmol) in an open vial and 9,9'-spirobi[fluorine] (5.0 g, 7.91 mmol) spread on a watch glass were placed at the bottom and top rack in a desiccator. An outlet tube was installed on the desiccator to vent HBr that is formed during the reaction which proceeded for 5 days. A dark green solid product was collected and recrystallized from dichloromethane/methanol (2:1) to isolate a white solid product that was dried using vacuum. ¹H NMR (400 MHz, CDCl₃, 25 °C): δ = 7.45 (d, 4H), 7.11 (dd, 4H), 7.7-38 (d, 4H)

3.2.4 Synthesis of 9,9'-spirobi[fluorine]-4,4',5,5'-tetracarbaldehyde (SFTA)

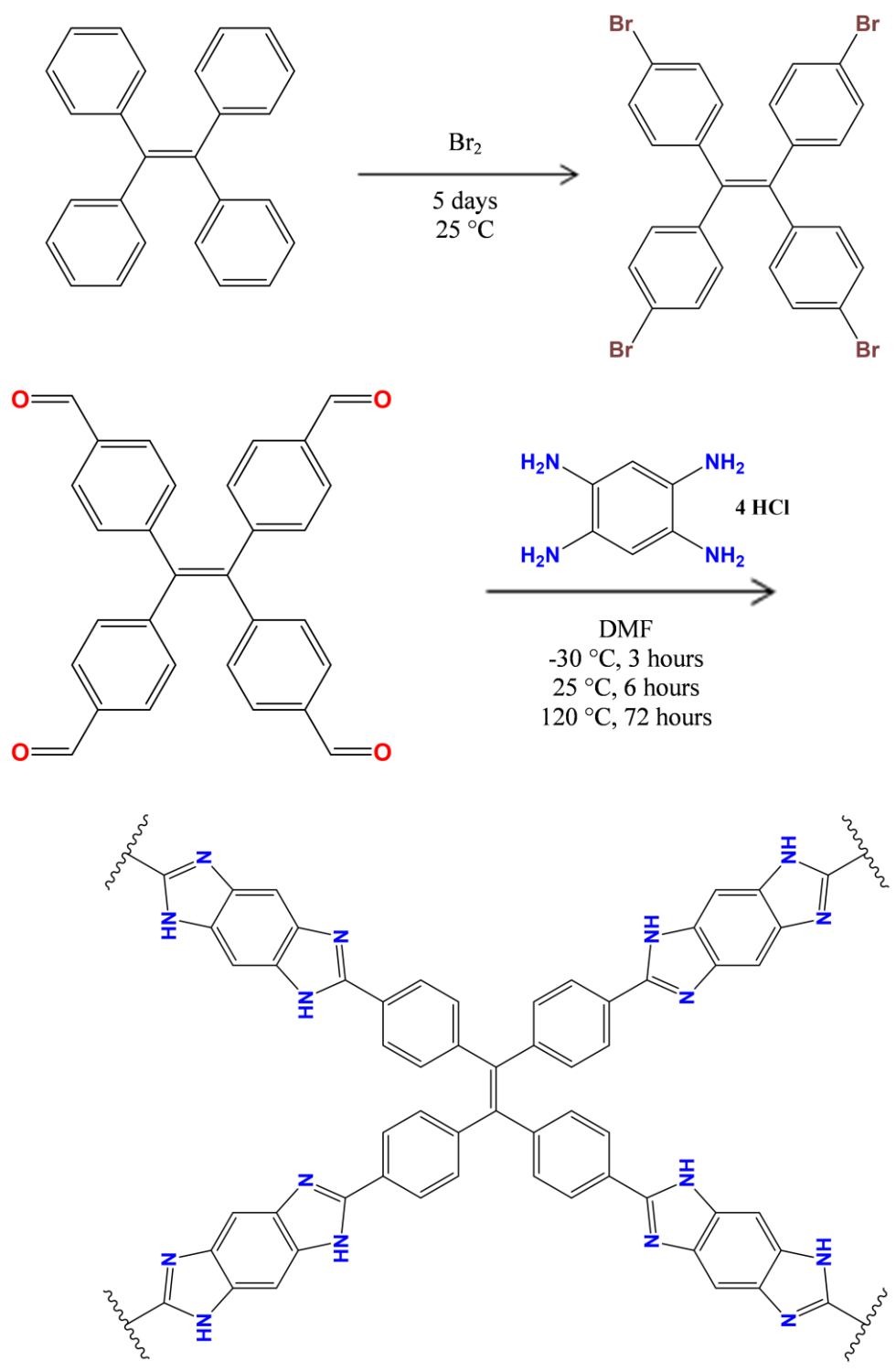
In a 250 mL Schlenk flask, TSF (1.5 g, 2.37 mmol) was dissolved in dry THF (150 mL) under a N₂ atmosphere. The solution was cooled to -78 °C and -BuLi (2.5 M solution in n-hexane, 9.5 mL, 23.7 mmol) was added dropwise while stirring. The flask was allowed to warm up to -60 °C over an hour forming a bright burgundy solution. The reaction mixture was then cooled back to -78 °C and treated dropwise with anhydrous DMF (3.7 mL, 47.4 mmol). The resultant white opaque mixture was treated with 3 M HCl (46 mL) and the organic layer removed by rotary evaporation. The remaining aqueous layer was extracted by CHCl₃ and the extract washed with water, dried over MgSO₄ and filtered. The crude light yellow product was isolated by rotary evaporation and further purified by flash column chromatography using silica gel and CH₂Cl₂ as an eluent to afford a cream colored solid product in 59% yield (0.60 g, 1.40 mmol). ¹H NMR (400 MHz, CDCl₃, 25 °C): δ = 7.85 (d, 4H), 7.35 (dd, 4H), 7.70 (d, 4H), 10.31 (s, 4H)
Anal. Calcd. for C₂₉H₁₆O₄: C, 81.30%; H, 3.76%; O 14.94% Found C, 74.76%; H, 5.34%; O (N/A)

3.2.5 Synthesis of BILP-30 (Scheme 3.1)⁸

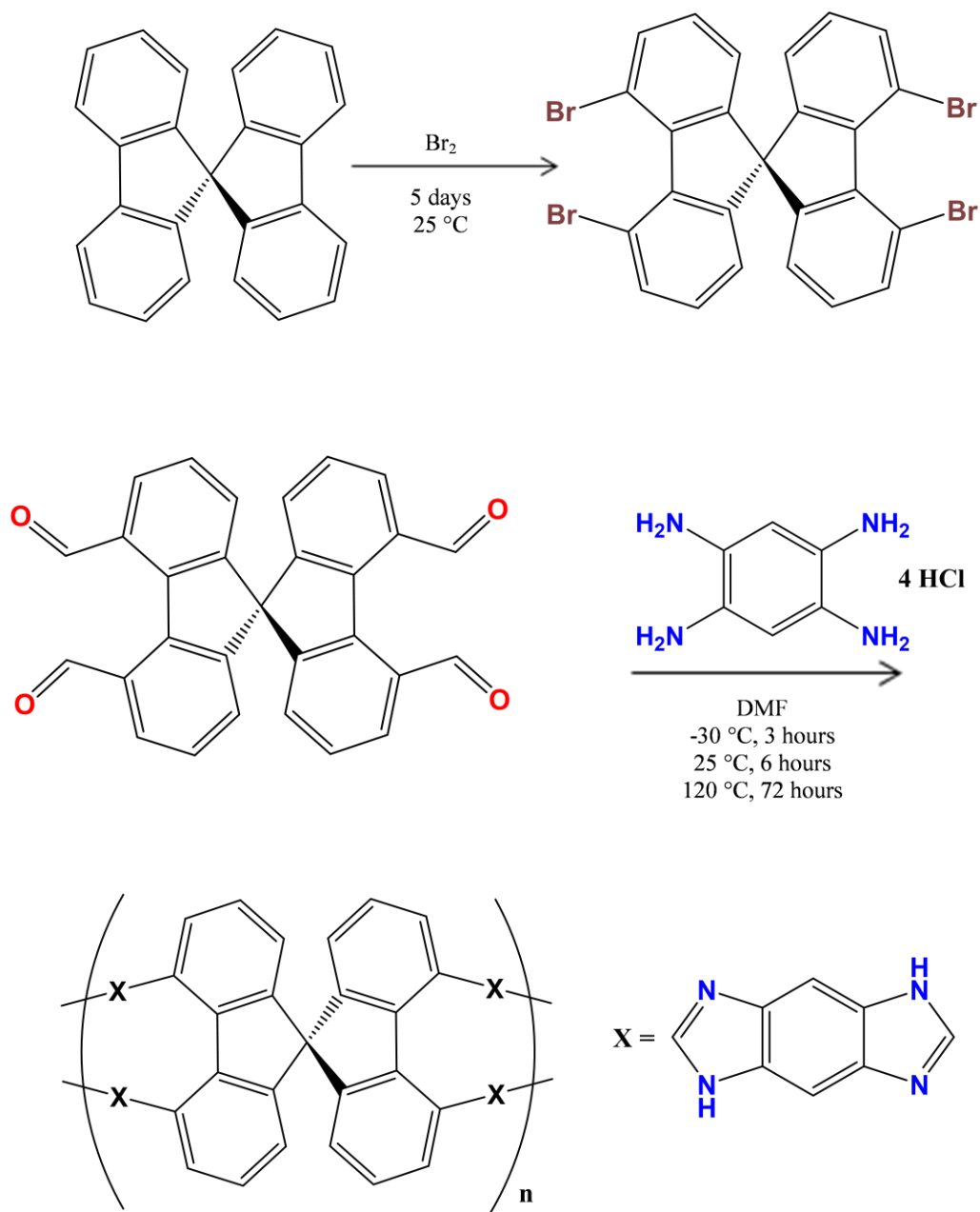
Tetra(4-formylphenyl)ethylene (50 mg, 0.112 mmol) was charged into a Schlenk flask (100 ml) and dissolved in 30 ml anhydrous DMF. The solution was cooled to -30 °C and treated dropwise with 15 ml solution of 1,2,4,5-Benzenetetramine tetrahydrochloride (mg, mmol) in anyhrdous DMF kept stirring at -30 °C for 3 h. The resultant brown slurry was allowed to warm up to room temperature overnight. The reaction mixture was bubbled with air for 15 minutes, transferred to an oven and heated to 130 °C and incubated for 72 h. The resulting brown polymer was isolated via filtration over a medium glass frit and subsequently washed with DMF, acetone, water, 2M HCl, 2M NaOH, water, and acetone. Anal. Calcd. for C₄₂H₅₂N₈: C, 78.28%; H, 4.38%; N 17.38% Found C, 59.9%; H, 5.1%; N 13.29%

3.2.6 Synthesis of BILP-31 (Scheme 3.2)⁸

SFTA (45 mg, 0.105 mmol) was charged into a Schlenk flask (100 ml) and dissolved in 30 ml anhydrous DMF. The solution was cooled to -30 °C and treated dropwise with 15 ml solution of 1,2,4,5-Benzenetetramine tetrahydrochloride (30mg, 0.21 mmol) in anyhrdous DMF kept stirring at -30 °C for 3 h. The resultant brown slurry was allowed to warm up to room temperature overnight. The reaction mixture was bubbled with air for 15 minutes, transferred to an oven and heated to 130 °C and incubated for 72 h. The resulting brown polymer was isolated via filtration over a medium glass frit and subsequently washed with DMF, acetone, water, 2M HCl, 2M NaOH, water, and acetone. Anal. Calcd. for C₄₀H₂₆N₆: C, 77.65%; H, 4.24%; N 18.11% Found C, 51.77%; H, 4.54%; N 11.64%



Scheme 3.1: Synthetic route for BILP-30

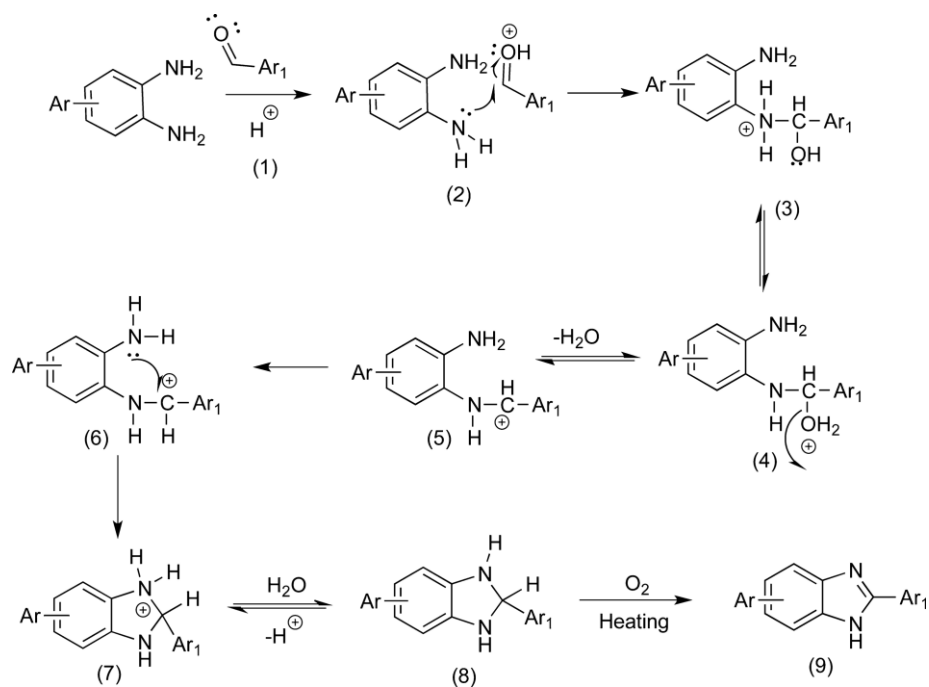


Scheme 3.2: Synthetic route for BILP-31

3.3 Results and Discussion

3.3.1 Synthesis and Characterization

The synthesis of BILPs was carried out following a procedure we previously reported implementing an acid catalyzed poly-condensation reaction between an aryl-*o*-diamine (HCl salts) and aryl-aldehyde building blocks. The reaction is proposed to proceed by the HCl from the amine salt protonation of the oxygen in the aldehyde monomer and catalysis of an imine bond formation. This is followed by a molecular oxygen supported dehydration and cyclization of the imidazole group (Scheme 3.3).⁹



Scheme 3.3: Proposed Mechanism of Imidazole Moiety Formation by the Catalytic Acid Process

Similar to previous reports, BILP-30 and -31 are insoluble in common organic solvents and their structural integrity stays intact upon soaking in concentrated 2M solutions of HCl and NaOH indicating their remarkable chemical stability. The formation of benzimidazole linkers

was confirmed by FT-IR spectra of the polymers (Figure 3.1). Characteristic N-H stretching bands at $\sim 3415\text{ cm}^{-1}$ (free) and $\sim 3225\text{ cm}^{-1}$ (hydrogen bonded) as well as an intense band (C=N) at $\sim 1620\text{ cm}^{-1}$. The skeleton vibrations of the imidazole rings are evident by peaks at 1500 cm^{-1} and 1450 cm^{-1} . Stretching bands of C-N are observed at 1355 cm^{-1} and N-H bending bands at 1640 cm^{-1} . Thermogravimetric analysis (TGA) was used to evaluate the thermal stability of BILP-30 and -31 (Figure 3.2) with both polymers displaying only about 12% weight loss up to $\sim 400\text{ }^\circ\text{C}$. The amorphous nature of BILP-30 and -31 was evident in their featureless powder X-ray diffraction patterns (Figure 3.3). Scanning electron microscopy (SEM) images reveal spherical aggregates of various sizes for both polymers (Figure 3.4).

3.3.2 Porosity Measurements and Textural Properties

The porosity of BILP-30 and -31 were evaluated *via* N_2 (77 K) adsorption-desorption isotherms presented in Figure 3.5. Both polymers display a sharp N_2 uptake at very low pressure ($P/P_o < 0.01$) which signifies the permanent microporous nature of the polymers.¹⁰ A gradual increase in the N_2 uptake at higher relative pressures (0.04-0.9) depicts the presence of a small percentage of mesopores. This trend was slightly more prominent in BILP-30 than it is in BILP-31, suggesting the presence of a higher ratio of mesopores.¹⁰ The Brunauer-Emmett-Teller (BET) method was applied to calculate the specific surface areas of the polymers using the adsorption branch of N_2 isotherms (Table 3.1). The polymers possess good porosity at surface areas of $926\text{ m}^2/\text{g}$ and $887\text{ m}^2/\text{g}$ for BILP-30 and BILP-31 respectively which are comparable to previously reported BILPs.^{8,11-13} The use of rigid star-shaped monomers and with the absence of long linkers precludes the amount of interpenetration in the polymers formed.¹⁴ The pore size distributions (PSD) of BILP-30 and -31 were elucidated from QSDFT fittings of the adsorption branch of N_2 (77 K) isotherm with carbon as adsorbent and slit/cylindrical pores (Figure 3.7).

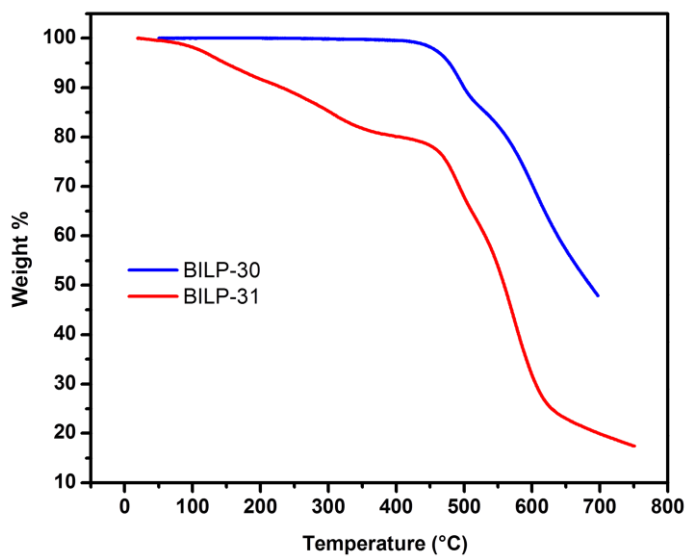


Figure 3.2: Thermogravimetric analysis of BILP-30 and BILP-31

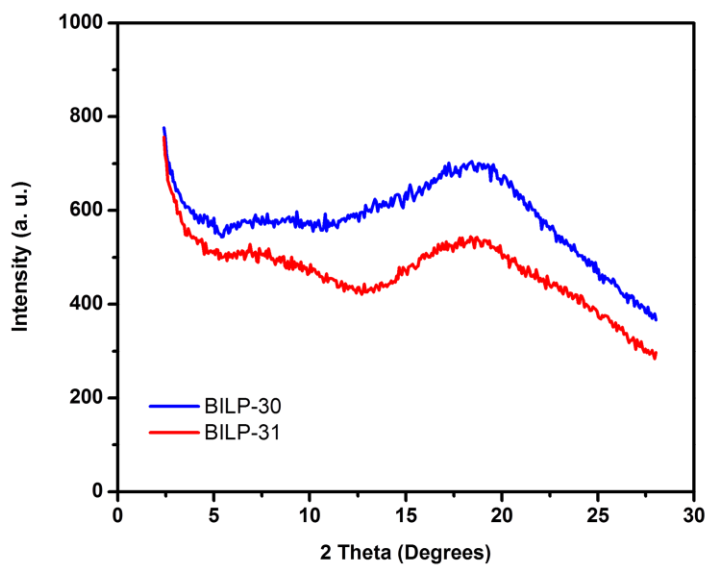


Figure 3.3: Powder X-ray diffraction patterns of BILP-30 and BILP-31



Figure 3.4 (a): Scanning electron microscopy (SEM) images of BILP-30

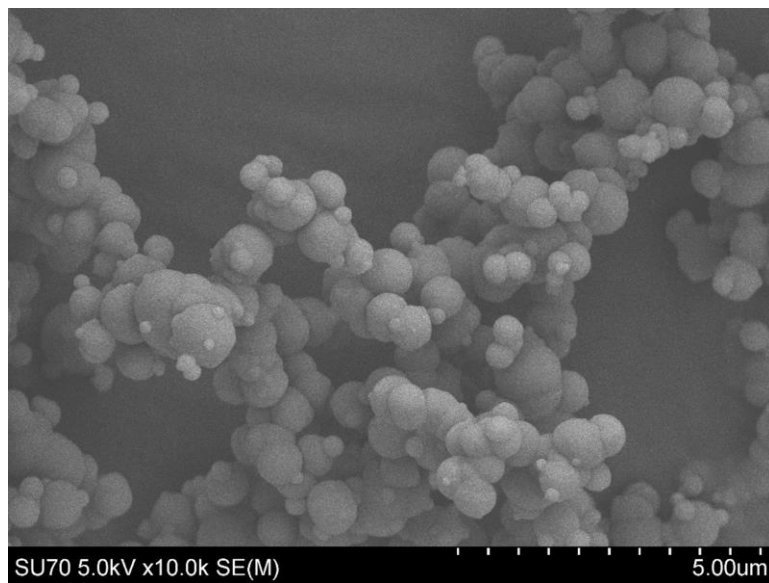


Figure 3.4 (b): Scanning electron microscopy (SEM) images of BILP-31

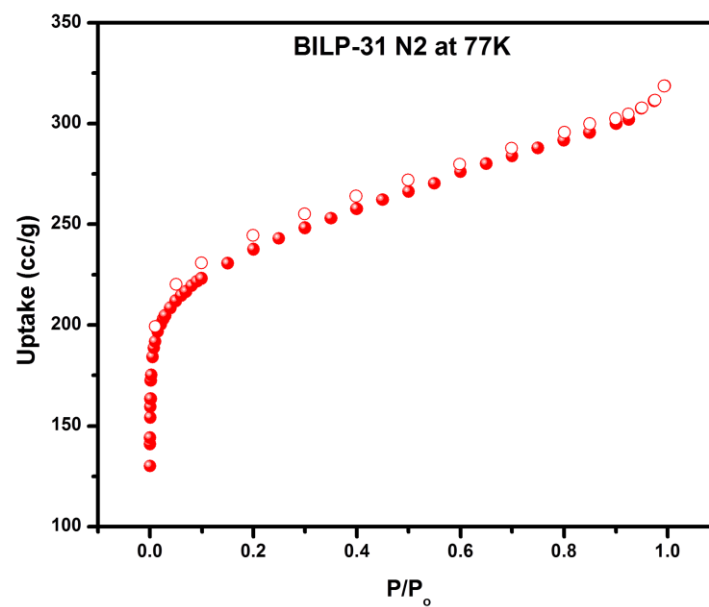
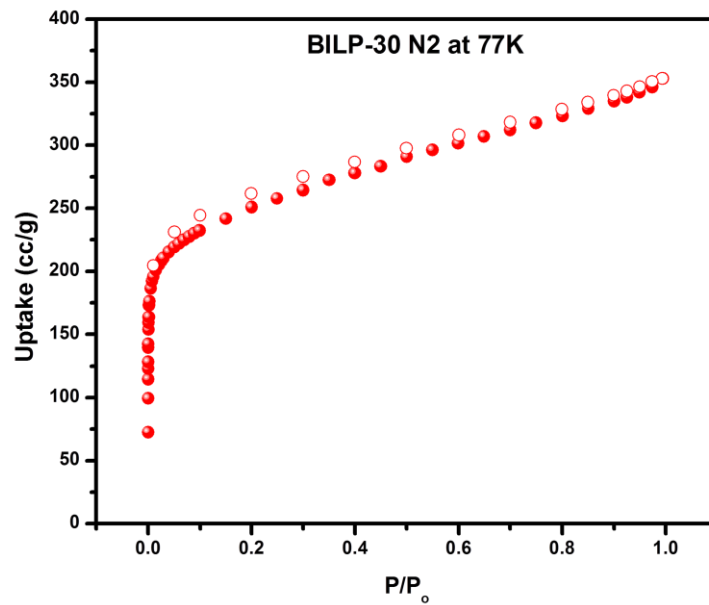


Figure 3.5: N₂ isotherms of BILP-30 and BILP-31 at 77 K

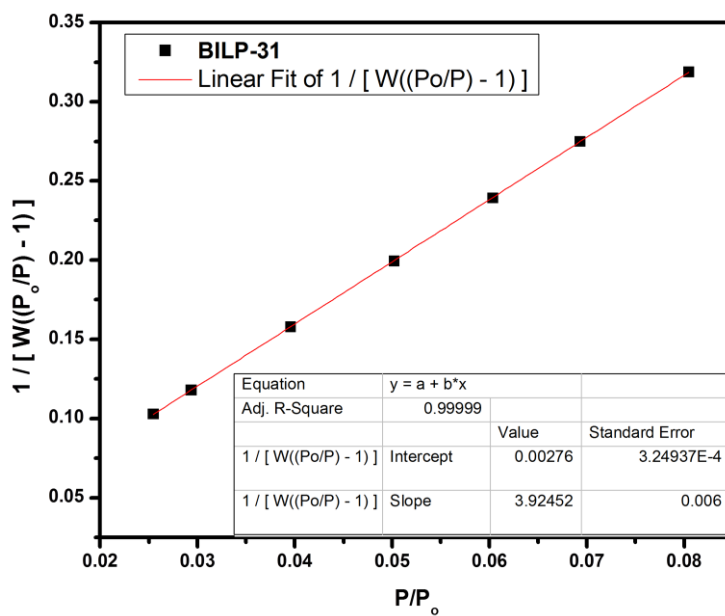
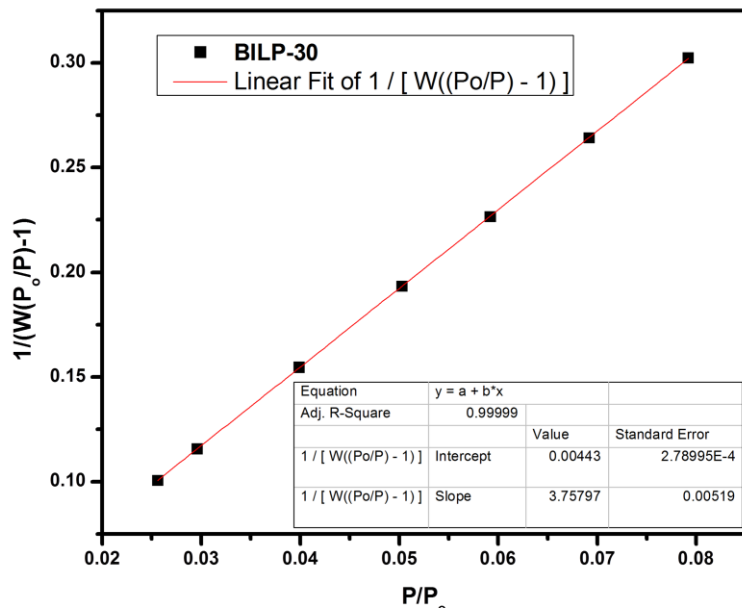


Figure 3.6: BET plot of BILP-30 and BILP-31 from N₂ isotherms at 77 K.

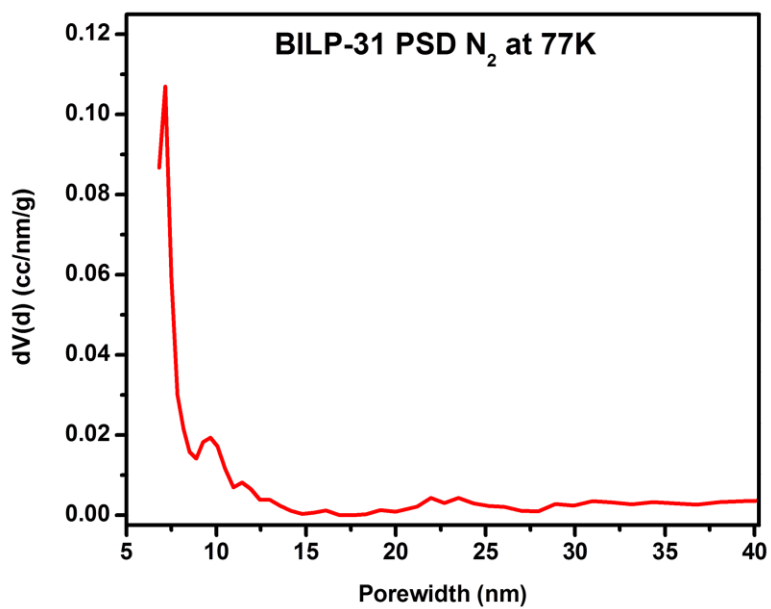
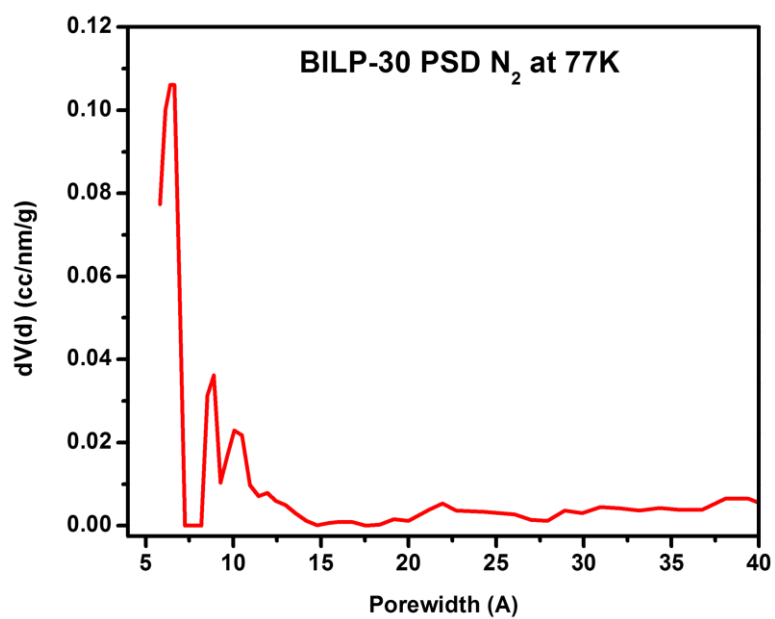


Figure 3.7: Pore size distribution of BILP-30 and BILP-31 from N_2 isotherms at 77 K

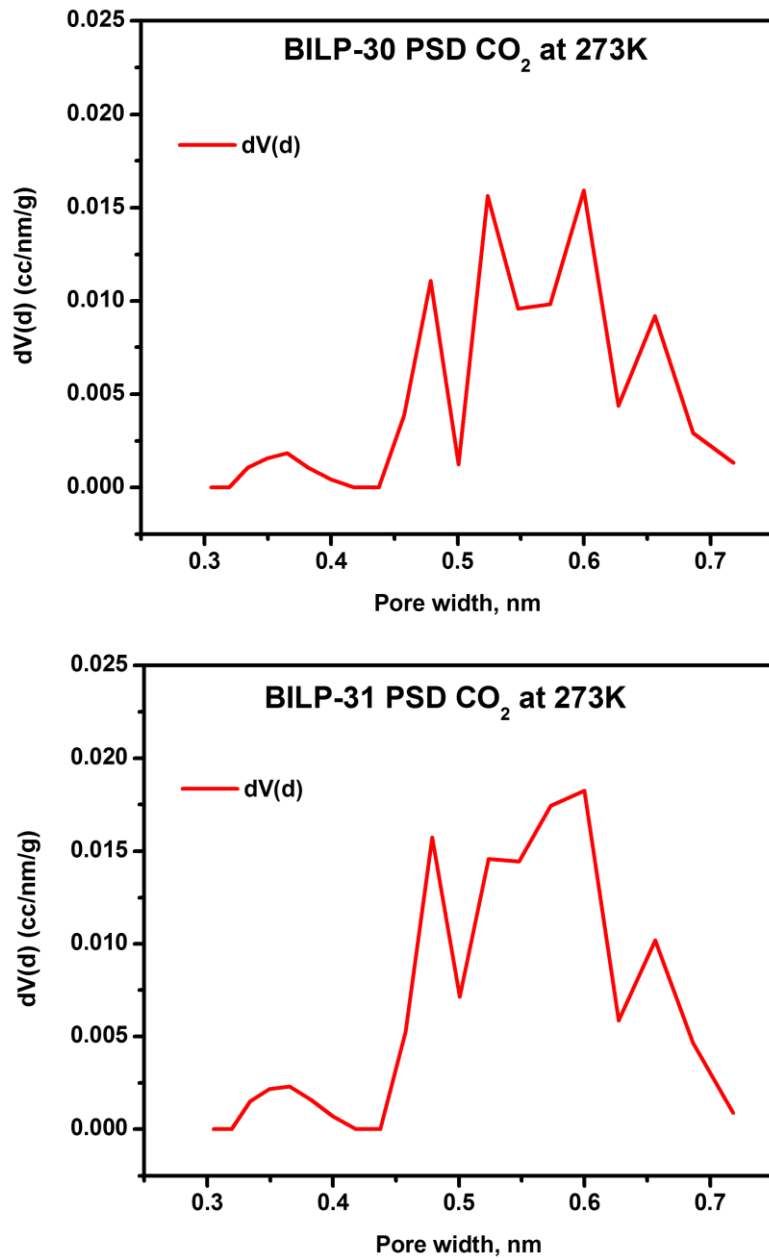


Figure 3.8: Pore size distribution of BILP-30 and BILP-31 from CO₂ isotherms at 273 K

BILP-30 and BILP-31 have dominant pores of around 0.83 and 0.79 nm respectively. The total pore volumes determined from single point adsorption values at $P/P_0 = 0.95$ are $0.53 \text{ cm}^3/\text{g}^{-1}$ and $0.48 \text{ cm}^3/\text{g}^{-1}$ for BILP-30 and -31 respectively. The micropore volume analysis from the quenched solid density functional theory (QSDFT) fitting showed that BILP-31 had a slightly higher percentage of micropores (57.7%) than BILP-30 (51.1%). Furthermore, the profile of ultramicropores, pores with width less than 0.7 nm, were elucidated by non-local density functional theory (NLDFT) fitting of the CO_2 isotherms at 273 K (Figure 8). Here, similar ultramicropore size distributions were observed, however, BILP-31 ($0.297 \text{ cm}^3/\text{g}^{-1}$) displays a slightly higher ultramicropore volume than BILP-30 ($\text{cm}^3/\text{g}^{-1}$). This is a significant observation as the nature and degree of presence of different types of pores in porous polymers play a critical role in their gas sorption and selectivity properties.

Table 3.1: Textural Properties of BILP-30 and -31

	^a $\text{SA}_{(\text{BET})}$	^b PSD	^c Pore Vol. _(Tot.)	^d Pore Vol. _(Mic.)	^e Pore Vol. _(Ult. Mic.)
	$\text{m}^2 \text{ g}^{-1}$	nm	$\text{cm}^3 \text{ g}^{-1}$	$\text{cm}^3 \text{ g}^{-1}$	$\text{cm}^3 \text{ g}^{-1}$
BILP-30	926	0.67	0.53	0.271(51.1)	0.0221
BILP-31	887	0.72	0.48	0.277(57.7)	0.0297

^aBrunauer–Emmett–Teller (BET) surface area. ^bDominant pore size determined by QSDFT fittings of N_2 isotherms at 77K. ^cTotal pore volume at $P/P_0 = 0.95$. ^dMicropore volume determined by DFT (the values in parenthesis are the percentage of micropore volume relative to total pore volume) ^ePore volume of ultramicropores (<0.7 nm) determined from CO_2 isotherms at 273K.

3.3.3 CO_2 Uptake Studies

Microporous materials possessing pores pre-dominantly below 0.1 nm have been known to exhibit desirable CO_2 capture and separation properties.¹⁵ To further elucidate such properties of BILP-30 and -31, single CO_2 gas isotherms were measured at 273 (Figure 3.9) and 298 K

(Figure 3.10). The CO₂ isotherms display minimal hysteresis indicating regenerability of the polymers by pressure reduction at ambient pressure or applying vacuum. The isotherms are also characterized by a steep rise at low pressures underlining strong interactions between CO₂ molecules and pore walls. This is due to the Lewis basic nature of imidazole moieties which display a strong affinity for acidic and polarizable CO₂ molecules.^{8,12,13} In comparison, BILP-31 displays a slightly higher CO₂ (4.47 and 3.14 mmol g⁻¹ at 273 and 298K respectively) uptake than BILP-30 (4.25 and 2.77 mmol g⁻¹ at 273 and 298K respectively) at 1 bar (Table 3.2). The higher uptake of BILP-31 can be attributed to its relatively narrow micropores which lead to enhanced interaction between CO₂ and the polymer's pore walls.⁴ The binding affinity of CO₂ to the polymers' pore walls was evaluated via their heat of adsorption, Q_{st} values, calculated using the Virial equation. At zero coverage, BILP-30 and -31 displayed Q_{st} values of 30.4 and 31.2 kJ mol⁻¹ respectively (Figure 3.11). The binding affinities gradually decrease with increasing CO₂ loading due to saturation of binding sites. The Q_{st} values of the BILPs are within close proximity of the optimum value for CO₂ capture from flue gas (~33 kJ mol⁻¹) as previously postulated in literature. The binding affinity of BILP-30 and -31 are within range of other BILPs and other nitrogen rich polymers including ALPs,^{4,16} azo-COPs¹⁷ and PECONFs.¹⁸ The CO₂ uptake at 1 bar is not a conclusive depiction of a porous material's performance to capture CO₂ from gas mixtures as the partial pressure of CO₂ varies depending on the ratio of gases present in the mixture. Given the partial pressure of CO₂ in flue gas, in the range of 0.1-0.15 bar, it is essential to assess the CO₂ uptake of polymers at the relevant low pressure to evaluate their potential application in post-combustion CO₂ capture applications. The CO₂ uptake of BILP-30 and -31 at 0.15 bar and 298K were found to be 0.84 and 1.07 mmol g⁻¹ respectively. These low pressure

values are comparable with previously reported benzimidazole polymers with BILP-31 displaying higher uptake than all ALPs.

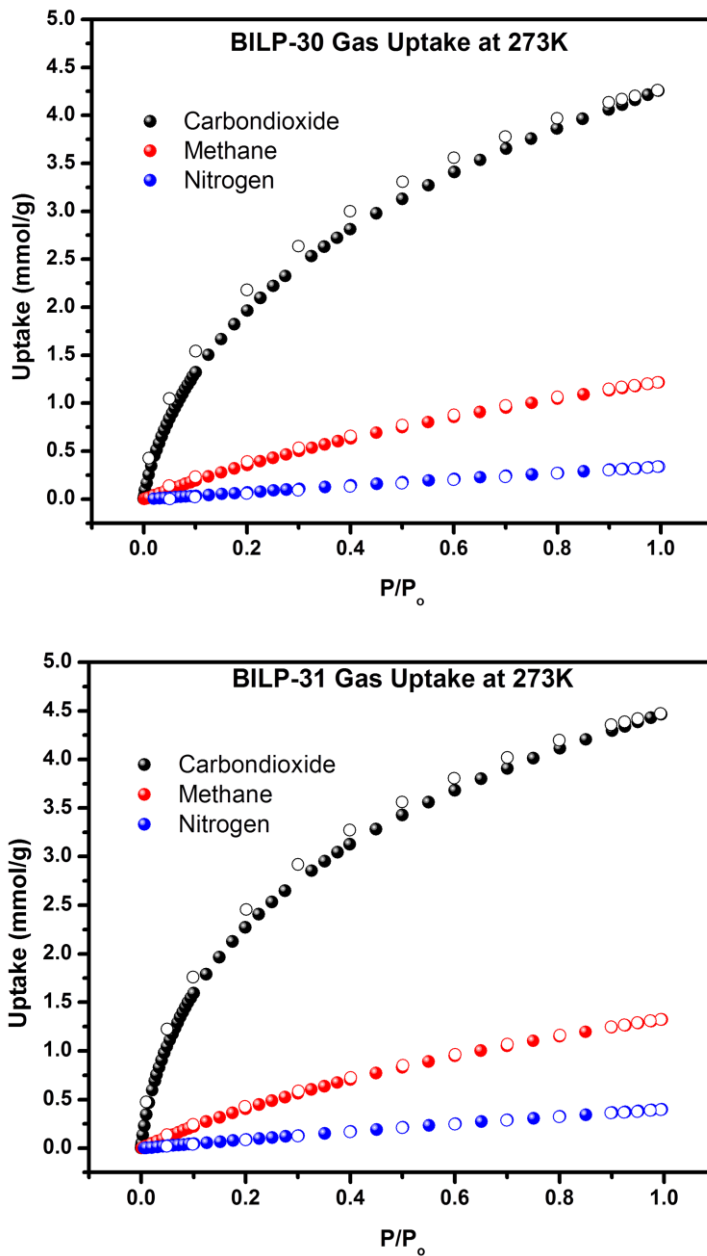


Figure 3.9: CO₂, CH₄ and N₂ uptake isotherms of BILP-31 at 273 K and 298 K

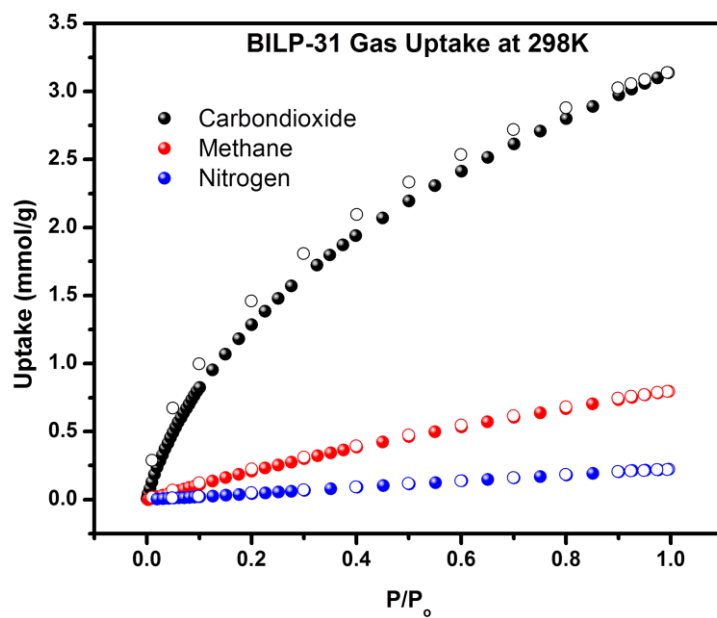
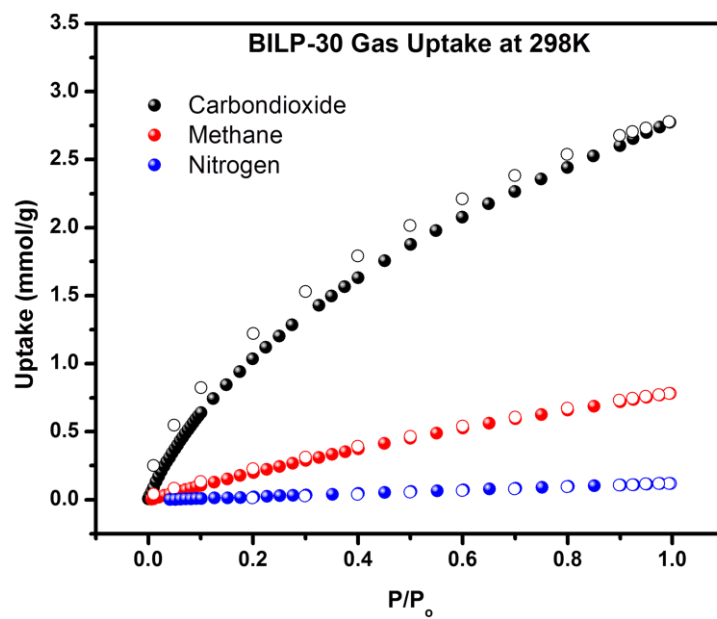


Figure 3.10: CO₂, CH₄ and N₂ uptake isotherms of BILP-31 at 273 K and 298 K

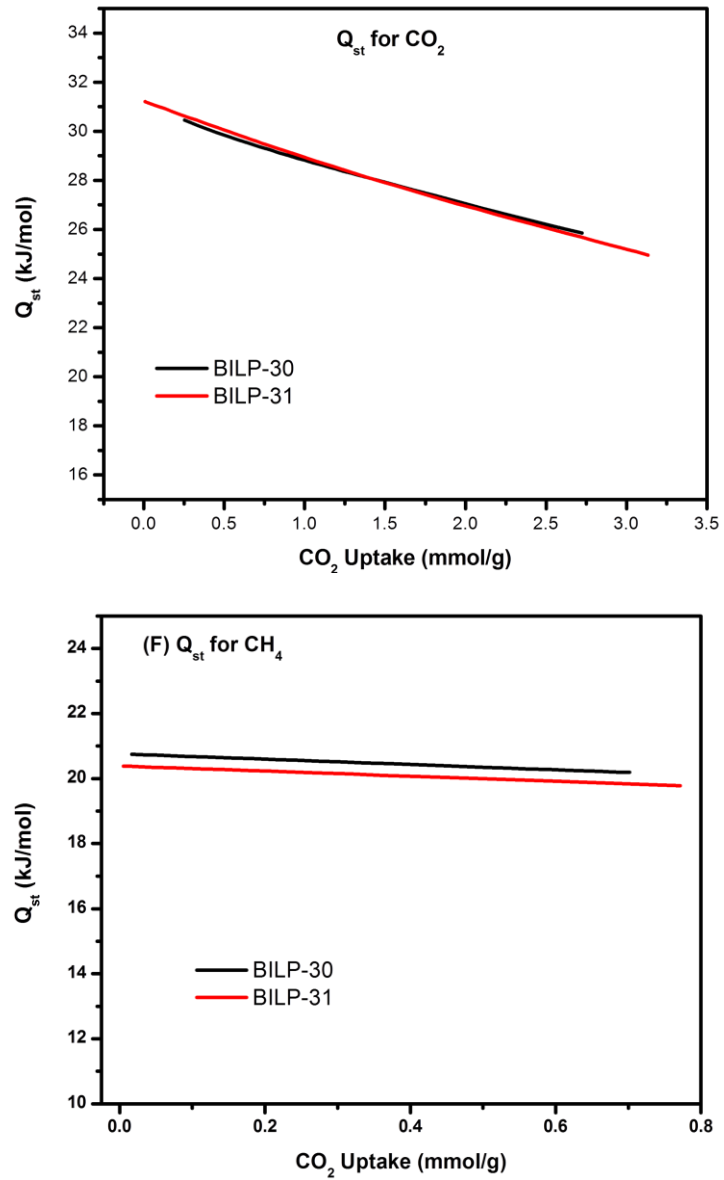


Figure 3.11: Isosteric heat of adsorption of CO₂ and CH₄ for BILP-30 and BILP-31 determined from virial equation.

3.3.4 Gas Selectivity Studies: CO₂ over N₂ and CH₄

BILP-30 and -31 possess some key properties including respectable surface area, Q_{st} , CO₂ uptake as well as narrow pores which make them promising candidates for selective capture of CO₂ in predominantly CO₂/N₂ and CO₂/CH₄ gas mixtures. To assess the viability of the BILPs for selective capture of carbondioxide over methane and nitrogen, single gas adsorption and desorption isotherms of CO₂, CH₄, and N₂ were collected at 273 and 298 K from 0-1 bar. By employing the ideal adsorbed solutions theory (IAST), a method that has been broadly established to deduce the selectivity values of adsorbents in gas mixtures from single-component isotherms, a thorough evaluation of BILPs' performance in CO₂ separations applications could be done. Selectivity values for BILP-30 and -31 were calculated for flue gas (CO₂:N₂ = 10:90) and landfill gas (CO₂:CH₄ = 50:50) at 273 and 298 K, as presented in Figure 3.12 and 3.13 respectively.

BILP-31 shows the higher CO₂/N₂ (70) and CO₂/CH₄ (11) selectivity at 273 K (Table 3.2) arising from its higher Q_{st} value resulting in high CO₂ uptake in the low pressure region. The trend of porous materials with higher binding affinity for CO₂ displaying high uptake and selectivity has been previously observed. It should be noted that CO₂/N₂ IAST selectivity for BILP-31 at 273 K is the highest observed for any BILP at this temperature. At 298 K, BILP-30 displays the higher CO₂/N₂ IAST selectivity of 61.4 which is amongst the best performing BILPs reported to date. BILP-101 has a CO₂/N₂ IAST selectivity of 70.1 due its ultramicroporous nature while TBILP-1 had a selectivity value of 62 aided by its bi-functional nature derived from its triazine and benzimidazole moieties. The higher selectivity of BILP-30 at 298 K stems from its relatively narrow pore size which is conducive for low N₂ uptake in contrast to CO₂ due to the higher kinetic diameter of the latter besides the ability of CO₂ to be polarized for dipole-

quadrupole interactions between CO₂ and imidazole functionalized pore walls. Additionally, the improved selectivity in BILP-30 is in line with the general trend of a trade-off between CO₂ capacity and CO₂/N₂ selectivity although this is not always to be expected. The CO₂/CH₄ selectivity is calculated at higher partial gas pressure of both gases therefore the uptake at these pressures has a direct correlation with selectivity. Previous reports have established that, CO₂ uptake is heavily dependent on pore functionality whereas CH₄ uptake is more influenced by surface area.¹⁹ This is in agreement with the high CO₂/CH₄ selectivity values for BILP-31 which has lower surface area than BILP-30.

When comparing the CO₂/N₂ selectivity at 273 versus 298 K, a decrease in value from 70 to 43 respectively is observed for BILP-31 while a slight increase in value is observed for BILP-30, from 57 to 60 respectively. This peculiar behavior in selectivity differences has been previously observed in porous organic polymers depending on the nature of their textural properties. Particularly, the concept of nitrogen-phobicity which is the phenomenon of increase in CO₂/N₂ selectivity with rising adsorption temperatures can suggest a rationale as to the differing selectivity behaviors of BILP-30 and -31. Nitrogen-phobicity is a concept that is has been observed to rely on the nature of the pore within in the porous polymers as opposed to their chemical functionality as it has been verified in polymers with identical functionalities. The increase in CO₂/N₂ selectivity with higher adsorption temperatures were attributed to polymers bearing a significant portion of mesopores leading to a decrease in N₂ uptake at such high temperatures.²⁰ Analyzing the N₂ isotherms at 77 K, BILP-31 displays a slightly more gradual increase of N₂ uptake at P/P₀ = 0.04-0.9 suggesting a lower level of mesopores present in the polymers. A quantitative analysis of the mesopore volume in the polymers using QSDFT fittings indicates BILP-30 and -31 bear 0.13 and 0.09 cc/g in the mesoporous volumes respectively.

Hence, the higher presence of mesopores present in BILP-30 results in the lower N_2 uptake at 298 K and 1 bar (0.12 mmol g^{-1}) relative to BILP-31 (0.22 mmol g^{-1}) leading to the high selectivity observed for BILP-30.

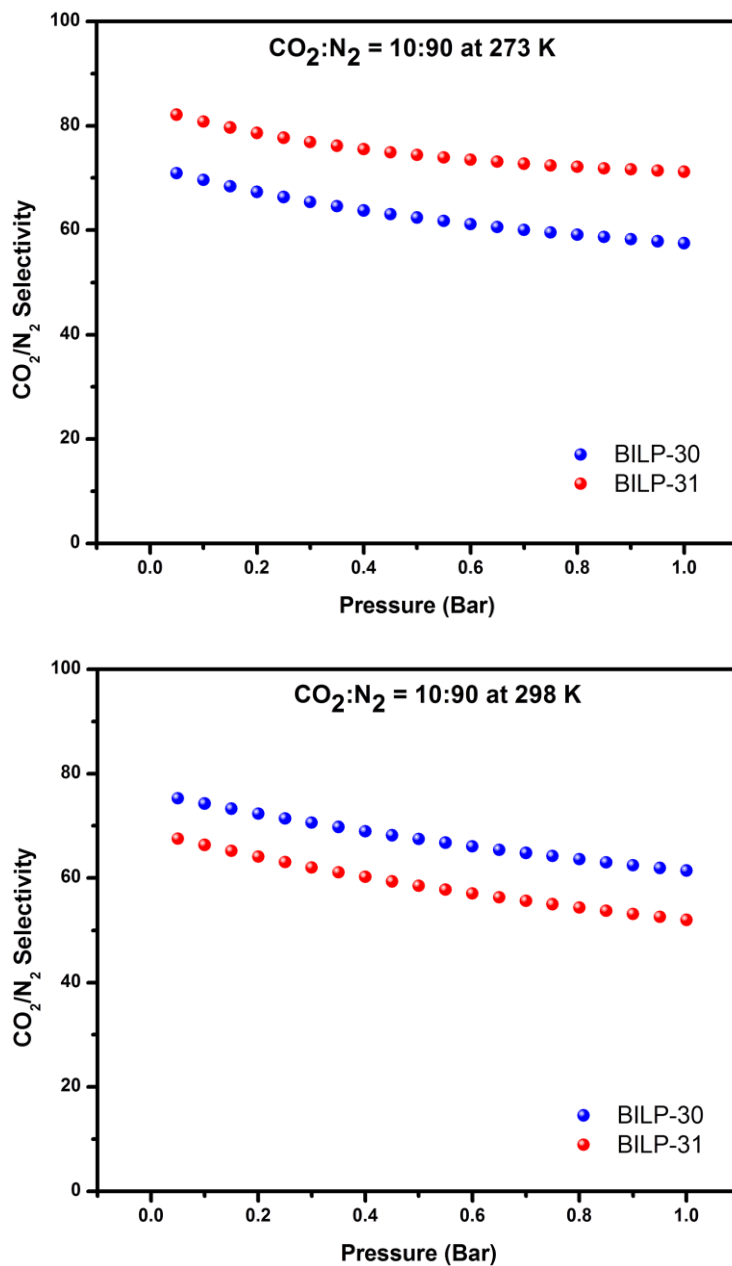


Figure 3.12: IAST CO₂/N₂ selectivity at 273K and 298 K of BILP-30 and BILP-31

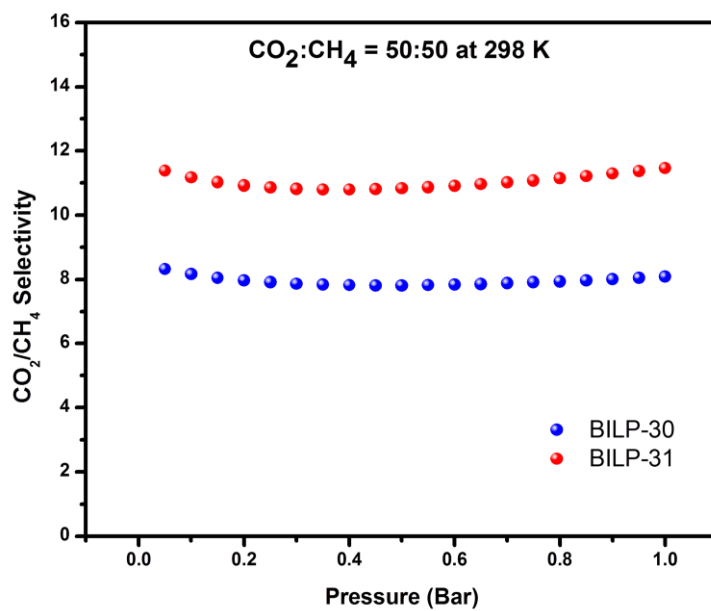
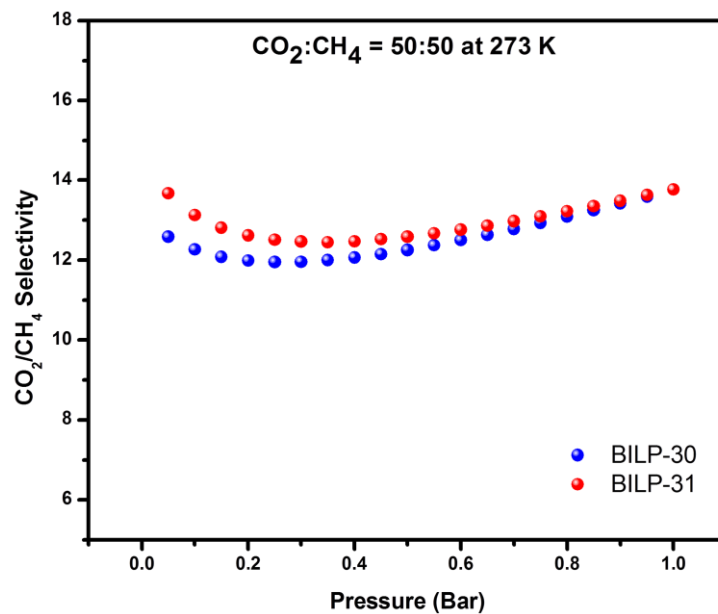


Figure 3.13: IAST CO₂/CH₄ selectivity at 273K and 298 K for BILP-30 and BILP-31

Table 3.2: Gas uptakes, heat of adsorption and selectivity of BILPs

Polymer	^a CO ₂ uptake at 1 bar			^a CH ₄ uptake at 1 bar			^a N ₂ uptake at 1 bar		^b Selectivity	
	273K	298K	Q _{st}	273K	298K	Q _{st}	273K	298K	CO ₂ /N ₂	CO ₂ /CH ₄
BILP-30	4.26	2.77	30.4	2.07	1.22	20.8	0.34	0.12	57 (61)	5 (4)
BILP-31	4.47	3.14	31.2	1.33	0.80	20.4	0.40	0.19	70 (52)	14 (11)

^aGas uptake in mmol g⁻¹, and isosteric heat of adsorption (Q_{st}) at zero coverage in kJ mol⁻¹. ^bSelectivity (mol mol⁻¹, at 1.0 bar) calculated by IAST method at mole ratio of 10:90 for CO₂/N₂ and mole ratio of 50:50 for CO₂/CH₄ at 273 K and (298 K)

3.3.5 Performance of BILP-30 and BILP-31 in CO₂ Separation from Flue Gas Using VSA

Assuming a CO₂:N₂ molar composition of 10:90, the performance of the BILPs in CO₂ separation was assessed at 298 K under vacuum swing adsorption settings. The five sorbent criteria outlined by Bae and Snurr,²¹ (discussed in detail in Chapter 2) were calculated and presented in Table 3.3 along with other top performing porous materials. The parameters were calculated by setting the adsorption pressure (P^{ads}) to 1 bar and the desorption pressure (P^{des}) to 0.1 bar. BILP-31 has a higher working capacity compared to BILP-30 due to its higher Q_{st} for CO₂ and high uptake when the partial pressure of CO₂ in flue gas mixture is taken into account. The working capacity of BILP-31 was at 0.68 mol kg⁻¹ which exceeds MOFs such as ZIF-78,²¹ SNU-CI-sca²² and MOF-4b. It is also superior to some of the best performing POPs including ALPs, BILPs and TBILPs. In terms of the sorbent selection parameter, S, value, BILP-30 (337.4) performs better than BILP-31 (154.4) due to the high working capacity of BILP-30 for nitrogen. The S value for BILP-30 is amongst the highest of the best performing porous materials.

Table 3.3. VSA evaluation criteria for CO₂ separation from flue gas^a

	N_I^{ads}	ΔNI	%R	α_{12}^{ads}	S
BILP-30	0.63	0.54	86.44	61.42	337.40
BILP-31	0.81	0.69	85.30	52.02	227.24
ALP-5 ⁴	2.07	1.67	80.90	8.30	75.00
BILP-101 ⁶	0.95	0.80	84.80	70.30	556.00
SNU-Cl-sca ²²	1.99	0.41	87.30	38.00	262.00
Zeolite-13X ²¹	3.97	1.35	54.20	86.20	128.00
Ni-MOF-74 ²¹	6.23	3.20	73.70	41.10	83.50

^aCO₂/N₂ = 10:90, T = 298 K, P^{ads} = 1 bar, and P^{des} = 0.1 bar.

3.3.6 Performance of BILP-30 and BILP-31 in CO₂ Separation from Landfill Gas Using VSA

Landfill gas is an attractive alternative as a source of energy as it does not result in the emission of greenhouse gases. However, the significant amount of CO₂, 40-60%, found in landfill gas needs to be separated in order to enhance energy density as well as prevent corrosion of fuel vessels and pipelines. Given the high CO₂/CH₄ selectivity of BILP-30 and -31, their performance in CO₂ separation from CO₂:CO₄ molar ratios of 50:50 with adsorption and desorption pressures of 1 and 0.1 bar respectively were evaluated. BILP-31 shows a higher working capacity than BILP-30 due to its high CO₂ uptake. The high CO₂/CH₄ selectivity and high working capacity contribute to BILP-31 having the highest S value amongst some of the best performing POPs reported to date (Table 3.4).

Table 3.4. VSA evaluation criteria for CO₂ separation from landfill gas^a

	N_I^{ads}	ΔNI	% R	α_{12}^{ads}	S
BILP-30	1.92	1.56	81.16	8.09	64.63
BILP-31	2.33	1.84	79.16	11.46	135.68
ALP-1 ¹⁶	2.04	1.73	85.1	5.8	35.1
ALP-5 ⁴	2.07	1.67	80.9	8.3	75
BILP-12 ²³	2.01	1.71	85.3	6	33.7
TBILP-2 ¹²	2.2	1.84	83.7	7.6	62.5
BILP-6-NH ₂	2.63	2.14	81.3	8.4	76
NPOF-1-NH ₂	2.53	2.1	82.9	9.9	91

^aCO₂/CH₄ = 50:50, T = 298 K, P^{ads} = 1 bar, and P^{des} = 0.1 bar.

3.3.7 Conclusion

In this project, two new BILP polymers have been designed and synthesized. The aldehyde monomers used were selected considering a topology-directed approach for the fabrication of POPs using rigid and star shaped monomers. The porosity and gas uptake properties of the polymers were assessed and subsequent analysis of these properties enabled a thorough depiction for the potential of polymers in application for CO₂ separation from flue and landfill gas using VSA processes. BILP-31 displays a respectable Q_{st} value for CO₂ of 31.2 kJ mol⁻¹ relative to other BILPs and POPs alike. At 1 bar, BILP-31 has a higher CO₂ uptake of 4.17 and 3.13 mmol g⁻¹ at 273 and 298 K respectively. This is due to its high Q_{st} for CO₂ and higher micropore volume. In terms of CO₂/N₂ selectivity at 298 K, BILP-30 is superior due to its narrow pore size while BILP-31 has a higher CO₂/CH₄ selectivity influenced by the high CO₂ uptake at higher partial pressures. Furthermore, the selective capture of CO₂ from flue gas and landfill gas under VSA conditions were investigated and the results rationalized via the textural

and gas uptake properties of the polymers as well as compared to some of the best performing polymers reported to date.

3.3.8 References

- (1) Xing, W.; Liu, C.; Zhou, Z.; Zhang, L.; Zhou, J.; Zhuo, S.; Yan, Z.; Gao, H.; G., W.; Qiao, S. Z. No Title. *Energy Environ. Sci.* **2012**, *5*, 7323–7327.
- (2) Xia, Y.; Mokaya, R.; Walker, G. S.; Zhu, Y. No Title. *Adv. Energy Mater.* **2011**, *1*, 678–683.
- (3) Talapaneni, S. N.; Buyukcakir, O.; Je, S. H.; Srinivasan, S.; Seo, Y.; Polychronopoulou, K.; Coskun, A. No Title. *Chem. Mater.* **2015**, *27*, 6818–6826.
- (4) Arab, P.; Parrish, E.; Islamoglu, T.; El-kaderi, H. M. Synthesis and Evaluation of Porous Azo-Linked Polymers for Carbon Dioxide Capture and Separation. *Mater. Chem. A* **2015**, 20586–20594.
- (5) Zou, X.; Rena, H.; Zhu, G. Topology-Directed Design of Porous Organic Frameworks and Their Advanced Applications. *Chem. Commun.* **2013**, *49*, 3925–3936.
- (6) Sekizkardes, A. K.; Culp, J. T.; Islamoglu, T.; Marti, A.; Hopkinson, D.; Myers, C.; El-Kaderi, H. M.; Nulwala, H. B. An Ultra-Microporous Organic Polymer for High Performance Carbon Dioxide Capture and Separation. *Chem. Commun. (Camb)*. **2015**, *51* (69), 13393–13396.
- (7) Bhunia, A.; Vasylyeva, V.; Janiak, C. From a Supramolecular Tetranitrile to a Porous Covalent Triazine-Based Framework with High Gas Uptake Capacities. *Chem. Commun.* **2013**, *49*, 3961–3963.
- (8) Rabbani, M. G.; El-Kaderi, H. M. Synthesis and Characterization of Porous Benzimidazole-Linked Polymers and Their Performance in Small Gas Storage and Selective Uptake. *Chem. Mater.* **2012**, *24* (8), 1511–1517.
- (9) Altarawneh, S.; Islamoglu, T.; Sekizkardes, A. K.; El-kaderi, H. M. Effect of Acid-

- Catalyzed Formation Rates of Benzimidazole-Linked Polymers on Porosity and Selective CO₂ Capture from Gas Mixtures. *Environ. Sci. Technol.* **2015**, *49* (7), 4715–4723.
- (10) Thommes, M.; Kaneko, K.; Neimark, A. V.; Olivier, J. P.; Rodriguez-Reinoso, F.; Rouquerol, J.; Sing, K. S. W. Physisorption of Gases, with Special Reference to the Evaluation of Surface Area and Pore Size Distribution (IUPAC Technical Report). *Pure Appl. Chem.* **2015**, *87*, 1051–1069.
- (11) Islamoglu, T.; Behera, S.; Kahveci, Z.; Tessema, T.-D.; Puru, J.; El-kaderi, H. M. Enhanced Carbon Dioxide Capture from Land Fill Gas Using Bifunctionalized Benzimidazole-Linked Polymers. *ACS Appl. Mater. Interfaces* **2016**, *8*, 14648–14655.
- (12) Sekizkardes, A. K.; Altarawneh, S.; Kahveci, Z.; Islamoglu, T.; El-kaderi, H. M. Highly Selective CO₂ Capture by Triazine-Based Benzimidazole-Linked Polymers. *Macromolecules* **2014**, *47*, 8328–8334.
- (13) Altarawneh, S.; Behera, S.; Jena, P.; El-Kaderi, H. M. New Insights into Carbon Dioxide Interactions with Benzimidazole-Linked Polymers. *Chem. Commun. (Camb)*. **2014**, *50* (27), 3571–3574.
- (14) Demirocak, Derviş Emre; Ram, M. K. ; Srinivasan, S.; Goswami, D. Yogi; Stefanakos, E. K. A Novel Nitrogen Rich Porous Aromatic Framework for Hydrogen and Carbon Dioxide Storage. *J. Mater. Chem. A* **2013**, *1*, 13800–13806.
- (15) Ben, T.; Li, Y.; Zhu, L.; Zhang, D.; Cao, D.; Xiang, Z.; Yao, X.; Qiu, S. Selective Adsorption of Carbon Dioxide by Carbonized Porous Aromatic Framework (PAF). *Energy Environ. Sci.* **2012**, *5*, 8370–8376.
- (16) Arab, P.; Rabbani, M. G.; Sekizkardes, A. K.; Islamoglu, T.; El-kaderi, H. M. Copper(I)-Catalyzed Synthesis of Nanoporous Azo-Linked Polymers: Impact of Textural Properties

- on Gas Storage and Selective Carbon Dioxide Capture. *Chem. Mater.* **2014**, *26*, 1385–1392.
- (17) Patel, H. A.; Je, S. H.; Park, J.; Chen, D. P.; Jung, Y.; Yavuz, C. T.; Coskun, A. Unprecedented High-Temperature CO₂ Selectivity in N₂-Phobic Nanoporous Covalent Organic Polymers. *Commun. Nat.* **2013**, *4*, 1357.
- (18) Mohanty, P.; Kull, L. D.; Landskron, K. Porous Covalent Electron-Rich Organonitridic Frameworks as Highly Selective Sorbents for Methane and Carbon Dioxide. *Nat. Commun.* **2011**, *2*, DOI: 10.1038/ncomms1405.
- (19) Islamoglu, T.; Rabbani, Mohammad Gulam El-Kaderi, H. M. Impact of Post-Synthesis Modification of Nanoporous Organic Frameworks on Small Gas Uptake and Selective CO₂ Capture. *J. Mater. Chem. A* **2013**, *1*, 10259–10266.
- (20) Lee, J. H.; Lee, H. J.; Lim, S. Y.; Kim, B. G.; Choi, J. W. Combined CO₂-Philicity and Ordered Mesoporosity for Highly Selective CO₂ Capture at High Temperatures. *J. Am. Chem. Soc.* **2015**, *137* (22), 7210–7216.
- (21) Bae, Y.-S.; Snurr, R. Q. Development and Evaluation of Porous Materials for Carbon Dioxide Separation and Capture. *Angew. Chemie - Int. Ed.* **2011**, *50* (49), 11586–11596.
- (22) Xie, L.-H. .; Suh, M. P. High CO₂-Capture Ability of a Porous Organic Polymer Bifunctionalized with Carboxy and Triazole Groups. *Chem. - Eur. J.* **2013**, *19* (35), 11590–11597.
- (23) Sekizkardes, A. K.; Kahveci, Z.; El-kaderi, H. M. Application of Pyrene-Derived Benzimidazolelinked Polymers to CO₂ Separation under Pressure and Vacuum Swing Adsorption Settings. *J. Mater. Chem. A* **2014**, *2*, 12492–12500.

Chapter 4

Highly Porous Pyrene Driven Azo-Functionalized Porous Nanofibers for CO₂ Capture and Separation Applications

4.1 Introduction

Chemical functionality of porous organic polymers has been found to be highly influential in enhancing the CO₂ binding affinity to pore walls and therefore implicative of their CO₂ uptake as well as selectivity over gases such as nitrogen and methane. Functional groups that introduce dipole-quadrupole and/or hydrogen bonding between CO₂ and porous frameworks have been utilized to improve the performance of porous sorbents in selective CO₂ capture application. This approach has been implemented by using both post- and pre-synthetic modification of sorbents. Alternatively, the use of building blocks rich in polar groups such as nitrogen and oxygen has been extensively explored. Recent reports of porous organic polymers functionalized by nitrogen-nitrogen double bonds, azo-bonds, have introduced a class of materials with exceptional CO₂ adsorption and selectivity with potential for targeted applications in selective CO₂ capture from flue gas and landfill gas mixtures.¹⁻⁴ In this project, a new azo-bond functionalized polymer, Azo-Py, has been synthesized using a 1,3,6,8-tetra(4-aminophenyl)pyrene monomer and a CuBr catalyzed oxidative homocoupling reaction.⁵ We have shown that the electron rich and rigid pyrene core of 1,3,6,8-tetra(4-aminophenyl)pyrene leads to a highly porous polymer exhibiting a solid state packing behavior resulting in a nanofiber morphology. This was facilitated by π - π stacking of the highly conjugated pyrene group. Furthermore, the CO₂ uptake and separation performance of Azo-Py were studied for flue gas and landfill gas mixtures.

4.2. Experimental Section

4.2.1 General Techniques and Materials

All solvents, starting materials and reagents were purchased from Acros Organics and used without any further purification unless otherwise noted. 4-Aminophenylboronic acid pinacol ester and tetrakis(triphenylphosphine)palladium(0) were purchased from Aldrich. Air sensitive materials and reactions were handled or carried out in an inert atmosphere (nitrogen gas) using glove box or Schlenk line techniques. Elemental analysis was done at American University of Sharjah, UAE. Liquid ^1H NMR was conducted using a Varian Mercury-400 MHz NMR spectrometer. FT-IR spectra were obtained using a Nicolet-Nexus 670 spectrometer equipped with an attenuated total reflectance accessory. Thermal stability of the synthesized polymers was assessed using a Perkin thermo-gravimetric analyzer with a temperature ramp rate of $5\text{ }^\circ\text{C}/\text{min}$ under N_2 flow. Scanning electron microscope (SEM) images were obtained to the morphology of the polymers using a Hitachi SU-70 FE-SEM. The samples were prepared by dispersion onto a double sided carbon tape attached to a sample holder followed by a platinum coating for 70 seconds at 1×10^{-6} bar. Powder X-ray diffraction data were collected using a Panalytical X'pert pro multipurpose diffractometer by a $\text{Cu K}\alpha$ radiation with a 2θ range of 2-30. Porosity and gas uptake studies were conducted using a Quantachrome Autosorb iQ volumetric analyzer using gases of ultra- high purity grade. Typically, an Azo-Py sample (~40-50 mg) was loaded into a pre-weighed 9 mm large bulb Quantachrome cell which was then hooked up to the degassing station of the gas analyzer. The sample was then degassed at $120\text{ }^\circ\text{C}$ and 1.0×10^{-5} bar for 12h. The degassed sample and cell were refilled with helium, weighed and hooked up to the analysis station of the gas analyzer. Adsorption temperatures were attained using a temperature

controlled water/ethylene glycol mixture bath for 273 and 298 K and a refrigerated bath of liquid nitrogen for 77 K.

4.2.2 Synthesis of 1,3,6,8-tetrabromopyrene

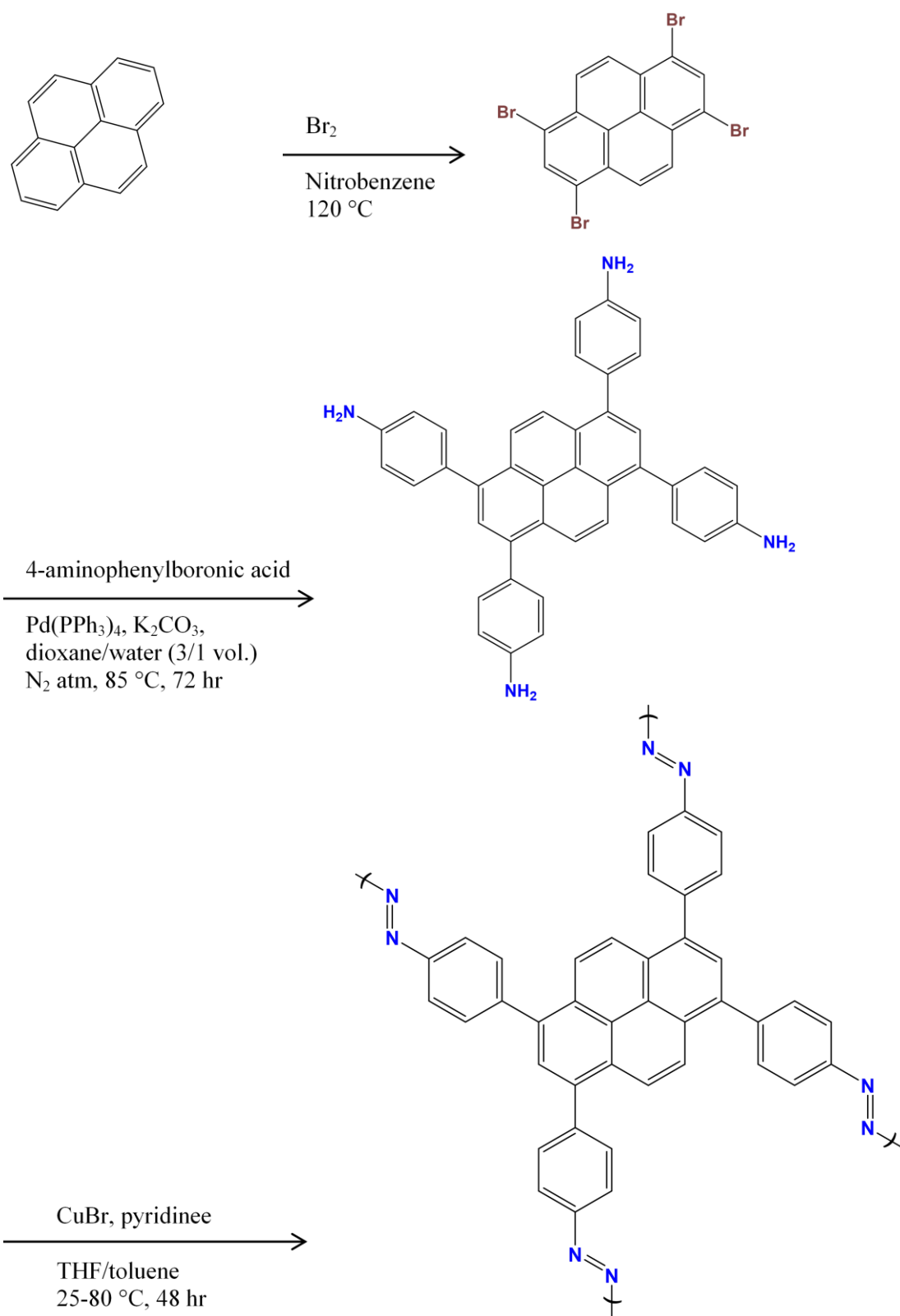
Tetrabromopyrene was synthesized following a previously reported procedure.⁶ Briefly, a solution of pyrene (5.0 g, 0.025 mol) in nitrobenzene was heated to 120 °C to which neat bromine (18 g, 0.23 mmol) was added dropwise while stirring vigorously. The resulting mixture was maintained at 120 °C for 4 hours and cooled down to room temperature. The precipitate was filtered, washed with excess ethanol and dried under vacuum to yield a pale-green solid product (10.3 g, 86%). The product was found to be insoluble in common organic solvents as reported.

4.2.3 Synthesis of 1,3,6,8-tetra(4-aminophenyl)pyrene

1,3,6,8-tetra(4-aminophenyl)pyrene was synthesized by adopting a previously reported method.⁷ A 250 mL Schlenk flask was charged with a mixture of dioxane:water (60 mL, 3:1 vol.), tetrabromopyrene (1.0 g, 1.93 mmol), 4-Aminophenylboronic acid pinacol ester (2.0 g, 9.1 mmol), tetrakis(triphenylphosphine)palladium(0) (0.21 g, 0.2 mmol), and potassium carbonate (1.45 g, 10.5 mmol). The mixture was degassed by bubbling with nitrogen gas for 30 minutes while stirring and refluxed at 100 °C for 72 hours. The reaction mixture was allowed to cool and the crude product isolated by filtration, washed with excess water and excess methanol and dried under vacuum to yield a light green solid product (0.65 g, 65%). ¹H NMR (400 MHz, d₆-DMSO, 25 °C): δ = 8.12 (s, 4 H), 7.79 (s, 2 H), 7.35 (d, 4 H), 6.78 (d, 4H), 5.31 (s, 8 H).

4.2.4 Synthesis of Azo-Py

Azo-Py was synthesized following a procedure established and further optimized by El-Kaderi *et. al.*^{3,4} A solution of CuBr (25 mg, 0.174 mmol) and pyridine (110 mg, 1.391 mmol) in 11 mL of toluene was stirred at 25 °C for 3 hours in a 50 mL round bottom flask and open air



Scheme 4.1: Synthetic route for the preparation of Azo-Py

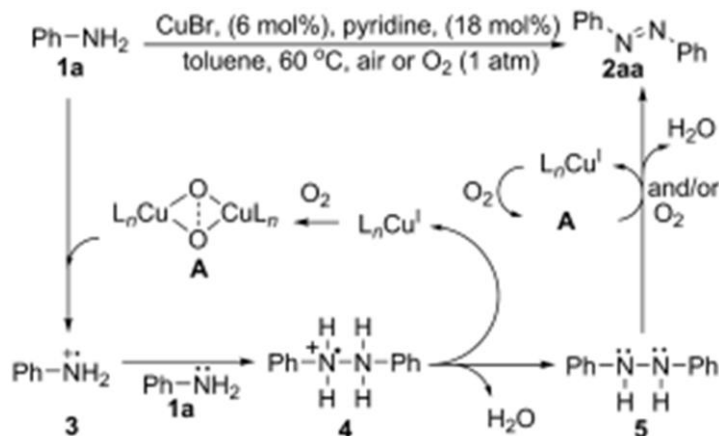
atmosphere. To this solution, 1,3,6,8-tetra(4-aminophenyl)pyrene (100 mg, 0.176 mmol) dissolved in 11 mL THF was added. The mixture was stirred in an open air atmosphere at 25 °C for 24 hours, refluxed at 60 °C for 12 hours, and then at 80 °C for 12 hours. A burgundy colored solid was isolated by filtration and subsequently washed with THF and water. The obtained powder was stirred in HCl (100 mL, 2 M) for 12 h, then filtered and washed with water. The powder was further treated with NaOH (2 M), water, ethanol, THF, and chloroform. The final product was dried at 120 °C under vacuum (150 mTorr) to give Azo-Py as a burgundy colored powder (82 mg, 83%). Anal. Calcd. for C₄₀H₂₂N₄: C, 86.00%; H, 3.97%; N 10.03% Found C, 70.76%; H, 4.39%; N 8.23%

4.3 Results and Discussion

4.3.1 Synthesis and characterization of Azo-Py

Azo-Py was prepared via an oxidative homocoupling of an aniline functionalized monomer with a pyrene core yielding robust azo bonded linkages as presented in Scheme 1. This polymerization reaction has carried out following our recent report which outlined the optimum amount of CuBr, solvent composition as well as temperature ramp profile in order to enhance the porosity of the resulting polymer.³ The mechanism for the CuBr catalyzed azo-bond formation has been proposed by Jiao *et. al* in a study where both symmetric and unsymmetric substituted azobenzenes have been prepared (Scheme 2).⁵ They propose that the copper(I) salt is chelated by a pyridine ligand and oxidized by oxygen molecule resulting in an active (μ - η^2 : η^2 -peroxo)dicopper(II) complex (A). A single electron oxidation of the amino group facilitated by the copper(II) forms a radical cation (3). The cation then couples with an amino group to form a three-electron sigma bond (4) which proceeds to donate two protons and one electron leading to

hydrazine (5). Finally, the hydrazine is further oxidized by the $(\mu-\eta^2:\eta^2\text{-peroxo})\text{dicopper(II)}$ complex or O_2 to form the azo bond.⁵



Scheme 4.2: Proposed mechanism of Azo bond formation by the catalytic acid process⁵

Azo-Py is insoluble in common organic solvents such as water, THF, chloroform, toluene, and ethanol depicting its structure as a highly cross-linked framework. Polymerization of Azo-Py was confirmed using FITR spectroscopy (Figure 4.1). Vibration bands in the region of 1415-1400 cm^{-1} signify the presence of azo-bonds expected in Azo-Py. Also, the decrease in intensity of the N-H stretching bands at 3200-3450 cm^{-1} indicates the consumption of secondary amines of the monomer taking part in the azo bond formation. It should be noted that unreacted terminal amines are seen as expected in the FTIR spectra of Azo-Py. The thermal stability of Azo-Py was assessed by thermogravimetric analysis (TGA) which showed stability up to 500 °C (Figure 4.2). Powder X-ray diffraction revealed an amorphous material as there were no distinct peaks in the spectra (Figure 4.3). Scanning electron microscopy (SEM) images show Azo-Py formed a nanofibrous morphology similar to previously reported BILPs bearing a pyrene core.^{8,9} It is presumed that these nanofibers, which are about 0.2 nm in thickness and varying length, result from π - π stacking interactions induced by the rigid and highly conjugated pyrene cores.

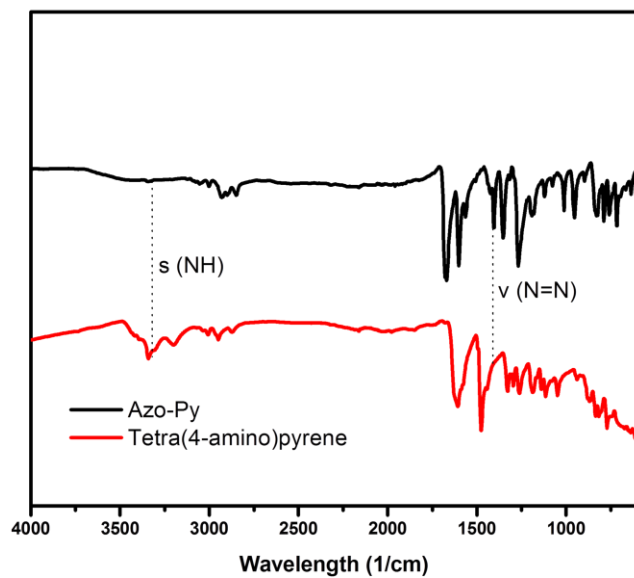


Figure 4.1: FT-IR spectra of of Azo-Py and tetra(4-amino)pyrene

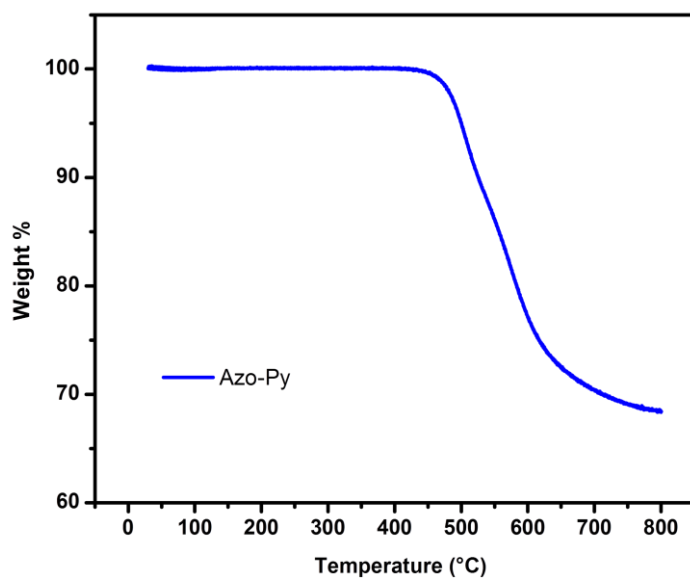


Figure 4.2: Thermogravimetric analysis of Azo-Py

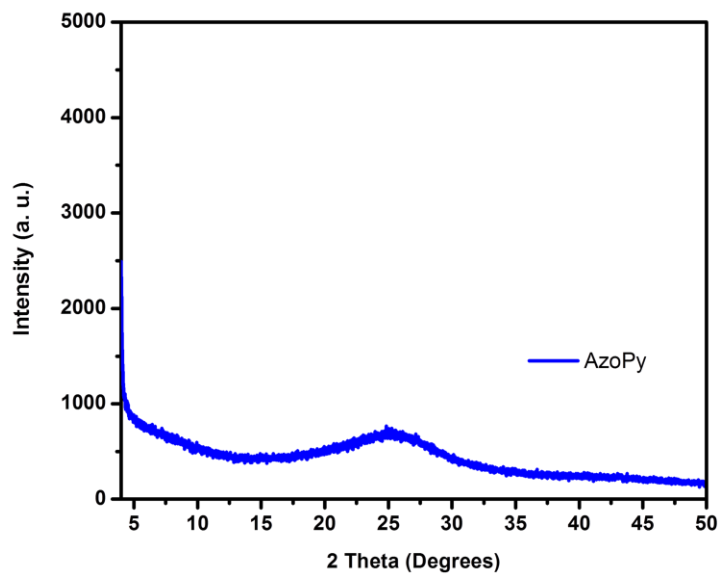


Figure 4.3: Powder X-ray diffraction patterns of Azo-Py



Figure 4.4: Scanning electron microscopy (SEM) image of Azo-Py

4.3.2 Porosity and textural properties

The porosity and textural properties of Azo-Py were characterized from its nitrogen isotherm at 77 K (Figure 4.4). A steeply increasing uptake is observed at lower pressure ranges (<0.035) followed by a decline in the slope of uptake in higher pressure ranges (0.035-0.9). This trend is indicative of a material with a highly microporous nature as well as a minor mesoporous pore size distribution.^{10,11} Textural properties of Azo-Py are summarized in Table 4.1. The Brunauer-Emmett-Teller (BET) model was used to calculate the specific surface area from the adsorption branch of Azo-Py which was $1259 \text{ m}^2 \text{ g}^{-1}$. This surface area is higher than previously reported azo-bond functionalized POPs including ALPs ($412\text{-}1235 \text{ m}^2 \text{ g}^{-1}$)^{3,4}, azo-COPs ($493\text{-}729 \text{ m}^2 \text{ g}^{-1}$)¹ and azo-POFs ($439\text{-}712 \text{ m}^2 \text{ g}^{-1}$)². Particularly, it is higher than some of the BILPs bearing a pyrene backbone including BILP-10, 11 and 13 ($658\text{-}787 \text{ m}^2 \text{ g}^{-1}$).⁸ A direct comparison can be made with BILP-10 ($787 \text{ m}^2 \text{ g}^{-1}$) as it is the benzimidazole linked analog to Azo-Py. In terms of surface area, Azo-Py is significantly superior. This is a testament to optimized synthetic route implemented for achieving high porosity in ALPs that we recently reported.³ However, BILP-12 displays a higher surface area than Azo-Py due to the incorporated triptycene building which has an internal molecular free volume (IMFV).¹² A pore size distribution curve was generated by fitting the adsorption branch of the N_2 isotherm at 77 K to QSDFT model for slit and cylindrical pores for carbon (Figure 4.6). The curve shows a dominant pore size centered at 0.64 nm for Azo-Py. The total pore volume of the polymer was deduced from a single adsorption, $P/P_0 = 0.95$, and found to be $0.699 \text{ cm}^3 \text{ g}^{-1}$. The micropore volume was also determined to be $0.377 \text{ cm}^3 \text{ g}^{-1}$ making up 53.9% of the total pore volume. Additionally, the profile of ultra-micropores ($< 0.7 \text{ nm}$) was elucidated by NLDFT fitting of the adsorption branch of the CO_2 isotherm at 273 K (Figure 4.7) with the ultra-micropore volume quantified to be $0.016 \text{ cm}^3 \text{ g}^{-1}$.

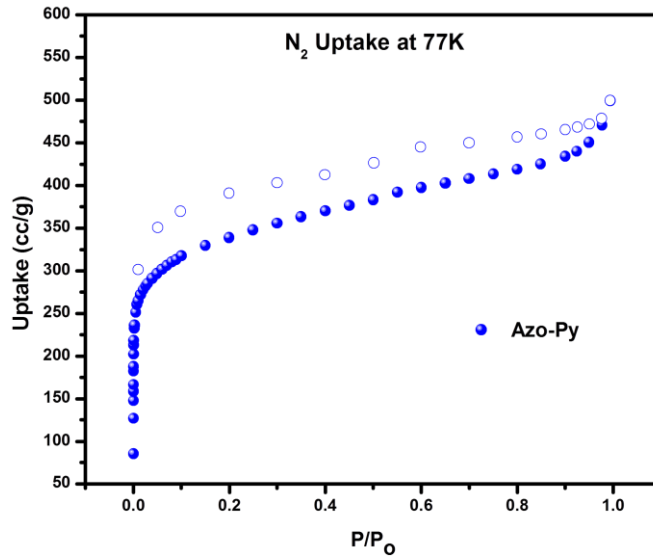


Figure 4.5: N₂ isotherm of Azo-Py at 77 K

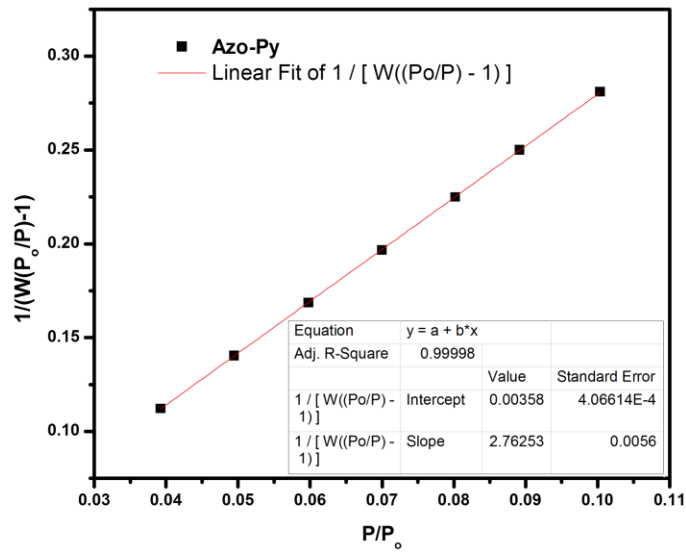


Figure 4.6: BET plot of Azo-Py from N₂ isotherm at 77 K

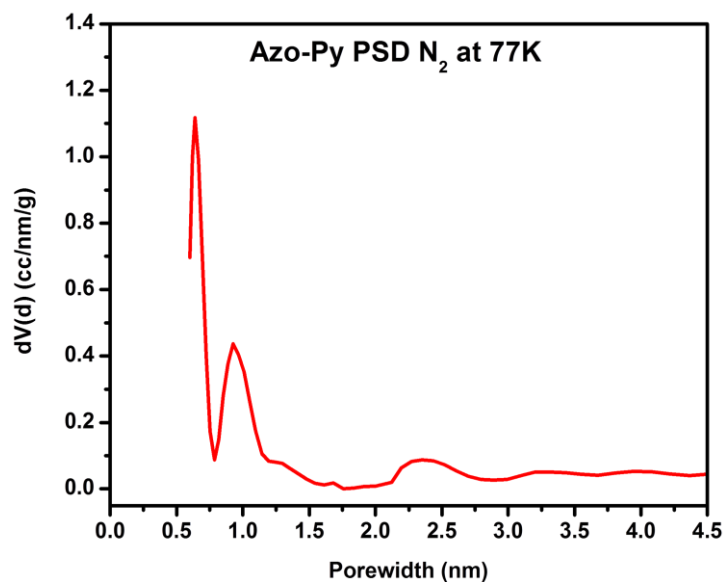


Figure 4.7: Pore size distribution of Azo-Py from N₂ isotherms at 77 K

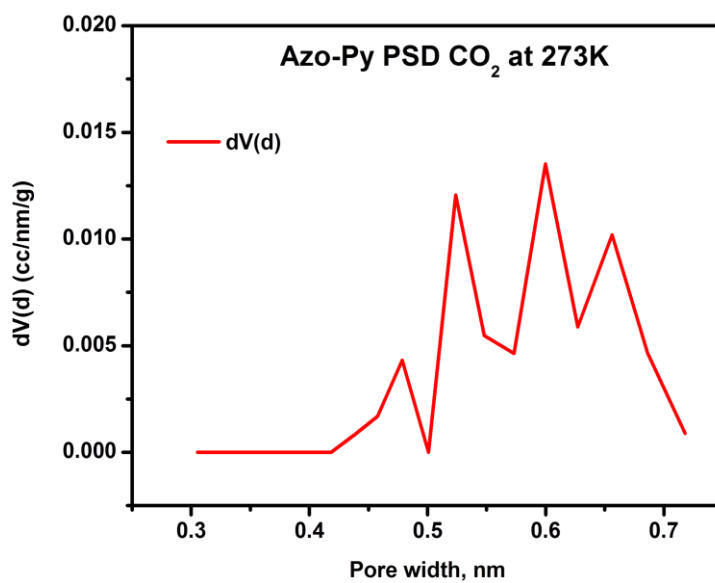


Figure 4.8: Pore size distribution of Azo-Py from CO₂ isotherms at 273 K (pores with <0.7 nm in diameter)

Table 4.1: Textural Properties of Azo-Py

	^a SA _(BET)	^b PSD	^c Pore Vol.	^d Vol. _(Mic)	^e Vol. _(U. Mic)
	m ² g ⁻¹	nm	cm ⁻³ g ⁻¹	cm ⁻³ g ⁻¹	cm ⁻³ g ⁻¹
Azo-Py	1259	1.06	0.699	0.377(53.9)	0.0158

^aBrunauer–Emmett–Teller (BET) surface area. ^bDominant pore size determined by QSDFT fittings of N₂ isotherms at 77K. ^cTotal pore volume at P/ P₀ = 0.95. ^dMicropore volume determined by DFT (the values in parenthesis are the percentage of micropore volume relative to total pore volume) ^ePore volume of ultramicropores (< 0.7 nm) determined from CO₂ isotherms at 273K.

4.3.3. Gas uptake studies

The textural properties discussed above including the high surface area, microporous nature and narrow pore size have proven to be effective in enhancing the CO₂ uptake in porous frameworks. Additionally, the incorporation of azo-bonds in porous sorbents has been theoretically and experimentally validated to enhance CO₂ uptake facilitated via Lewis acid base interactions between CO₂ and the azo functionalities.¹³ With that in consideration, the CO₂ uptake capacity of Azo-Py was investigated by collecting low pressure CO₂ isotherms at 273 and 298 K presented in Figure 4.9 and summarized in Table 4.2. The CO₂ isotherms display a steep rise in the low pressure region and no significant hysteresis in the adsorption and desorption curves. These are characteristic of a porous material desirable for selective CO₂ capture as well as easily reversible adsorption processes for regeneration of sorbent at a low energy cost. At 273 K and 1 bar, Azo-Py has a CO₂ uptake of 4.79 mmol g⁻¹ which is higher than BILP-10, -11 and -13 (2.6-4.0 mmol g⁻¹). Consistent with the surface area difference Azo-Py had a lower CO₂ uptake than BILP-12 (5.1 mmol g⁻¹).⁸ This is indicative of the direct correlation between surface area and CO₂ uptake that has been observed in most porous polymers. In relation to other azo

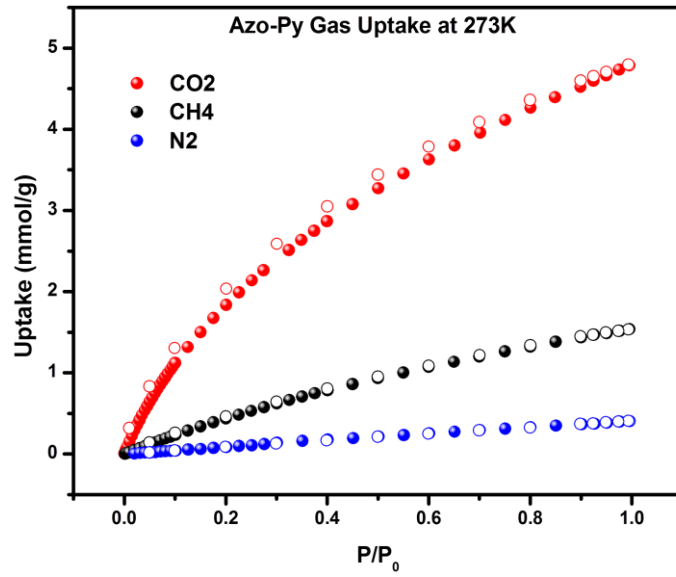


Figure 4.9 (a): CO₂, CH₄ and N₂ uptake isotherms of Azo-Py at 273 K

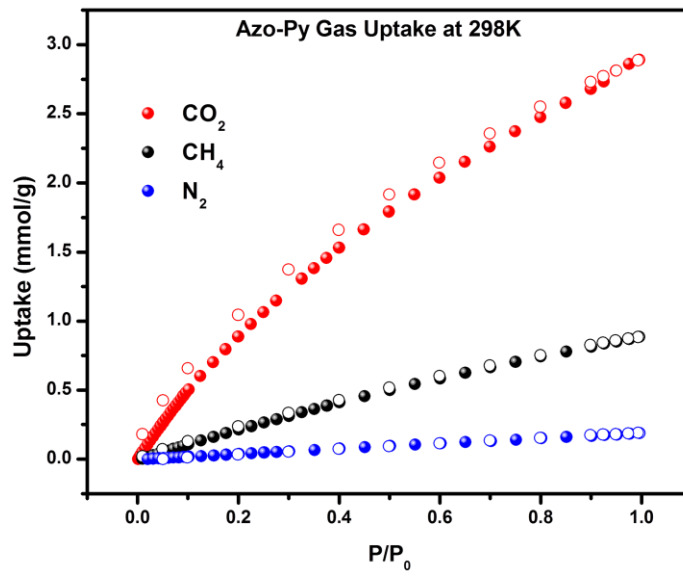


Figure 4.9 (b): CO₂, CH₄ and N₂ uptake isotherms of Azo-Py at 298 K

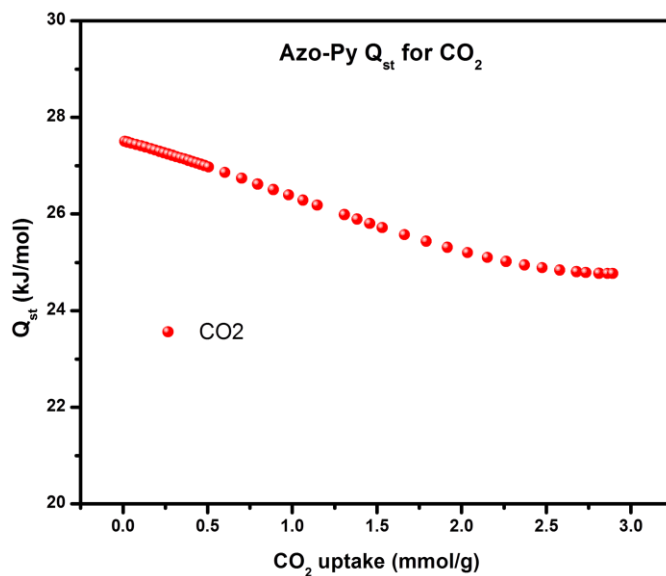


Figure 4.10 (a): Azo-Py isosteric heat of adsorption for CO_2

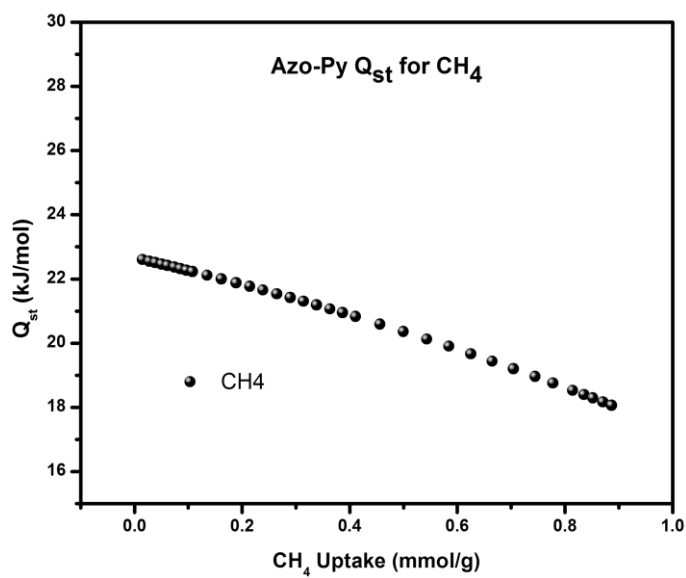


Figure 4.10 (b): Azo-Py isosteric heat of adsorption for CH_4

functionalized polymers, Azo-Py has a higher CO₂ uptake at 273 K and 1 bar than all ALPs (2.5 - 4.7 mmol g⁻¹) except for ALP-1 (5.37 mmol g⁻¹).^{3,4} While at 298 K and 1 bar, Azo-Py has a CO₂ uptake of 2.89 mmol g⁻¹ which is higher than azo-COPs (1.2-1.5 mmol g⁻¹) and azo-POFs (1.2-1.5 mmol g⁻¹) but slightly lower than ALP-1 (3.2 mmol g⁻¹) and ALP-5 (2.94 mmol g⁻¹). This is due to the triptycene based framework of ALP-1 which results in high IMFV enhancing the total uptake at 1 bar while ALP-1 has a high binding affinity to CO₂ due to its narrow pore size. The CH₄ uptake of Azo-Py at 1 bar was recorded at 1.54 and 0.89 mmol g⁻¹ at 273 and 298 k respectively. This was higher than all pyrene derived BILPs⁸ and all ALPs except ALP-1. The binding affinity of Azo-Py for gas molecules was quantified via isosteric heat of adsorption, Q_{st}, by fitting the CO₂ and CH₄ isotherms at 273 and 298 K with the virial equation. The CO₂ Q_{st} value for Azo-Py at zero surface coverage was quantified to be 27.5 kJ mol⁻¹. From the Q_{st} curves generated (Figure 4.10), it is evident that the strength of interaction between gas molecules and the polymer pore walls decreases with more loading as the interaction sites and pore volumes are increasingly saturated. The Q_{st} for CH₄ was calculated to be 22.6 kJ mol⁻¹ with depreciation in binding affinity observed with increasing gas loading as well.

Table 4.2: Gas uptakes, heat of adsorption and selectivity of Azo-Py

Adsorbent	CO ₂ uptake at 1 bar			CH ₄ uptake at 1 bar			N ₂ uptake at 1 bar		Selectivity	
	273K	298 K	Q _{st}	273 K	298 K	Q _{st}	273 K	298 K	CO2/N2	CO2/CH4
Azo-Py	4.79	2.89	27.5	1.54	0.89	22.6	0.40	0.19	55.1(42.4)	10.9(7.8)

Gas uptake in mmol g⁻¹, and isosteric heat of adsorption (Q_{st}) at zero coverage in kJ mol⁻¹. Selectivity (mol mol⁻¹, at 1.0 bar) calculated by IAST method at mole ratio of 10:90 for CO₂/N₂ and mole ratio of 50:50 for CO₂/CH₄ at 273 K and (298 K)

4.3.4. Selective CO₂ capture over N₂ and CH₄

Motivated by the azo-functionality, microporosity, high CO₂ uptake and suitable binding affinity of Azo-Py, the selective CO₂ capture potential of Azo-Py was evaluated using two methods: IAST and initial slope. Selectivity studies were conducted from analysis of single gas isotherms of CO₂, CH₄ and N₂. As described earlier, IAST is a widely recognized method for deducing the selective gas capture behavior of porous sorbents from single gas isotherms while taking into account the composition of the targeted gas mixtures. In this case, flue gas composed predominantly of CO₂ and N₂ with ratios of CO₂:N₂ at 10:90 and landfill gas composed predominantly of CO₂ and CH₄ with ratios of CO₂:CH₄ at 50:50 were analyzed (Figure 4.11). For flue gas compositions, the CO₂/N₂ IAST selectivity of Azo-Py at 1 bar was calculated at 55.1 and 42.4 at 273 and 298 K respectively. These values are comparable to other nitrogen bearing organic polymers ALPs,^{3,4} BILPs¹⁴ and functionalized NPOFs.¹⁵ The decrease in selectivity from 273 to 298 K is a trend that has been observed before in POPs that lack the presence of a large portion of pores in the mesoporous range.^{16,17} The CO₂/CH₄ selectivity of Azo-Py at 1 bar was 10.9 and 7.8 for 273 and 298 K respectively. These values are also comparable to our previously published azo-functionalized polymers. Furthermore, selectivities were calculated using the Henry law constants. These constants were obtained from the initial slope of the adsorption branch of the isotherms (Figure 4.12). The CO₂/N₂ selectivities were found to be 39.6 (273K and 29.2 (298 K) while CO₂/CH₄ selectivities were 7.04 (273 K) and 4.8 (298 K).

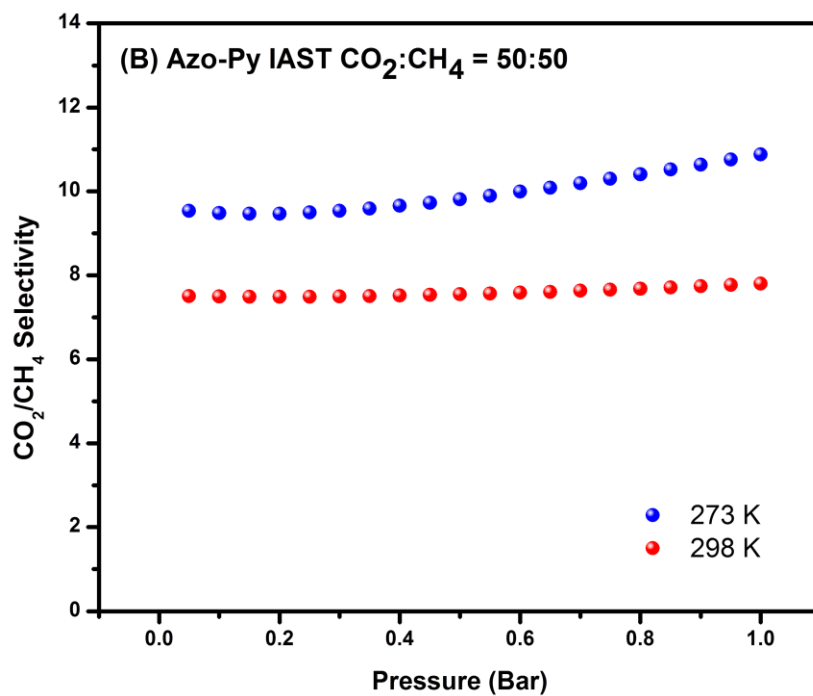
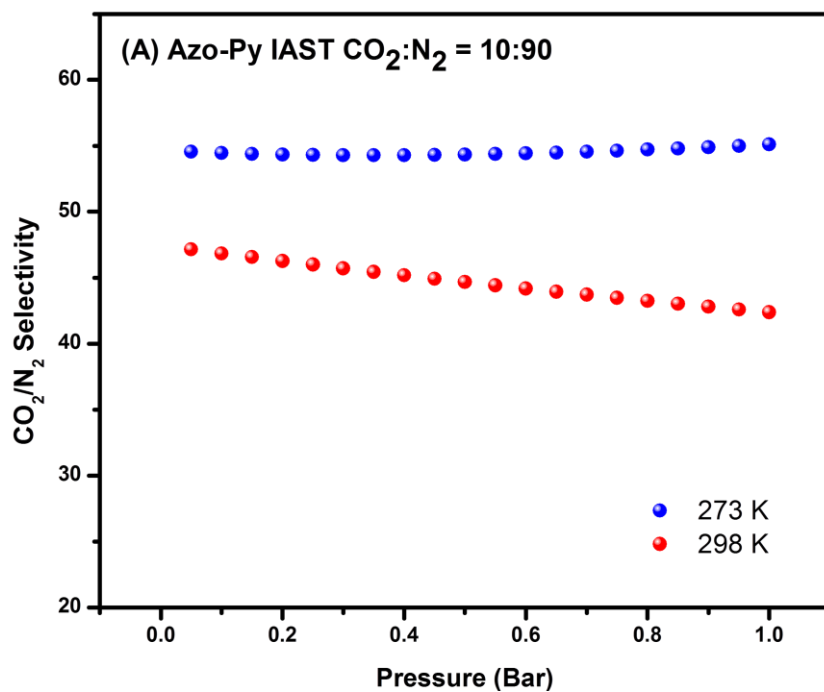


Figure 4.11. IAST selectivity of CO_2/N_2 (10:90) (A) and CO_2/CH_4 (50:50) at 273 K and 298 K.

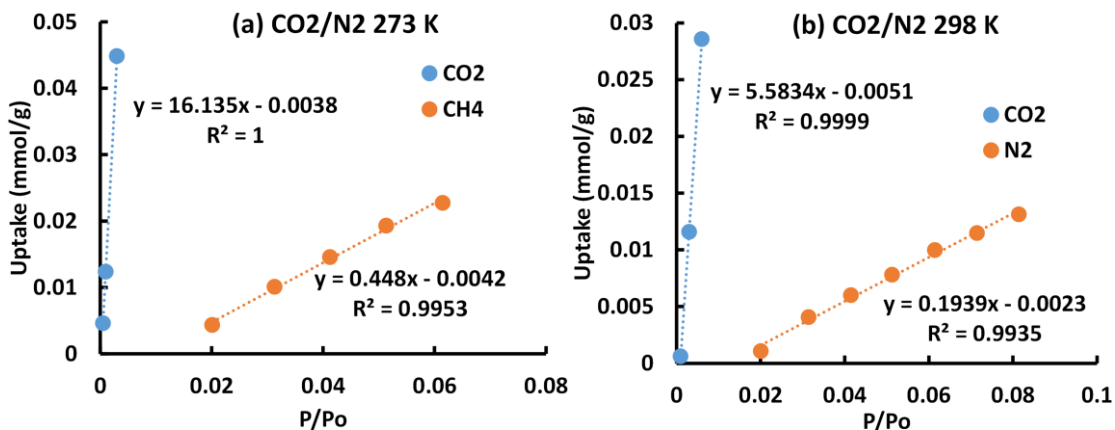


Figure 4.12 (a): Initial slope determination of CO₂ and N₂ low pressure adsorption for CO₂/N₂ selectivity calculations at 273 and 298 K

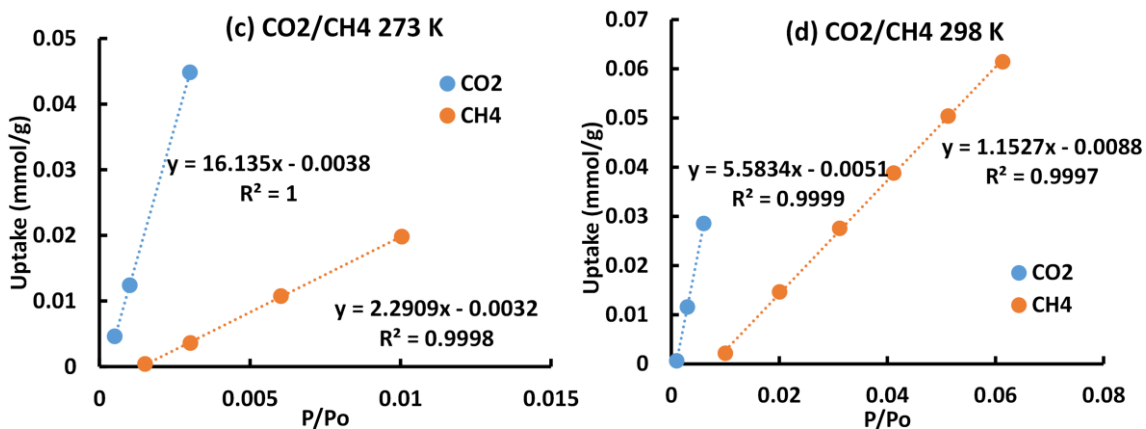


Figure 4.12 (b): Initial slope determination of CO₂ and CH₄ low pressure adsorption for CO₂/CH₄ selectivity calculations at 273 and 298 K

4.3.5 Sorbent evaluation criteria of Azo-Py for CO₂ separation

Recently a report by Bae and Snurr has outlined a set of parameters that can provide an assessment for a sorbent's ability in selectively capturing CO₂ under specific conditions and targeted gas mixtures.¹⁸ Specifically the following sorbent criteria parameters were calculated: CO₂ uptake under adsorption conditions (N_I^{ads}), working capacity for (ΔN_I), adsorbent regenerability (R), selectivity under adsorption (α_{12}^{ads}) and sorbent selection parameter (S) which is a combination of the selectivity and working capacity. Following this approach the sorbent evaluation criteria of Azo-Py for flue gas (Table 4.3) and landfill gas (Table 4.4) were calculated and compared to some of the best performing sorbents in literature. Conditions for flue gas (CO₂/N₂ = 10/90) and landfill gas (CO₂/CH₄ = 50/50) were evaluated under vacuum swing adsorption (VSA) conditions at 298 K and adsorption pressure of 1 bar and desorption pressure of 0.1 bar. For CO₂ separation from flue gas mixtures, Azo-Py displays a respectable S value due to its moderate selectivity and low working capacity for nitrogen. For landfill gas purification, Azo-Py has a high working capacity resulting in competitive S value relative to the best performing sorbents in literature.

Table 4.3. VSA evaluation criteria for CO₂ separation from flue gas^a

	N_I^{ads}	ΔN_I	% R	α_{12}^{ads}	S
Azo-Py	0.68	0.60	87.9	42.4	178.2
ALP-1	0.57	0.51	88.6	28.0	85.2
ALP-5 ⁴	2.07	1.67	80.90	8.30	75.0
BILP-101 ¹⁹	0.95	0.80	84.80	70.30	556.0
SNU-Cl-sca ²⁰	1.99	0.41	87.30	38.00	262.0
Zeolite-13X ¹⁸	3.97	1.35	54.20	86.20	128.0
Ni-MOF-74 ¹⁸	6.23	3.20	73.70	41.10	83.50

^aCO₂/N₂ = 10:90, T = 298 K, P^{ads} = 1 bar, and P^{des} = 0.1 bar.

Table 4.4. VSA evaluation criteria for CO₂ separation from landfill gas^a

	N_I^{ads}	ΔN_I	% R	α_{12}^{ads}	S
Azo-Py	2.04	1.73	84.86	7.8	63.83
ALP-1 ³	2.04	1.73	85.1	5.8	35.1
ALP-5 ⁴	2.07	1.67	80.9	8.3	75
BILP-12 ⁸	2.01	1.71	85.3	6	33.7
TBILP-2 ¹⁴	2.2	1.84	83.7	7.6	62.5
BILP-6-NH ₂ ²¹	2.63	2.14	81.3	8.4	76
NPOF-1-NH ₂ ²²	2.53	2.1	82.9	9.9	91

^aCO₂/CH₄ = 50:50, T = 298 K, P^{ads} = 1 bar, and P^{des} = 0.1 bar.

4.4 Conclusion

In conclusion, a new azo-functionalized POP, Azo-Py was synthesized by incorporating a highly conjugated pyrene core into the polymer framework. The influence of the pyrene moiety in the solid-state packing of the polymer is evident by the formation of nanofibers that are assembled by strong π - π stacking interactions. Azo-Py displays high porosity with a surface area of 1259 m² g⁻¹ and high microporosity as a result of the rigid pyrene core. These characteristics induced CO₂ uptakes of 4.79 mmol g⁻¹ (273 K) and 2.89 mmol g⁻¹ (298 K) at 1 bar along with binding affinities conducive for easy regeneration, Q_{st} 27.5 kJ mol⁻¹. Furthermore, the CO₂ separation performance of Azo-Py from flue and land fill gas was evaluated displaying competitive S values amongst other porous sorbents.

References

- (1) Patel, H. A.; Je, S. H.; Park, J.; Chen, D. P.; Jung, Y.; Yavuz, C. T.; Coskun, A. Unprecedented High-Temperature CO₂ Selectivity in N₂-Phobic Nanoporous Covalent Organic Polymers. *Commun. Nat.* **2013**, *4*, 1357.
- (2) Lu, J.; Zhang, J. Facile Synthesis of Azo-Linked Porous Organic Frameworks via Reductive Homocoupling for Selective CO₂ Capture. *J. Mater. Chem. A* **2014**, *2* (34), 13831–13834.
- (3) Arab, P.; Rabbani, M. G.; Sekizkardes, A. K.; Islamoglu, T.; El-kaderi, H. M. Copper(I)-Catalyzed Synthesis of Nanoporous Azo-Linked Polymers: Impact of Textural Properties on Gas Storage and Selective Carbon Dioxide Capture. *Chem. Mater.* **2014**, *26*, 1385–1392.
- (4) Arab, P.; Parrish, E.; Islamoglu, T.; El-kaderi, H. M. Synthesis and Evaluation of Porous Azo-Linked Polymers for Carbon Dioxide Capture and Separation. *Mater. Chem. A* **2015**, 20586–20594.
- (5) Zhang, C.; Jiao, N. Copper-Catalyzed Aerobic Oxidative Dehydrogenative Coupling of Anilines Leading to Aromatic Azo Compounds Using Dioxygen as an Oxidant. *Angew. Chemie - Int. Ed. Commun.* **2010**, *49* (35), 6174–6177.
- (6) Venkataramana, G.; Sankararaman, S. Synthesis, Absorption, and Fluorescence-Emission Properties of 1,3,6,8-Tetraethynylpyrene and Its Derivatives. *Eur. J. Org. Chem.* **2005**, *19*, 4162–4166.
- (7) Jin, Shangbin ; Sakurai, Tsuneaki ; Kowalczyk, Tim ; Dalapati, Sasanka ; Xu, Fei ; Wei, Hao ; Chen, Xiong ; Gao, Jia ; Seki, Shu ; Irle, Stephan ; Jiang, D. Two-Dimensional Tetrathiafulvalene Covalent Organic Frameworks: Towards Latticed Conductive Organic

- Salts. *Chem. - A Eur. J.* **2015**, *20*, 14608–14613.
- (8) Sekizkardes, A. K.; Kahveci, Z.; El-kaderi, H. M. Application of Pyrene-Derived Benzimidazolelinked Polymers to CO₂ Separation under Pressure and Vacuum Swing Adsorption Settings. *J. Mater. Chem. A* **2014**, *2*, 12492–12500.
- (9) Rabbani, M. G.; Sekizkardes, A. K.; El-Kadri, O. M.; Kaafarani, B. R.; El-Kaderi, H. M. Pyrene-Directed Growth of Nanoporous Benzimidazole-Linked Nanofibers and Their Application to Selective CO₂ Capture and Separation. *J. Mater. Chem.* **2012**, *22*, 25409–25417.
- (10) Thommes, M.; Kaneko, K.; Neimark, A. V.; Olivier, J. P.; Rodriguez-Reinoso, F.; Rouquerol, J.; Sing, K. S. W. Physisorption of Gases, with Special Reference to the Evaluation of Surface Area and Pore Size Distribution (IUPAC Technical Report). *Pure Appl. Chem.* **2015**, *87*, 1051–1069.
- (11) Zhang, X. .; Lu, J. .; Zhang, J. Porosity Enhancement of Carbazolic Porous Organic Frameworks Using Dendritic Building Blocks for Gas Storage and Separation. *Chem. Mater.* **2014**, *26* (13), 4023–4029.
- (12) Rabbani, M. G. .; Reich, T. . E. .; Kassab, R. M. .; Jackson, K. T. .; El-Kaderi, H. M. High CO₂ Uptake and Selectivity by Triptycene-Derived Benzimidazole-Linked Polymers. *Chem. Commun.* **2012**, *48*, 1411–1413.
- (13) Nagaraja, C. M.; Haldar, Ritesh; Maji, Tapas Kumar; Rao, C. N. R. Chiral Porous Metal-Organic Frameworks of Co(II) and Ni(II): Synthesis, Structure, Magnetic Properties, and CO₂ Uptake. *Cryst. Growth Des.* **2012**, *12* (2), 975–981.
- (14) Sekizkardes, A. K.; Altarawneh, S.; Kahveci, Z.; Islamoglu, T.; El-kaderi, H. M. Highly Selective CO₂ Capture by Triazine-Based Benzimidazole- Linked Polymers.

- Macromolecules* **2014**, *14*, 8328–8334.
- (15) Islamoglu, T.; Rabbani, Mohammad Gulam El-Kaderi, H. M. Impact of Post-Synthesis Modification of Nanoporous Organic Frameworks on Small Gas Uptake and Selective CO₂ Capture. *J. Mater. Chem. A* **2013**, *1*, 10259–10266.
- (16) Saleh, M.; Baek, S. B.; Lee, H. M.; Kim, K. S. Triazine-Based Microporous Polymers for Selective Adsorption of CO₂. *J. Phys. Chem. C* **2015**, *119* (10), 5395–5402.
- (17) Lee, J. H.; Lee, H. J.; Lim, S. Y.; Kim, B. G.; Choi, J. W. Combined CO₂-Philicity and Ordered Mesoporosity for Highly Selective CO₂ Capture at High Temperatures. *J. Am. Chem. Soc.* **2015**, *137* (22), 7210–7216.
- (18) Bae, Y.-S.; Snurr, R. Q. Development and Evaluation of Porous Materials for Carbon Dioxide Separation and Capture. *Angew. Chemie - Int. Ed.* **2011**, *50* (49), 11586–11596.
- (19) Sekizkardes, A. K.; Culp, J. T.; Islamoglu, T.; Marti, A.; Hopkinson, D.; Myers, C.; El-Kaderi, H. M.; Nulwala, H. B. An Ultra-Microporous Organic Polymer for High Performance Carbon Dioxide Capture and Separation. *Chem. Commun. (Camb)*. **2015**, *51* (69), 13393–13396.
- (20) Xie, L.-H. .; Suh, M. P. High CO₂-Capture Ability of a Porous Organic Polymer Bifunctionalized with Carboxy and Triazole Groups. *Chem. - Eur. J.* **2013**, *19* (35), 11590–11597.
- (21) Islamoglu, T.; Behera, S.; Kahveci, Z.; Tessema, T. D.; Jena, P.; El-Kaderi, H. M. Enhanced Carbon Dioxide Capture from Landfill Gas Using Bifunctionalized Benzimidazole-Linked Polymers. *ACS Appl. Mater. Interfaces* **2016**, *8* (23), 14648–14655.
- (22) Islamoglu, T. .; Kim, T. .; Kahveci, Z. .; El-Kadri, O. M. .; El-Kaderi, M. H. Systematic

Postsynthetic Modification of Nanoporous Organic Frameworks for Enhanced CO₂
Capture from Flue Gas and Landfill Gas. *J. Phys. Chem. C* **2016**, *120* (5), 2592–2599.

Chapter 5

Compatible incorporation of benzimidazole linked polymers into Matrimid to yield mixed matrix membranes with superior CO₂/N₂ selectivity

5.1 Introduction

Polymer membranes have been prevalent in gas separation applications through the years due to their easy processability. However, they present a drawback by their trade-off between permeability and selectivity as proposed by Robeson.¹ To address this issue, researchers have pursued the incorporation of porous materials ranging from zeolites,²⁻⁴ MOFs¹⁰⁻¹³,⁵⁻⁸ and carbon molecular sieves,^{3,9,10} into a polymer matrix to produce a class of materials known as mixed matrix membranes (MMMs). A common challenge encountered in MMMs performance for gas separation is the inadequate adhesion between the polymer matrix and the filler. This causes interfacial defects including voids, polymer rigidification, and filler pore blockage.^{11,16} In order to address this issue, BILP-101, a porous organic polymer has recently been evaluated as a promising class of material to be implemented as a filler material in a MMM.¹² POPs offer high chemical and physical stability along with high surface area, tunable functionality and textural properties. Their purely organic nature combined with desired surface functionalities need to be further explored for its potential to enhance the adhesion to polymer matrix and reduce interfacial defects in MMMs.

Benzimidazole linked polymers (BILPs) are highly porous nitrogen rich polymers prepared by the acid catalyzed condensation reaction between aryl-*o*-diamine and aryl-aldehyde building blocks.^{13,14} The chemical stability of benzimidazole groups along with their physisorptive affinity for CO₂ through Lewis acid-base (N \cdots CO₂) and aryl (C-H \cdots O=C=O) has garnered BILPs significant attention for CO₂ separation studies.^{15,16} BILP-4 is one of such polymers with

a highly cross-linked structure obtained by a metal free synthesis from simple building blocks.¹³ It has a high surface area and high CO₂ uptake at low STP. With these considerations in mind, we have prepared a series of BILP-4/ Matrimid MMMs, characterized their physicochemical properties as well as gas permeabilities to evaluate their ability to selectively capture CO₂ over N₂ and ultimately their potential for treatment of flue gas mixtures.

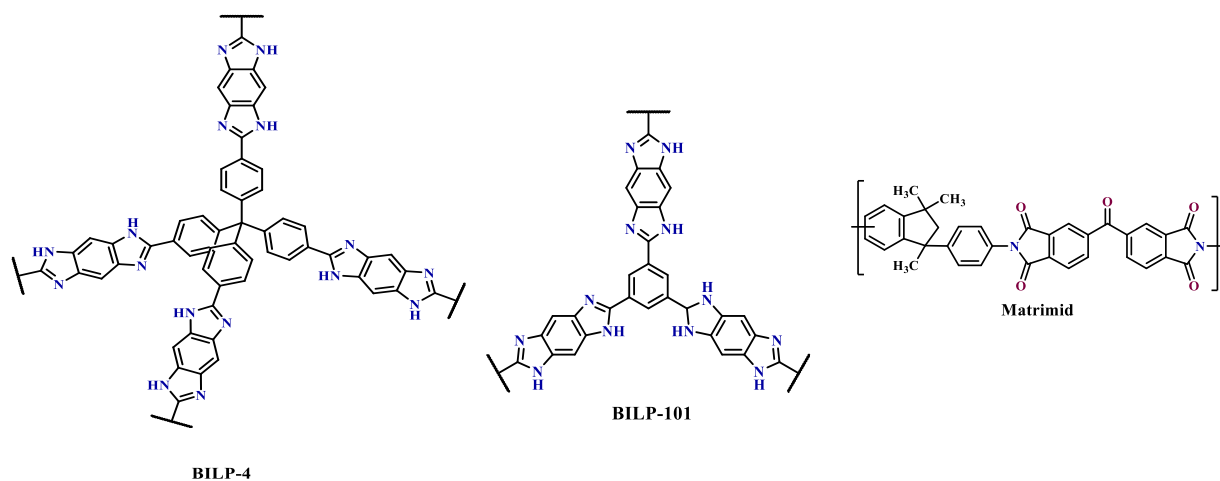


Figure 5.1: Structures of BILP-4, BILP-101 and Matrimid[®]

5.2 Experimental

5.2.1 Materials and instrumentation

All chemicals for BILP-4 and BILP-101 synthesis were purchased from Sigma Aldrich and were used without further purification. Matrimid[®] 5218 polymer was purchased from Huntsman Chemical (Figure 5.1). Tetrahydrofuran was purchased from Fisher Scientific. Fourier transformed infra-red (FT-IR) spectra were obtained using a Bruker Vertex 70. Thermogravimetric analysis (TGA) was performed using a TGA Q500 thermal analysis system. Surface area measurements were conducted using a Quantachrome Autosorb iQ₂ gas sorption analyzer. Scanning electron microscopy (SEM) was conducted using an FEI Quanta 600 scanning electron microscope.

5.2.2 Synthesis of BILP-4

BILP-4 (Figure 5.1) was synthesized following a method previously reported.¹³ Briefly, a 200 ml Schlenk flask was loaded 1,2,4,5-benzenetetramine tetrahydrochloride (55 mg, 0.19 mmol) and anhydrous DMF (30ml) and stirred to form a homogenous mixture. A solution of tetrakis(4-formylphenyl)methane (40 mg, 0.1 mmol) in 15 ml anhydrous DMF was added dropwise to the Schlenk flask at -30 °C. Upon the precipitation of a brown product the mixture was allowed to warm up to room temperature and kept stirring overnight. The reaction mixture was bubbled with air for 15 minutes, capped and incubated at 130 °C for a period of 72 hours. The resulting yellowish brown polymer was isolated by filtration and washed with DMF, acetone, water, 2M HCl, 2M HCl, water and acetone in that order. The product was soaked in acetone/CH₂Cl₂ (1:1, v:v) for 24 hours and dried at 120 °C under vacuum to yield the yellowish brown BILP-4 (54 mg, 91%).

5.2.3 Synthesis of BILP-101

This polymer was synthesized following methods mentioned above for BILP-4 using 1,2,4,5-benzenetetramine tetrahydrochloride (100 mg, 0.35 mmol) and 1,3,5-triformylbenzene (40 mg, 0.23 mmol). After drying, the final product BILP-7 (Figure 5.1) was obtained as a yellow brown powder (72 mg, yield 92%).

5.2.4 Membrane fabrication

The pristine Matrimid[®] and BILP/ Matrimid[®] MMMs were prepared using a recently reported technique.⁸ To prepare the pristine Matrimid[®], Matrimid[®] was dried at 120 °C under vacuum for 24 hours. This was dissolved in THF and mixed in a roller mixer and left standing overnight to rid of any gas bubbles. Matrimid[®] membranes were then cast on a glass plate confined in a glove bag purged with N₂ and saturated with THF so as to minimize humidity and

the rate of THF evaporation from the membrane. The membrane was then dried at 100 °C overnight, annealed at 225 °C in a vacuum oven for 2 hours and cooled down to room temperature.

The casting solution for the BILP/ Matrimid[®] MMMs was made by homogeneously dispersing activated BILP (120 °C overnight under vacuum) in THF using an ultrasonication water bath for 2 hours. A 30 wt% of Matrimid[®] solution in THF was then added to BILP dispersion, mixed in a roller mixer and ultrasonicated for 2 hours. This was repeated for the remaining Matrimid[®] solution at 30 wt% and 40 wt% increments. The BILP/ Matrimid[®] MMMs were cast using the same procedure for the pristine Matrimid[®] membranes discussed above. BILP mass loading to Matrimid[®] ratios of 10%, 15% and 25% were used to fabricate three different BILP/Matrimid[®] MMMs.

5.2.5 Gas separation performance testing

The gas separation performance testing of these membranes using constant volume-variable pressure system was reported in our previous reports.⁸ The membranes were cut into 1 inch in diameter coupons and loaded in a millipore high pressure holder for testing of these membranes at 22 °C. The effective areas of the membranes were 2.7 cm² with a pressure drop across the membranes of about 30 psi.

5.3 Results and Discussion

5.3.1 Characterization of BILP-4 and BILP-4/Matrimid[®] MMMs

The BET surface area of BILP-4 was deduced from a N₂ isotherm at 77K presented in Figure 5.2. The surface area of 1079 m²/g recorded is within agreement to previously reported value. The Type-1 isotherm is reversible with a sharp uptake in the pressure range of P/P₀ = 0.01-0.15 indicative of a large portion of micropores. This was supported by pore-size distribution (PSD)

curves modeled using nonlocal density functional theory (NLDFT) which showed dominant pore sizes of 0.63 nm (Figure 5.2). The low pressure CO₂ uptakes collected at 298 K are presented in Table 5.1. BILP-4 CO₂ uptake 158 mg g⁻¹ at 298 K (1 bar) is in close agreement with previously reported values.¹³

Table 5.1. Textural properties and CO₂ uptake of BILP-4 and BILP-101

<i>Polymer</i>	<i>BET Surface Area</i>	<i>Pore Volume</i>	<i>Pore Size</i>	<i>CO₂ uptake at 1 bar 298K</i>
BILP-4	1135 m ² /g	0.65 cc/g	0.71 nm	158 mg/g
BILP-101	536 m ² /g	0.41 cc/g	0.54 nm	108 mg/g

The incorporation of BILP-4 into Matrimid[®] was verified by comparing the FT-IR spectra of pristine Matrimid[®] membranes and BILP-4/Matrimid[®] MMMs (Figure 5.3). A broad peak at 3400-3500 cm⁻¹ absent in the pure Matrimid[®] membrane was evident in the membranes loaded with BILP-4, this is characteristic of free N-H and hydrogen bonded N-H peaks from the secondary amine in the imidazole ring of BILP-4. The thermal stability of the MMMs fabricated was assessed by non-oxidative thermogravimetric analyses (Figure 5.4). The decomposition onset temperature observed for Matrimid[®] was found to be around 445 °C with the weight unaffected up to 350 °C indicating minimum amount of solvent trapped in the membrane matrix during fabrication. With increased filler loadings, a trend of enhanced thermal stability up to 461, 470 and 474 °C of 10, 15 and 25 wt% BILP-4/Matrimid MMMs respectively was observed. This is caused by a thermal motion inhibition introduced by the interfacial interaction of Matrimid and BILP-4 polymers which increases the thermal energy barrier needed to mobilize the polymer chains.¹⁷ The morphology and interfacial effects of interaction between filler and polymer were assessed using cross-sectional SEM imaging (Figure 5.5). The Matrimid membrane is expectedly

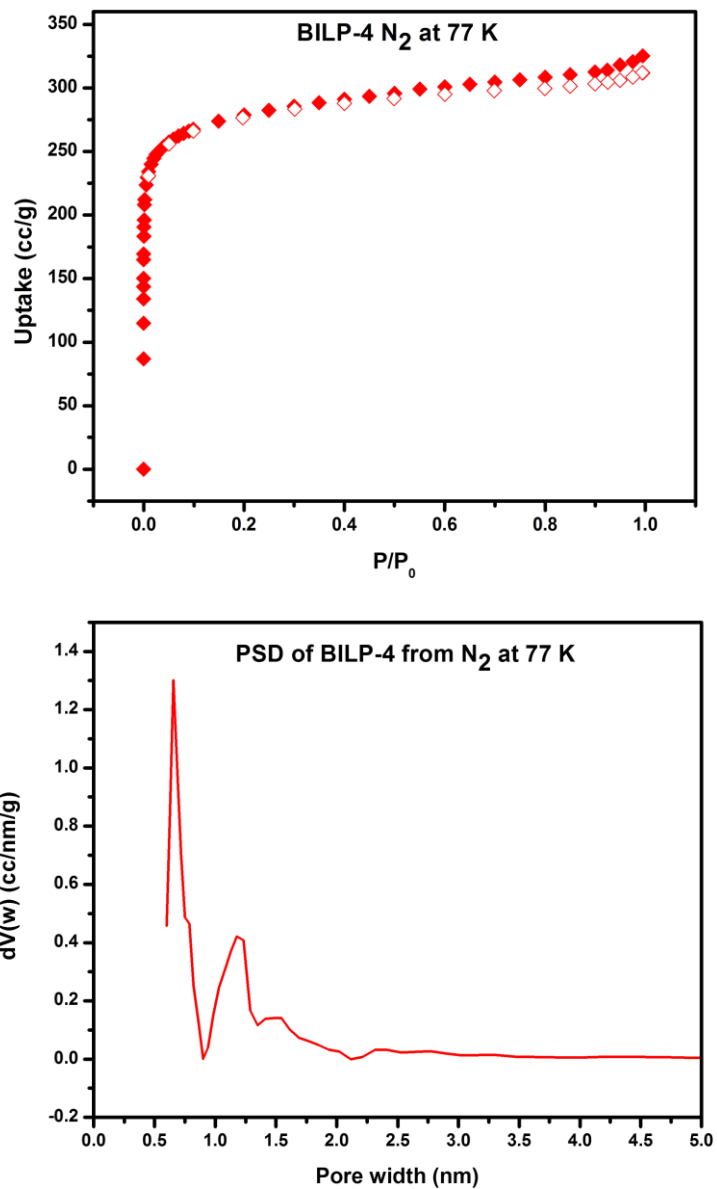


Figure 5.2: N₂ isotherm of BILP-4 at 77 K (top) and pore size distribution from NLDFIT fitting.

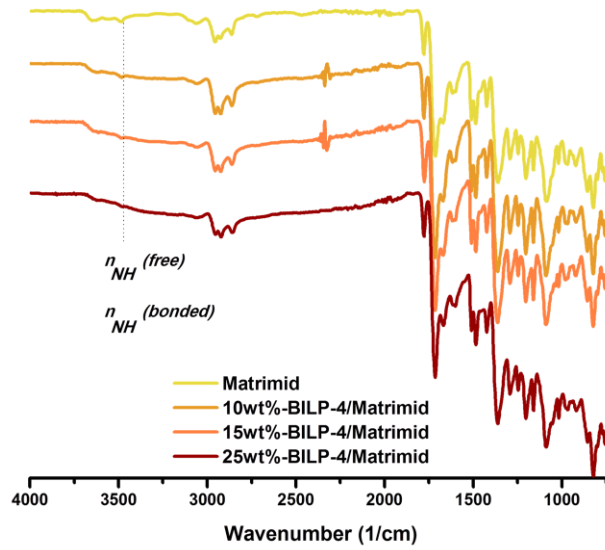


Figure 5.3: FT-IR spectra of pristine Matrimid[®] membranes and BILP-4/Matrimid[®] MMMs

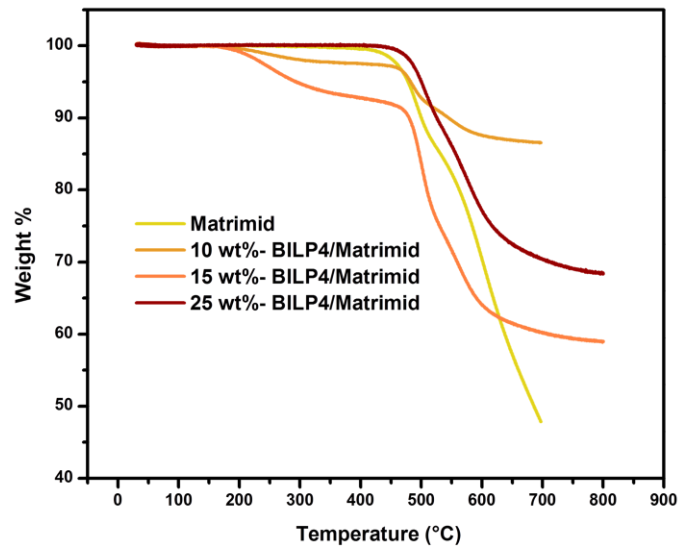
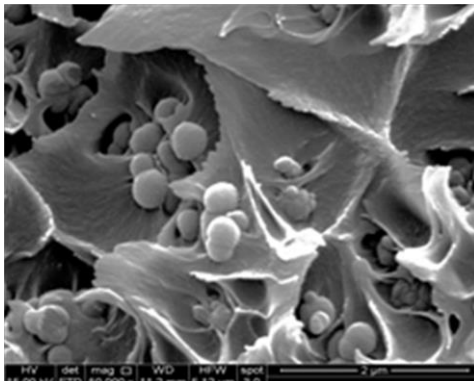
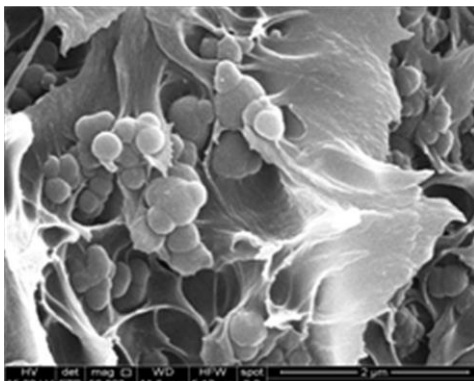


Figure 5.4: TGA of pristine Matrimid[®] membranes and BILP-4/Matrimid[®] MMMs

10 wt% BILP-4/ Matrimid



15 wt% BILP-4/ Matrimid



20 wt% BILP-4/ Matrimid

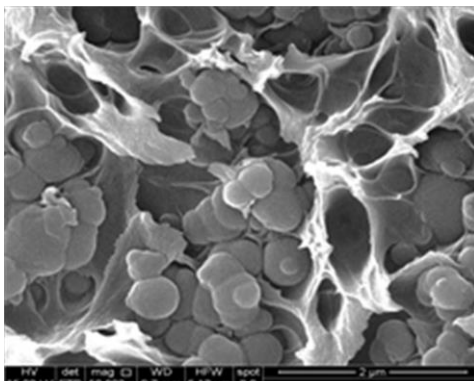


Figure 5.5: SEM images of pristine Matrimid[®] membrane and BILP-4/Matrimid[®] MMMs

free of any apparent defects. However, such defects become more prominent with increasing BILP-4 loadings with the 25% BILP-4 loading displaying the most concentration of defects. Concentric apertures are observed around filler particles which denote the presence of strong interfacial interaction in the membranes. Moreover, it should be noted that BILP-4 fillers are evenly distributed in the matrix, a desired effect in the MMM fabrication process. The SEM images also reveal the filler particles remain intact upon incorporation into the Matrimid matrix.

The mechanical properties of the BILP-4/Matrimid[®] MMMs evaluated using dynamic mechanical analysis are presented in Figure 5.6. The Young's Modulus values of BILP-4/Matrimid[®] MMMs are higher than the pristine Matrimid[®] membrane (1.56 GPa). An increase in the Young's Modulus values of MMMs with filler loading up to 2.5 GPa for 25wt% BILP-4 was recorded. This is an indication of a strong interfacial interaction between Matrimid[®] and the filler BILP-4 particles in agreement with previous reports of similar trends in MMMs of Matrimid[®] loaded with Cu-BPY-HFS MOFs and carbon molecular sieves.^{18,19} The glass transition temperature (T_g) of MMMs were determined using differential scanning microscopy (DSC). The T_g of BILP-4/Matrimid[®] membranes were all found to be higher than pure Matrimid[®] (Figure 5.7). MMMs with 15% and 25% BILP-4 have a T_g of 328 °C which is 3 °C higher than that of pure Matrimid[®]. This trend is in agreement with previous report where filler material interaction with polymer results in MMM rigidification and hence a restricted mobility of the polymer chains.^{20,21} In the case of BILP-4/ Matrimid, this interaction is enhanced by the hydrogen bonding between secondary amines of BILP-4 imidazoles and imide oxygens of Matrimid as well as π - π stacking between aromatic groups of the two materials (Figure 5.8).

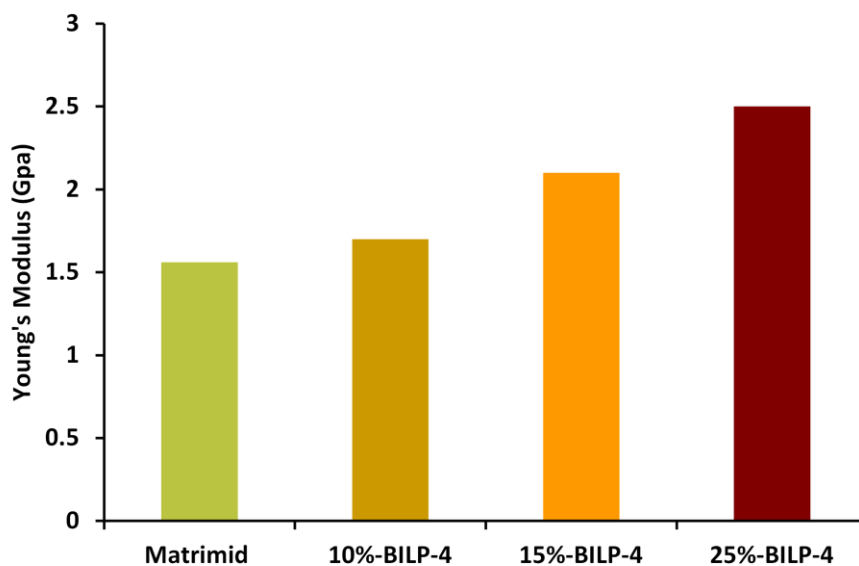


Figure 5.6: Young's Modulus of Matrimid[®] membrane and BILP-4/Matrimid[®] MMMs

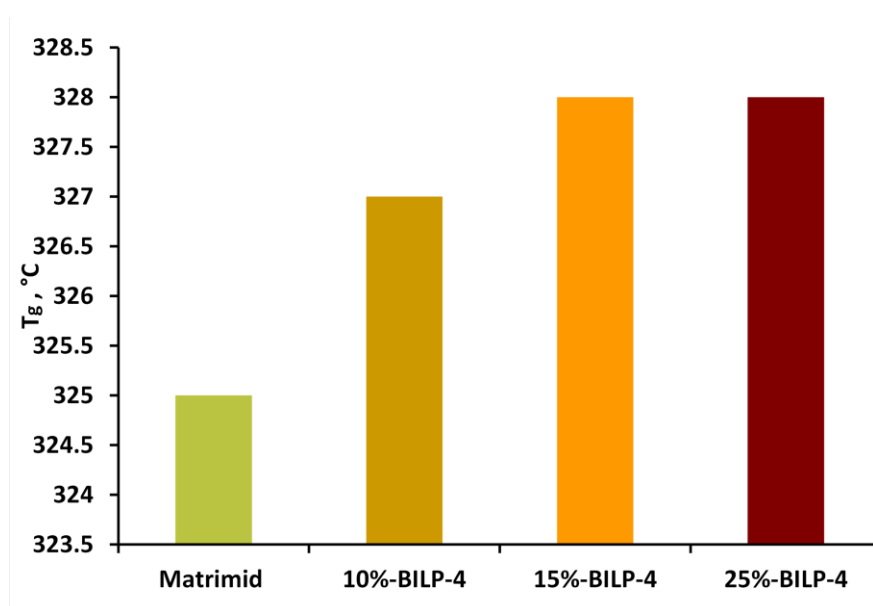


Figure 5.7: T_g of pristine Matrimid[®] membrane and BILP-4/Matrimid[®] MMMs

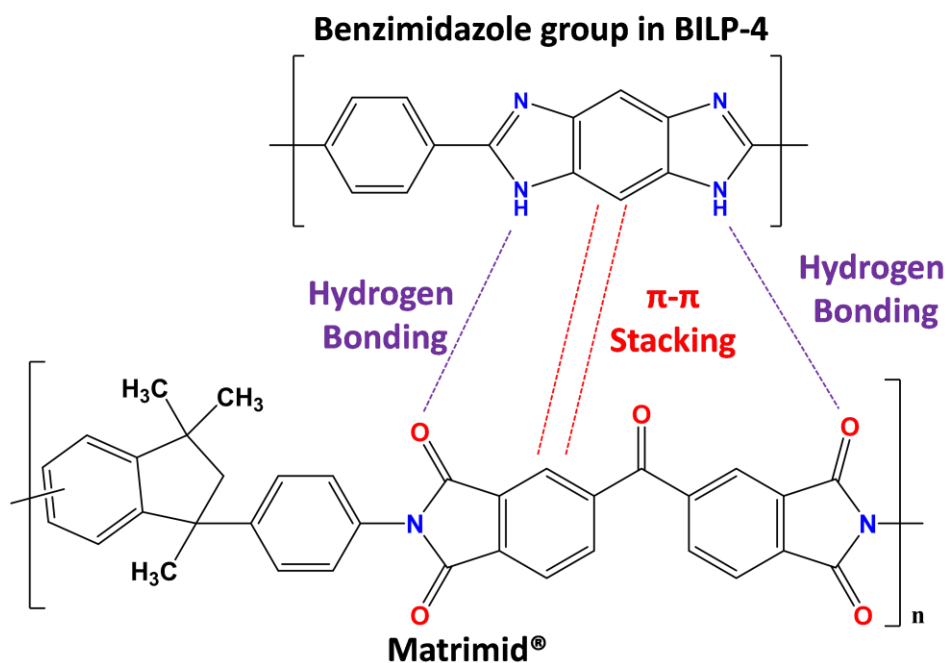


Figure 5.8: Interaction between benzimidazole moiety of BILPs and Mamtrimid®

5.3.2 Gas transport properties

The gas permeability properties of Matrimid and BILP-4/Matrimid membranes were obtained from pure gas CO₂ and N₂ permeation measurements. The performance of MMMs for CO₂ separation was evaluated by deducing the ideal selectivity values defined as the ratio of the permeability of the individual gases (Table 5.2). In agreement with literature reports, the CO₂ permeability of pure Matrimid membrane was measured at 8.7 Barrer with a CO₂/N₂ ideal selectivity of 29.^{8,6} For the BILP-4/Matrimid MMMs, the permeability values for CO₂ increase with BILP-4 loading to 13.2, 14.9 and 63.6 Barrer for loadings of 10 wt%, 15 wt% and 25wt% BILP-4 respectively. These enhancements in CO₂ permeability are attributed to resulting increase of fractional free volume in the MMMs: introduced by way of the inherent pores present in BILP-4 as well as interfacial voids generated between porous fillers and the Matrimid matrix. The large increase in permeability (over 6 times) at 25wt% BILP-4 loading indicates a high level of defect formation caused by agglomeration of filler particles in the membranes.

Table 5.2: CO₂ permeability and CO₂/N₂ ideal selectivity for Matrimid as well as BILP-4/Matrimid

Membrane	CO₂ Permeability (Barrer)	N₂ Permeability (Barrer)	CO₂/N₂ Selectivity
Matrimid	8.7	0.30	29.0
10 wt% BILP-4/Matrimid	13.2	0.41	32.0
15 wt%-BILP-4/Matrimid	14.9	0.38	38.9
25 wt%-BILP-4/Matrimid	63.8	2.52	25.3

The ideal selectivities of the MMMs were 32, 38.9 and 25.3 for 10, 15 and 25 wt% BILP-4 loadings. This suggests that the 15 wt% MMM had the optimum combination of filler to Matrimid interaction as well as optimum free volume due to polymer chain packing disruption that act as gas diffusion pathways. However, a different scenario occurs at 25 wt% BILP-4 loading where a dense presence of filler in Matrimid affords large aggregates which can result in defects in the matrix larger than the kinetic diameters of both CO₂ (3.3 Å) and N₂ (3.64 Å), evident in the high permeability values of both gases.

We also evaluated gas transport properties of MMMs by employing another benzimidazole linked porous polymer, BILP-101, in Matrimid. The motivation for conducting this study was dictated by two objectives; (i) supporting the suggested hypothesis on potential interaction between functional groups of BILPs and Matrimid and (ii) studying textural properties (pore size, pore volume, surface area) of fillers in polymeric membranes with respect to gas transport properties. Thus, we fabricated MMMs composed of 10, 15 and 25 % BILP-101 in Matrimid,

respectively and under the same fabrication conditions with BILP-4/Matrimid series (Experimental section).

In similar trend with BILP-4/Matrimid, BILP-101 based MMMs showed CO₂ permeability enhancement compared to neat Matrimid. Membranes with 10 and 15 wt % BILP-101 also exhibited higher CO₂/N₂ selectivity compared to Matrimid (Figure 5.9). However, CO₂/N₂ selectivity properties of MMMs dropped at higher BILP-101 loadings (>25wt%). Drastic depletion in CO₂/N₂ selectivity can be addressed by defect formation within 25 % BILP-101/Matrimid. On the other hand, CO₂ permeability and CO₂/N₂ selectivity enhancement in 10 and 15 % BILP-101/Matrimid MMMs can be attributed to the favorable interaction between functional groups of BILPs and Matrimid (Figure 5.8).

In the second objective, we aim to correlate textural property differences between BILP-4 and BILP-101 on the gas transport properties of membranes. Both BILPs are constructed from imidazole linkages within highly conjugated porous scaffold. BILP-4, however, features nearly two times more surface area compared to BILP-101 and its pore size is considerably larger. Given its larger pore size, BILP-4 possesses less CO₂/N₂ selectivity and larger CO₂ adsorption capacity as a sorbent material compared to BILP-101(Ref of BILP-101). Keeping these property differences in mind, we studied CO₂ and N₂ permeability properties of mixed matrix membranes composed of BILP-4 and BILP-101 fillers. We expected BILP-4 based MMMs to exhibit less CO₂/N₂ selectivity compared to BILP-101/Matrimid membranes. However, 10 and 15% BILP-4/Matrimid membranes showed more CO₂/N₂ selectivity compared to BILP-101 counterparts. These findings can be attributed to more CO₂ attractive groups provided in larger surface area and higher CO₂ adsorption properties of BILP-4 compared to BILP-101 (Table 5.1).

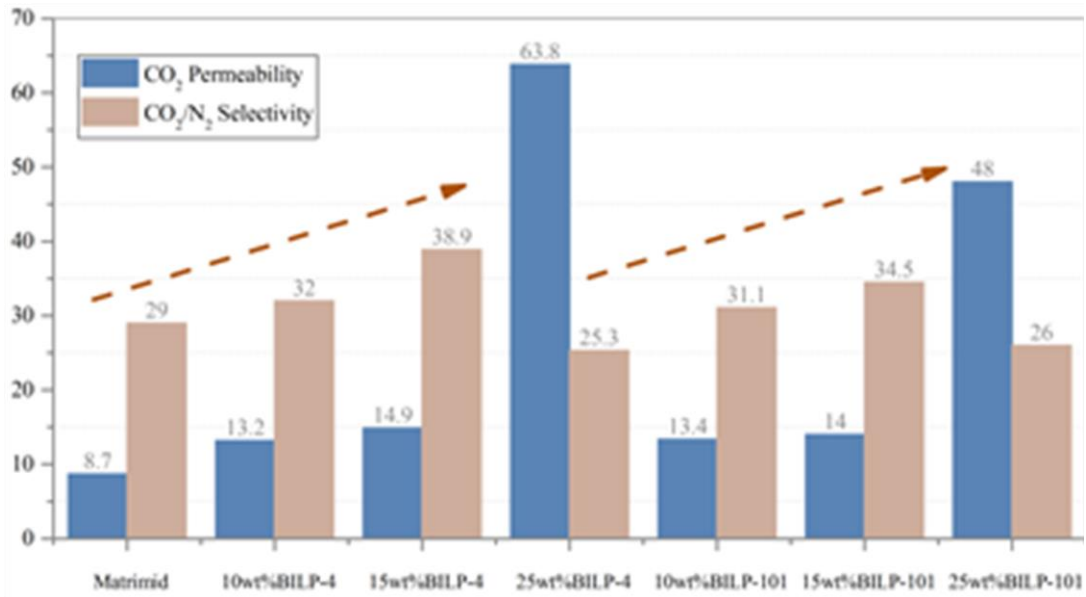


Figure 5.9: Gas transport properties of Matrimid-BILP MMMs

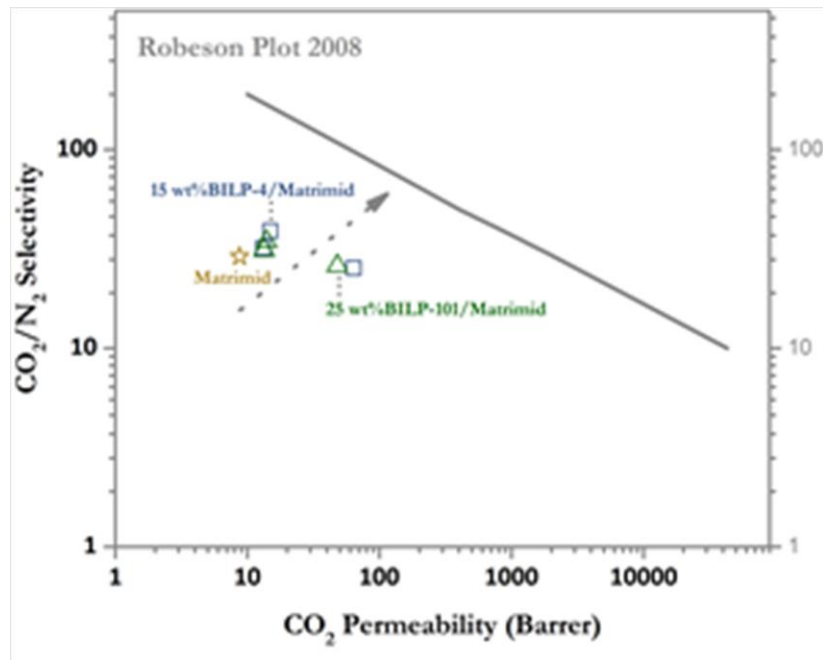


Figure 5.10: performances of Matrimid-BILP MMMs in Robeson Plot 2008

5.4 Conclusion

In this project, we have successfully fabricated MMMs by incorporating benzimidazole linked porous polymers (BILPs), which were synthesized by a facile polycondensation reaction, into a commercial organic polymer Matrimid. The MMMs produced display excellent stability under harsh thermal conditions which is key for applications in industrial settings. The chemical functionalities of the BILPs framework facilitate a strong interaction with the Matrimid polymer matrix. This was manifested in the uniform and compatible incorporation of two different BILPs BILP-4 and BILP-101 into the matrix as well as improved gas permeability and separation properties of the fabricated MMMs. This approach is advantageous in that it eliminates the necessity for pre- or post-synthetic functionalization of filler porous materials as previously explored in other reports.

5.5 References

- (1) Robeson, L. M. The Upper Bound Revisited. *J. Memb. Sci.* **2008**, *320* (1–2), 390–400.
- (2) Hillock, A. M. W.; Miller, S. J.; Koros, W. J. Crosslinked Mixed Matrix Membranes for the Purification of Natural Gas: Effects of Sieve Surface Modification. *J. Memb. Sci.* **2008**, *314* (1–2), 193–199.
- (3) Li, Y.; Guan, H. M.; Chung, T. S.; Kulprathipanja, S. Effects of Novel Silane Modification of Zeolite Surface on Polymer Chain Rigidification and Partial Pore Blockage in Polyethersulfone (PES)-Zeolite A Mixed Matrix Membranes. *J. Memb. Sci.* **2006**, *275* (1–2), 17–28.
- (4) Yong, H. H.; Park, H. C.; Kang, Y. S.; Won, J.; Kim, W. N. Zeolite-Filled Polyimide Membrane Containing 2,4,6-Triaminopyrimidine. *J. Memb. Sci.* **2001**, *188* (2), 151–163.
- (5) Bae, T. H.; Lee, J. S.; Qiu, W.; Koros, W. J.; Jones, C. W.; Nair, S. A High-Performance Gas-Separation Membrane Containing Submicrometer-Sized Metal-Organic Framework Crystals. *Angew. Chemie - Int. Ed.* **2010**, *49* (51), 9863–9866.
- (6) Perez, E. V.; Balkus, K. J.; Ferraris, J. P.; Musselman, I. H. Mixed-Matrix Membranes Containing MOF-5 for Gas Separations. *J. Memb. Sci.* **2009**, *328* (1–2), 165–173.
- (7) Ordoñez, M. J. C.; Balkus, K. J.; Ferraris, J. P.; Musselman, I. H. Molecular Sieving Realized with ZIF-8/Matrimid?? Mixed-Matrix Membranes. *J. Memb. Sci.* **2010**, *361* (1–2), 28–37.
- (8) Venna, S. R.; Lartey, M.; Li, T.; Spore, A.; Kumar, S.; Nulwala, H. B.; Luebke, D. R.; Rosi, N. L.; Albenze, E. Fabrication of MMMs with Improved Gas Separation Properties Using Externally-Functionalized MOF Particles. *J. Mater. Chem. A* **2015**, *3* (9), 5014–5022.

- (9) Chung, T. S.; Chan, S. S.; Wang, R.; Lu, Z.; He, C. Characterization of Permeability and Sorption in Matrimid/C60 Mixed Matrix Membranes. *J. Memb. Sci.* **2003**, *211* (1), 91–99.
- (10) Vu, D. Q.; Koros, W. J.; Miller, S. J. Mixed Matrix Membranes Using Carbon Molecular Sieves. *J. Memb. Sci.* **2003**, *211* (2), 311–334.
- (11) Moore, T. T.; Koros, W. J. Non-Ideal Effects in Organic-Inorganic Materials for Gas Separation Membranes. *J. Mol. Struct.* **2005**, *739* (1–3), 87–98.
- (12) Sekizkardes, A. K.; Kusuma, V. A.; Dahe, G.; Roth, E. A.; Hill, L. J.; Marti, A.; Macala, M.; Venna, S. R.; Hopkinson, D. Separation of Carbon Dioxide from Flue Gas by Mixed Matrix Membranes Using Dual Phase Microporous Polymeric Constituents. *Chem. Commun.* **2016**, *52* (79), 11768–11771.
- (13) Rabbani, M. G.; El-Kaderi, H. M. Synthesis and Characterization of Porous Benzimidazole-Linked Polymers and Their Performance in Small Gas Storage and Selective Uptake. *Chem. Mater.* **2012**, *24* (8), 1511–1517.
- (14) Islamoglu, T.; Behera, S.; Kahveci, Z.; Tessema, T. D.; Jena, P.; El-Kaderi, H. M. Enhanced Carbon Dioxide Capture from Landfill Gas Using Bifunctionalized Benzimidazole-Linked Polymers. *ACS Appl. Mater. Interfaces* **2016**, *8* (23), 14648–14655.
- (15) Altarawneh, S.; Behera, S.; Jena, P.; El-Kaderi, H. M. New Insights into Carbon Dioxide Interactions with Benzimidazole-Linked Polymers. *Chem. Commun. (Camb)*. **2014**, *50* (27), 3571–3574.
- (16) Rabbani, M. G.; Sekizkardes, A. K.; El-Kadri, O. M.; Kaafarani, B. R.; El-Kaderi, H. M. Pyrene-Directed Growth of Nanoporous Benzimidazole-Linked Nanofibers and Their Application to Selective CO₂ Capture and Separation. *J. Mater. Chem.* **2012**, *22*, 25409–

25417.

- (17) Alexandre, M.; Dubois, P. Polymer-Layered Silicate Nanocomposites: Preparation, Properties and Uses of a New Class of Materials. *Mater. Sci. Eng. R Reports* **2000**, *28* (1), 1–63.
- (18) Zhang, Y.; Musselman, I. H.; Ferraris, J. P.; Balkus, K. J. Gas Permeability Properties of Matrimid Membranes Containing the Metal-Organic Framework Cu-BPY-HFS. *J. Memb. Sci.* **2008**, *313* (1–2), 170–181.
- (19) Vu, D. Q.; Koros, W. J.; Miller, S. J. Effect of Condensable Impurity in CO₂/CH₄ Gas Feeds on Performance of Mixed Matrix Membranes Using Carbon Molecular Sieves. *J. Memb. Sci.* **2003**, *221* (1–2), 233–239.
- (20) Liu, R.; Qiao, X.; Chung, T. S. The Development of High Performance P84 Co-Polyimide Hollow Fibers for Pervaporation Dehydration of Isopropanol. *Chem. Eng. Sci.* **2005**, *60* (23), 6674–6686.
- (21) Khosravi, T.; Mosleh, S.; Bakhtiari, O.; Mohammadi, T. Mixed Matrix Membranes of Matrimid 5218 Loaded with Zeolite 4A for Pervaporation Separation of Water-Isopropanol Mixtures. *Chem. Eng. Res. Des.* **2012**, *90* (12), 2353–2363.

Chapter 6

Concluding Remarks

Due to the increasing emission of CO₂ into the atmosphere, the need to advance the methodologies used in carbon capture and sequestration processes is of paramount importance. To this end, we have presented in this dissertation a series of studies that contribute to this research field. The studies presented have thoroughly explored the potential for newly fabricated materials that employ adsorption and membrane gas separation mechanisms with potential to address the problem of CO₂ emission.

In the first project, we detail the single gas isotherm data analysis methods used to elucidate the performance of sorbents in gas capture and separation application. Moreover we present the design and working principle of a dynamic gas mixture breakthrough apparatus. The working principle of the breakthrough setup mimics the dynamic and real life gas mixtures involved in CO₂ separation from post combustion flue gas exhausts. The separation performance of a new class of heteroatom (N and O) doped porous carbons derived from a Pyrazole precursor were evaluated and compared to IAST selectivity studies.

The high physico-chemical stability, high surface area and tunability of surface and pore functionality has garnered POPs significant attention as promising candidates as sorbents for the treatment of post combustion flue gas to reduce CO₂ emission into the atmosphere. In the second project, two new benzimidazole linked polymers (BILPs) have been designed and synthesized by employing a metal free acid catalyzed condensation reaction. The polymers porosity with surface area are of up to 926 m² g⁻¹ driven by the rigid and star shaped building blocks used. The basic imidazole functionality and microporous nature of BILPs resulted in a high CO₂ uptake of 3.14 mmol g⁻¹ with isosteric heat of adsorption (Q_{st}) value of 31.2 kJ mol⁻¹ at 298K and 1 bar for

BILP-31. BILP-30 displayed very good selectivity for CO₂ for flue gas (61.42) while BILP-31 was superior in CO₂ separation from landfill gas mixtures (11.5) at 298 K and 1 bar.

In the third project, a new POP incorporating a highly conjugated pyrene core into a polymer framework linked by azo-bonds is presented. Azo-Py displays a nanofibrous morphology induced by the π - π stacking of the electron rich pyrene core. Azo-Py has exceptional surface area of 1259 m² g⁻¹ and a microporous pore size distribution. These properties lead to high CO₂ uptakes of 4.79 mmol g⁻¹(273 K) and 2.89 mmol g⁻¹ (298 K) at 1 bar. Evaluation of the *S* value for CO₂ separation of Azo-Py revealed competitive values for flue gas (178.2) and landfill gas (63.83) at 298 K and 1 bar.

Finally, an alternative approach of using membranes for selective CO₂ capture is presented. Highly cross-linked benzimidazole linked polymers (BILPs) displaying high surface area were successfully incorporated into a commercial polyimide, Matrimid, polymer to form a series of new mixed matrix membranes (MMMs). The surface functionality of BILPs, BILP-4 and BILP-101 were exploited to assure the interaction with Matrimid matrix and to produce robust MMMs which displayed significantly improved CO₂ gas permeability. The ideal selectivities for CO₂/N₂ were calculated with enhancements as high as ~134% at 15 wt% BILP loading. This study also presents a comprehensive study on structure-property relationship between polymeric fillers and a matrix and evaluates the gas transport properties of MMMs accordingly.